Chapter 7: Trace Elements in Igneous Processes

7.1 Introduction

In this chapter we will consider the behavior of trace elements, particularly in magmas, and introduce methods to model this behavior. Though trace elements, by definition, constitute only a small fraction of a system of interest, they provide geochemical and geological information out of proportion to their abundance. There are several reasons for this. First, variations in the concentrations of many trace elements are much larger than variations in the concentrations of major components, often by many orders of magnitude. Second, in any system there are far more trace elements than major elements. In most geochemical systems, there are 10 or fewer major components that together account for 99% or more of the system. This leaves 80 trace elements. Each element has chemical properties that are to some degree unique, hence there is unique geochemical information contained in the variation of concentration for each element. Thus the 80 trace elements always contain information not available from the variations in the concentrations of major elements. Third, the range in behavior of trace elements is large and collectively they are sensitive to processes to which major elements are insensitive. One example is the depth at which partial melting occurs in the mantle. When the mantle melts, it produces melts whose composition is only weakly dependent on pressure, i.e., it always produces basalt. Certain trace elements, however, are highly sensitive to the depth of melting (because the phase assemblages are functions of pressure). Furthermore, on a large scale, the composition of the Earth's mantle appears to be relatively uniform, or at least those parts of it that give rise to basaltic magmas. Indeed, it has proved very difficult to demonstrate any heterogeneity in the mantle on the basis of the major element chemistry of the magmas it has produced. In contrast, it has been amply demonstrated that trace element concentrations of the mantle are quite variable. Trace elements, particularly when combined with isotope ratios, which we shall discuss the in next chapter, thus provide a chemical fingerprint of different mantle reservoirs. Finally, the behavior of trace elements is almost always simpler than that of major elements because trace elements obey Henry's Law (Chapter 3).

Trace element geochemistry has been of enormous use in understanding the evolution of the Earth. As we shall see in subsequent chapters, a fair amount of what we know about the evolution of the core, the mantle, and the crust has come from the study of trace element abundances. For example, the abundance of certain "siderophile" (a term we shall define shortly) trace elements in the mantle and mantle-derived rocks, provides reason to believe that segregation of the Earth's iron-nickel core must have been largely complete before the Earth had entirely accreted from the cloud of gas and dust surrounding the early Sun (the solar nebula). We also know, for example, that much of the upper mantle has undergone partial melting at some point in the past. These partial melts of the upper mantle have, through time, created the continental crust. From the abundances of trace gases in the mantle and their isotopic composition, we conclude that the solid portion of the Earth must have undergone extensive outgassing within the first few hundred million years of Earth history. As we shall see in subsequent chapters, magmas from a given tectonic setting tend to share patterns of trace element abundances. This allows the tectonic setting of anciently erupted magmas to be deduced.

Though our focus here will be on igneous processes, trace elements are equally useful in other geologic problems as well. For example, trace elements can provide useful clues as to the origin of sulfide ore deposits. The concentrations of trace elements such as cadmium in the fossil shells of micro-organisms provide information about the biological productivity and circulation patterns of ancient oceans, and the concentration of Sr in corals provides a measure of temperature of ancient seas. Indeed, throughout the earth sciences, trace element geochemistry has become a powerful tool.

Our purpose in this chapter is to add this tool to our geochemical toolbox. We will begin by considering the chemical properties of the various groups of trace elements, with particular emphasis on how they behave in nature. We then introduce quantitative means of describing trace element distribution. Our primary tool here will be the distribution, or partition, coefficient, which we first introduced in

CHAPTER 7: TRACE ELEMENTS

Chapter 3 (as K_D). We will examine how the distribution coefficient depends on temperature, pressure, composition, and the fundamental chemical properties of the element of interest. Finally, we develop equations to predict the behavior of trace elements during melting and crystallization. The knowledge of trace element behavior that we gain in this chapter will be useful in the following one where we discuss radiogenic isotope geochemistry, because all the radioactive elements and their daughter products, with a single exception, are trace elements. We will apply the tools we acquire here to understanding the evolution of the core, the mantle, and the crust in subsequent chapters.

7.1.1 WHAT IS A TRACE ELEMENT?

The term trace element is a bit hard to define. For igneous and metamorphic systems (and sedimentary rocks for that matter), an operational definition might be as follows: trace elements are *those elements that are not stoichiometric constituents of phases in the system of interest.* Clearly this definition is a bit fuzzy: a trace element in one system is not one in another. For example, potassium never forms its own phase in mid-ocean ridge basalts (MORB), its concentration rarely exceeding 1500 ppm; but K is certainly not a trace element in granites. For most silicate rocks, O, Si, Al, Na, Mg, Ca, and Fe are 'major elements'. H, C, S, K, P, Ti, Cr, and Mn are sometimes 'major elements' in the sense that they can be stoichiometric constituents of phases. These are often referred to as 'minor elements'. All the remaining elements are always trace elements, with the exception of a few rare, but important, circumstances such as pegmatites and ore deposits.

The above definition breaks down entirely for fluids and natural waters since there is only one phase, namely the fluid, and it's not stoichiometric. In seawater, anything other than Cl^-, SO_4^{2-}, CO_3^{2-},

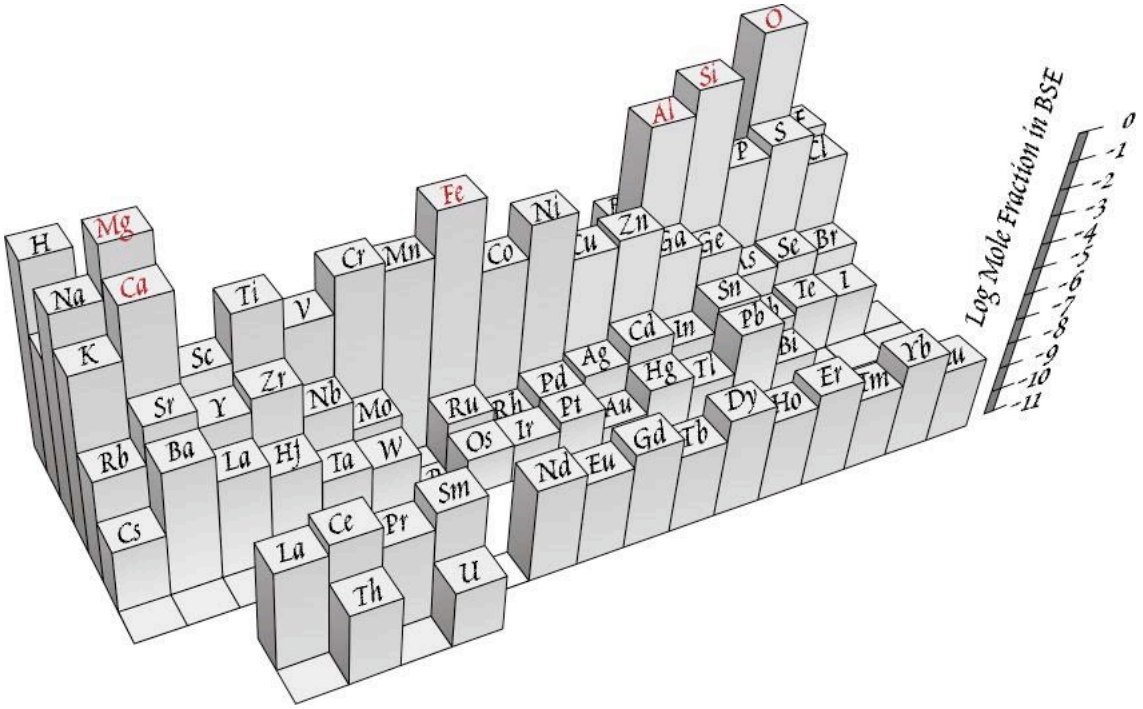

Figure 7.1. Three-dimensional histogram illustrating the abundance of the elements (as the log of mole fraction) in the silicate portion of the Earth (the "Bulk Silicate Earth"; BSE). Just 6 elements, oxygen, magnesium, silicon, iron, aluminum, and calcium make up 99.1% of the silicate Earth. If we include the core and consider the composition of the entire Earth, then only nickel, and perhaps sulfur, need be added to this list. The remaining elements, though sometimes locally concentrated (e.g., in the crust, in the hydrosphere, in ores) can be considered *trace elements*.

HCO_3^-, Mg^{2+}, Ca^{2+}, K^+ and Na^+ (and H_2O, of course) can be considered a trace constituent, though Sr^{2+}, HBO_3^-, and Br^- are sometimes considered major constituents also (constituents or species is a better term here than elements). These, including the last three, constitute over 99.99% of the total dissolved solids in seawater. Trace elements in seawater and in rocks do have one thing in common: *neither affect the chemical or physical properties of the system as a whole to a significant extent.* This might serve as a definition. However, trace (or at least minor) elements can determine the color of a mineral (e.g., the green color of chrome diopside), so even this definition has problems. And CO_2, with a concentration in the atmosphere of only 360 ppm, profoundly affects the transparency of the atmosphere to infrared radiation, and, as a result, Earth's climate. At even lower concentrations, ozone in the upper atmosphere controls the atmospheric transparency to ultraviolet radiation. So this definition is not satisfactory either.

Yet another possible definition of a trace element is: *an element whose activity obeys Henry's Law in the system of interest.* This implies sufficiently dilute concentrations that for trace element A and major component B, A-A interactions are not significant compared to A-B interactions.

There is perhaps no satisfactory quantitative definition of a trace element that will work in every situation. For our present purposes, any of these definitions might do, but bear in mind that a trace element in one system need not be a trace element in another.

7.2 Behavior of the Elements

7.2.1 Goldschmidt's Classification

No matter how we define the term "trace element", most elements will fall into this category, as is illustrated in Figure 7.1. That being the case, this is a good place to consider the geochemical characteristics of the elements. Goldschmidt* recognized four broad categories: atmophile, lithophile, chalcophile, and siderophile (Figure 7.2, Table 7.1). *Atmophile* elements are generally extremely volatile (i.e., they form gases or liquids at the surface of the Earth) and are concentrated in the atmosphere and hydrosphere. Lithophile, siderophile and chalcophile refer to the tendency of the element to partition into a silicate, metal, or sulfide *liquid* respectively. *Lithophile* elements are those showing an affinity for silicate phases and are concentrated in the silicate portion (crust and mantle) of the earth. *Siderophile* elements have an affinity for a metallic liquid phase. They are depleted in the silicate portion of the earth and presumably concentrated in the core. *Chalcophile* elements have an affinity for a sulfide liquid phase. They are also depleted in the silicate earth and may be concentrated in the core. Many sulfide ore deposits originated from aqueous fluids rather than sulfide liquid. A chalcophile element need not necessarily be concentrated in such deposits. As it works out, however, they generally are. Most elements that are siderophile are usually also somewhat chalcophile and visa versa.

There is some basis for Goldschmidt's classification in the chemistry of the elements. Figure 7.2 shows that the lithophile elements occur mainly at either end of the periodic table, siderophile elements are mainly group 8, 9 & 10 elements (and their neighbors), chalcophile elements are mainly group 11, 12 and the heavier group 13-16 elements, while the atmophile elements are mainly the noble gases. The distribution of the electropositive elements (those that give up an electron more readily than they accept one) among metal, sulfide, and silicate phases is controlled by the free energies of formation of the corresponding sulfides and silicates. By comparing the free energies of formation with those of ferrous

* Victor Goldschmidt (1888-1947) is often considered the 'father of geochemistry'. Goldschmidt earned a Ph.D. from the University of Oslo in 1911 and remained there until 1929, when he assumed the directorship of the Geochemisches Institut at the University of Göttingen. Because of the worsening political situation in Germany, he returned to Oslo in 1935. He was for a time imprisoned in a concentration camp after Germany invaded Norway in 1940. In 1942 he fled to Sweden and eventually to England. He returned to Oslo in 1946 but never fully recovered from the effects of imprisonment and died a year later. The Geochemical Society has named its most prestigious medal after him and co-sponsors, along with the European Association of Geochemistry, annual Goldschmidt Conferences.

TABLE 7.1. GOLDSCHMIDT'S CLASSIFICATION OF THE ELEMENTS

Siderophile	Chalcophile	Lithophile	Atmophile
Fe*, Co*, Ni*	(Cu), Ag	Li, Na, K, Rb, Cs	(H), N, (O)
Ru, Rh, PdZn, Cd, Hg	Be, Mg, Ca, Sr, Ba	He, Ne, Ar, Kr, Xe	
Os, Ir, Pt	Ga, In, Tl	B, Al, Sc, Y, REE	
Au, Re†, Mo†	(Ge), (Sn), Pb	Si, Ti, Zr, Hf, Th	
Ge*, Sn*, W‡	(As), (Sb), Bi	P, V, Nb, Ta	
C‡, Cu*, Ga*	S, Se, Te	O, Cr, U	
Ge*, As†, Sb†	(Fe), Mo, (Os)	H, F, Cl, Br, I	
	(Ru), (Rh), (Pd)	(Fe), Mn, (Zn), (Ga)	

*Chalcophile and lithophile in the earth's crust
†Chalcophile in the earth's crust
‡Lithophile in the earth's crust

sulfide and ferrous silicate, it is possible to deduce which elements are siderophile, those which are chalcophile and which are lithophile. For historical reasons, namely lack of ΔG_f^o data on silicates, the point is generally illustrated using the enthalpy of formation, ΔH_f, of the oxide. Since 'oxyphile' could arguably be a better term than lithophile, this is not such a bad thing. Table 7.2 gives some examples. Elements whose oxides have high $-\Delta G_f$ are lithophile. Why this is the case should be clear from our understanding of thermodynamics. States with the lowest free energy are the most stable: a high $-\Delta G_f$ indicates the oxide is much more stable than the metal. Elements whose oxides have $-\Delta G_f$ similar to that FeO combine with oxygen only about as readily as Fe, and are generally siderophile. Those elements whose oxides have low $|\Delta G°|$ are generally chalcophile.

Lithophile elements also have either very low electronegativities or very high ones and tend to form ionic bonds (although the basic silicate bond, the Si—O bond, is only about 50% ionic, metal–oxygen bonds in silicates are dominantly ionic). Siderophile and chalcophile elements have intermediate electronegativities and tend to form covalent or metallic bonds.

7.2.2 THE GEOCHEMICAL PERIODIC TABLE

Goldschmidt's classification is relevant mainly to distribution of elements in meteorites and to how elements distribute themselves between the Earth's major geochemical reservoirs: the core, the mantle and crust, and the hydrosphere and atmosphere. Since there is an overabundance of O in the outer part of the Earth, metallic liquids do not form, and siderophile elements have little opportunity to behave as such. Similarly, sufficient S is rarely available to form more than trace amount of sulfides. As a result, siderophile elements such as Ni and chalcophile elements such as Pb occur mainly in silicate phases in the crust and mantle.

We can, however, group the elements based on how they behave in the silicate portion of the Earth, the mantle and crust. Figure 7.3 illustrates this grouping. We first note that we have added sodium to those 6 elements whose molar abundance exceeds 1 percent (Figure 1), to form the group called major elements, and which we will not discuss in this chapter. Although the elements K, Ti, Mn, and P are often reported in rock analyses as major elements, we will include them in our discussion of trace elements. Let's now briefly examine the characteristics of the remaining groups.

Chapter 7: Trace Elements

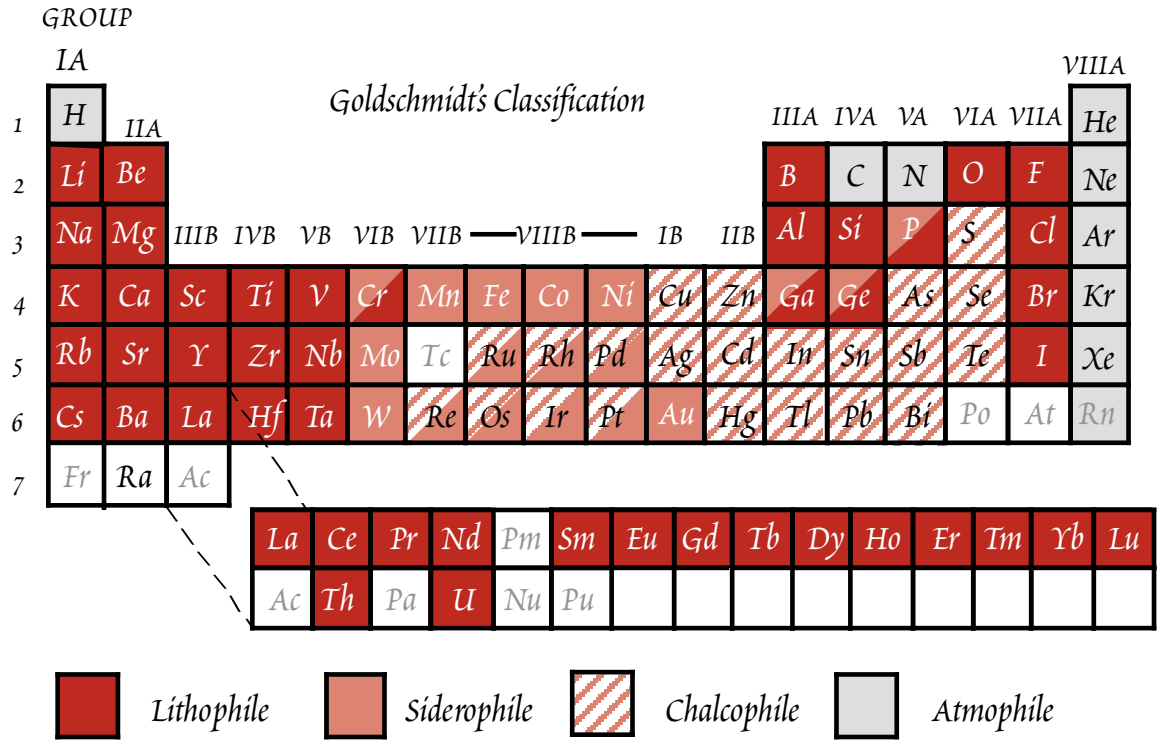

Figure 7.2. Goldschmidt's classification of the elements.

7.2.2.1 The Volatile Elements

The defining feature of the noble gases is their filled outer electron shell, making them chemically inert as well as volatile. Hence, they are never chemically bound in rocks and minerals. Furthermore, except for He, they are have rather large radii and cannot easily be accommodated in either cationic or anionic lattice sites of many minerals. Thus they are typically present at very low concentrations. Their concentrations are usually reported in STP cm^3/g at (i.e., cm^3/g at standard temperature and pressure: 273 K and 01.MPa; 1 cm^3/g =4.46 × 10^{-5} moles/g). Concentrations in silicate rocks and minerals are

Table 7.2. Free Energy of Formation of Some Oxides

Oxide	$-\Delta G_f^o$ (kJ/mole/oxygen)	Oxide	$-\Delta G_f^o$ (kJ/mole/oxygen)
CaO	604.0	In_2O_3	304.2
ThO_2	584.6	SnO_2	260.0
MgO	569.4	*FeO*	*245.9*
Al_2O_3	527.3	WO_3	247.3
ZrO_2	521.6	CdO	221.9
CeO_2	512.6	NiO	211.6
TiO_2	444.7	MoO_3	215.4
SiO_2	428.1	Sb_2O_3	207.9
Na_2O	398.3	PbO	189.3
Ta_2O_3	374.0	As_2O_3	180.1
MnO	362.8	Bi_2O_3	168.8
Cr_2O_3	353.1	CuO	127.6
ZnO	318.4	Ag_2O_3	10.9

CHAPTER 7: TRACE ELEMENTS

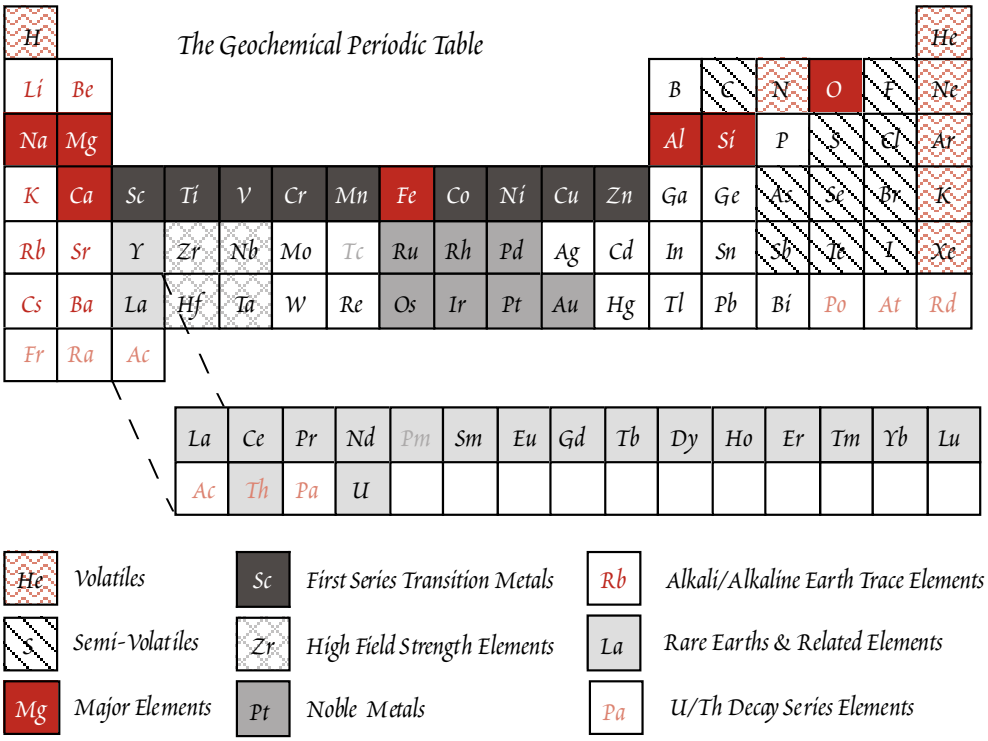

Figure 7.3. The Geochemical Periodic Table, in which elements are grouped according to their geochemical behavior.

typically 10^{-4} to 10^{-12} STP cm^3/g (10^{-1} to 10^{-9} ppm). Their solubility in silicate melts is a strong function of pressure, as well as both atomic radius and melt composition as is illustrated in Figure 7.4. Although they cannot form true chemical bonds with other atoms, they can be strongly adsorbed to crystal surfaces through van der Waals forces.

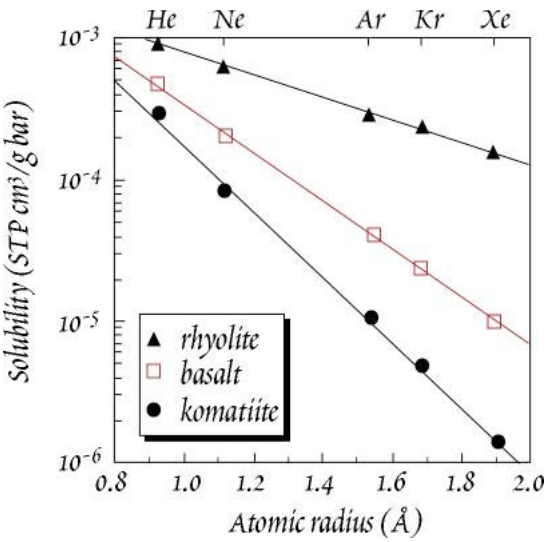

Figure 7.4. Solubility of the rare gases is melts of varying composition at 1200° to 1400° C. Solubility is a strong function of atomic radius and melt composition, but only a weak function of temperature. From Carroll and Draper (1994).

The very strong nature of the N–N bond makes nitrogen relatively unreactive once molecular nitrogen forms; consequently it, like the rare gases, is strongly partitioned into the atmosphere. However, it is quite capable of forming strong covalent bonds with other elements. In silicate minerals, N is probably primarily present as the ammonia ion rather than N_2. As such, it readily substitutes for K^+. As ammonia, it is highly soluble in aqueous fluids and is therefore readily transported by them. Ammonia, like N_2, is quite volatile, so both species partition readily into the gas phase of magmas. In aqueous solution, nitrogen will be present as nitrate (and trace amounts of ammonia, produced by breakdown of nitrogen-bearing organic compounds), as well as N_2. Nitrogen is a component of proteins and nucleic acids and as such is vital to all organisms. However, most plants can utilize only "fixed" nitrogen, that is nitrate or ammonia. In many natural waters, nitrate concentrations are held at very low concentrations because of biological utilization.

Chapter 7: Trace Elements

7.2.2.2 The Semi-Volatiles

The shared characteristic of this group is that they partition readily into a fluid or gas phase (e.g., Cl, Br) or form compounds that are volatile (e.g., SO_2, CO_2). Not all are volatile in a strict sense (volatile in a strict sense means having a high vapor pressure or low boiling point; indeed, carbon is highly refractory in the elemental form).

The partitioning of sulfur between liquid and gas phases is a strong function of f_{O_2}. At high oxygen fugacities, sulfur is present primarily as SO_2, but at low f_{O_2} it is present primarily as sulfide. The solubility of sulfide in silicate liquids is, however, low. At sufficiently high sulfur concentrations in magmas, sulfide and silicate liquids will exsolve. Sulfide liquids are rich in Fe and Ni and other chalcophile metals and are the source of many economically important ore deposits. Large volumes of sulfide liquid are rare, but microscopic droplets of sulfide liquids commonly occur in mid-ocean ridge magmas.

Similarly, the solubility of CO_2 in silicate magmas is limited and is a strong function of pressure. At low CO_2 concentrations, CO_2 exsolves from magmas to form a CO_2–H_2O gas phase. However, at higher CO_2/H_2O ratios and total CO_2 concentrations, carbonatite magmas can form in which $CaCO_3$ is the dominant component. On the whole, carbonatites are rare, but over the course of geologic history they have erupted on every continent. In certain localities, such as the modern East Africa Rift, they can be fairly common.

The remaining elements in this group are always present in trace concentrations and never reach saturation in magmas and hence never exsolve as independent gas or fluid phases. Rather, they partition into gas phase formed by exsolution of CO_2 and H_2O.

7.2.2.3 The Alkali and Alkaline Earth Elements

The alkali and alkaline earth elements have electronegativities less than 1.5 and a single valence state (+1 for the alkalis, +2 for the alkaline earths). The difference in electronegativity between these elements and most anions is 2 or greater, so the bonds these elements form are strongly ionic in character (Be is an exception, as it forms bonds with a more covalent character). Ionic bonds are readily disrupted by water due to its polar nature (see Chapter 3). The low ionic potential (ratio of charge to ionic radius) makes these elements relatively soluble in aqueous solution. Because of their solubility, they are quite mobile during metamorphism and weathering.

Because bonding is predominantly ionic, the atoms of these elements behave approximately as hard spheres containing a fixed point charge at their centers (these are among the group A or hard ions discussed in Chapter 6). Thus the factors that most govern their behavior in igneous rocks are *ionic radius and charge*. K, Rb, Cs, Sr, and Ba, are often collectively termed the *large-ion-lithophile (LIL) elements*. As the name implies, these elements all have large ionic radii, ranging from 118 picometers (pm) for Sr to 167 pm for Cs. The major minerals in basaltic and ultramafic rocks have two kinds of cationic lattice sites: small tetrahedral sites occupied by Si and Al (and less often by Fe^{3+} and Ti^{4+}) and larger octahedral ones usually occupied by Ca, Mg, or Fe and more rarely by Na. The ionic radii of the heavy alkali and alkaline earth elements are larger than the radii of even the larger octahedral sites. As a result, substitution of these elements in these sites results in local distortion of the lattice, which is energetically unfavorable. These elements thus tend to be concentrated in the melt phase when melting or crystallization occurs. Such elements are called *incompatible elements*. Incompatible elements are defined as those elements that partition readily into a melt phase when the mantle undergoes melting. Compatible elements, conversely, remain in the residual minerals when melting occurs. Over the history of the Earth, partial melting of the mantle and eruption or intrusion of the resulting magmas on or in the continental crust has enriched the crust in incompatible elements.

In contrast to the heavy alkaline earths, Be has an ionic radius smaller than most octahedral sites. Substitution of a small ion in a large site is also energetically unfavorable as the bond energy is reduced. Thus Be is also an incompatible element, though only moderately so. While Li has an ionic radius similar to that of Mg and Fe^{2+}, its substitution for one of these elements creates a charge imbalance that requires a coupled substitution. This is also energetically unfavorable, hence Li is also an incompatible element, though again only moderately so.

CHAPTER 7: TRACE ELEMENTS

7.2.2.4 The Rare Earth Elements and Y

The rare earths are the two rows of elements commonly shown at the bottom of the periodic table. The first row is the *lanthanide* rare earths, the second is the *actinide* rare earths. However, the term "rare earths" is often used in geochemistry to refer to only to the lanthanide rare earths. We will follow that practice in this book, though we will discuss both the actinide and lanthanides in this section. Only two of the actinides, U and Th, have nuclei stable enough to survive over the history of the Earth. Y shares the same chemical properties, including charge and ionic radius, as the heavier rare earths, and as a result behaves much like them.

As the alkalis and alkaline earths, the rare earths and Y are strongly electropositive; the lathanide have electronegativities of 1.2 or less, the actinides U and Th have slightly higher electronegativities. As a result, they form predominantly ionic bonds, and the hard charged sphere again provides a good model of their behavior. The lanthanide rare earths are in the +3 valence state over a wide range of oxygen fugacities. At the oxygen fugacity of the Earth's surface, however, Ce can be partly or wholly in the +4 state and Eu can be partly in the +2 state at the low oxygen fugacities of the Earth's interior. Th is always in a +4 valence state, but U may be in a +4 or +6 valence state, depending on oxygen fugacity (or pε, if we chose to quantify the redox state that way). Unlike the alkali and alkaline earth elements, they are relatively insoluble in aqueous solutions, a consequence of their higher charge and high ionic potential and resulting need to be coordinated by anions. The one exception is U in its fully oxidized U^{6+} form, which forms a soluble oxyanion complex, UO_2^{2-}.

The rare earths are transition metals. In the transition metals, the *s* orbital of the outermost shell is filled before filling of lower electron shells is complete. In atoms of the period 6 transition elements, the *6s* orbital is filled before the *5d* and *4f* orbitals. In the lanthanide rare earths, it is the *4f* orbitals that are being filled, so the configuration of the valence electrons is similar in all the rare earth, hence all exhibit similar chemical behavior. Ionic radius, which decreases progressively from La^{3+} (115 pm) to Lu^{3+} (93 pm), illustrated in Figure 7.5, is thus the characteristic that governs their relative behavior.

Because of their high charge and large radii, the rare earths are incompatible elements. The degree of incompatibilities varies, however. Highly charged U and Th are highly incompatible elements, as are the lightest rare earths. However, the heavy rare earths have sufficiently small radii that they can be accommodated to some degree in many common minerals. The heaviest rare earths readily substitute for Al^{3+} in garnet, and hence can be concentrated by it. Eu, when in its 2+ state, substitutes for Ca^{2+} in plagioclase feldspar more readily than the other rare earths. Thus plagioclase is often anomalously rich in Eu compared to the other rare earths, and other phases in equilibrium with plagioclase become relatively depleted in Eu as a consequence.

The systematic variation in lathanide rare earth behavior is best illustrated by plotting the log of the *relative abundances* as a function of atomic number (this sort of plot is sometimes called a Masuda, Masuda-Coryell, or Coryell plot, but most often is simply termed a rare earth plot or diagram). Relative abundances are calculated by dividing the concentration of each rare earth by its concentration in a set of normalizing values, such as the concentrations of rare earths in chondritic meteorites. Why do we use relative abundances? As we shall see in Chapter 10, the abundances of even numbered elements in the solar system (and most likely the cosmos) are greater than those of neighboring odd-

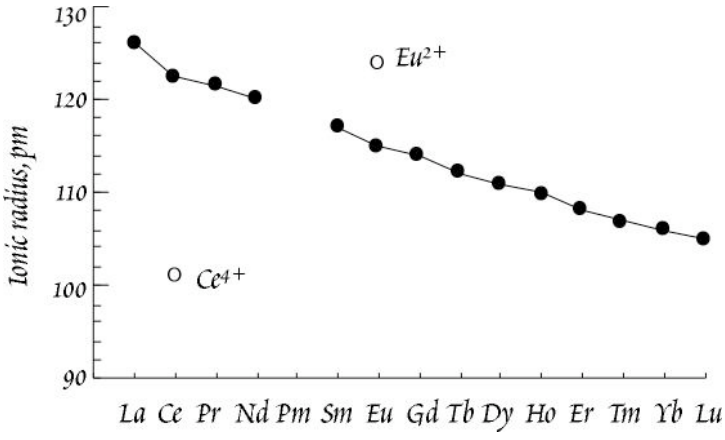

Figure 7.5. Ionic radii of the lanthanide rare earth elements (3+ state except where noted). Promethium (Pm) has no isotope with a half-life longer than 5 years.

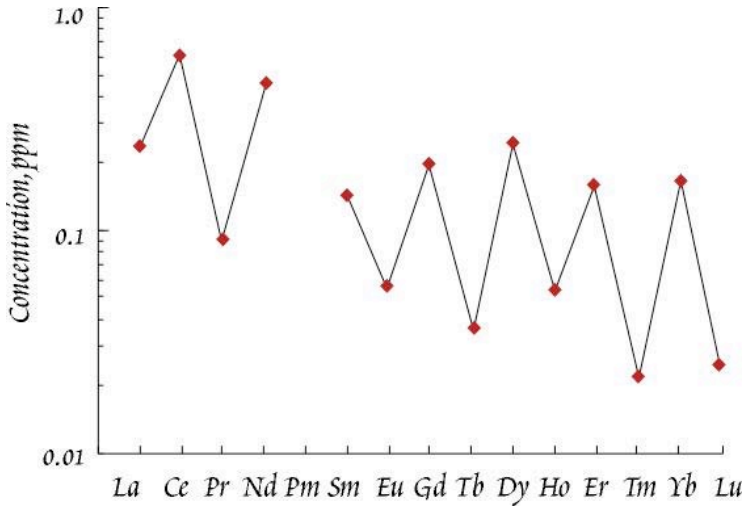

Figure 7.6. Concentrations of the rare earths in the carbonaceous chondritic meteorite Orgueil.

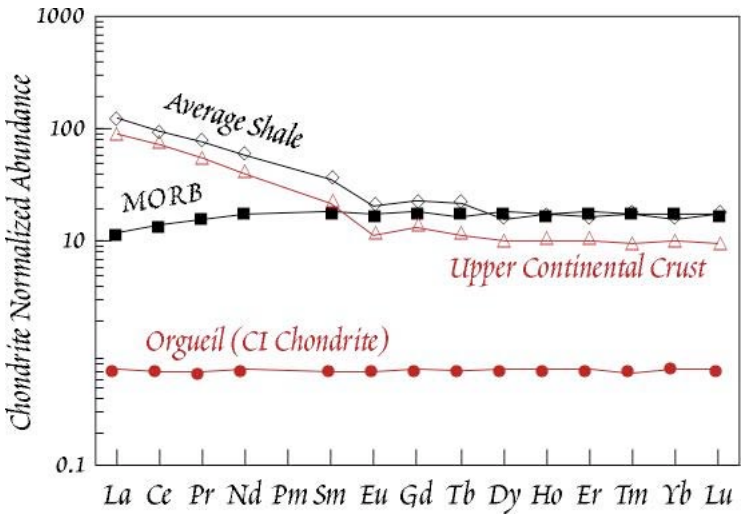

Figure 7.7. A rare earth plot showing rare earth patterns for average upper continental crust (Rudnick and Fountain, 1995), average shale, average mid-ocean ridge basalt, and the meteorite Orgueil. As a carbonaceous chondrite, Orgueil has lower rare earth concentrations than the average of ordinary chondrites used for normalization.

numbered elements. Furthermore, because of the way the elements have been created, abundances generally decrease with increasing atomic number. Thus a simple plot of abundances produces a saw tooth pattern of decreasing abundances. This can be seen in Figure 7.6, which shows rare earth abundances in the CI chondrite Orgueil (CI chondrites are a class of meteorites that are taken to be the best representative of the average concentrations of non-volatile elements in the solar system; see Chapter 10). "Normalizing" the rare earth abundances to those of chondritic meteorites eliminates effects related to nuclear stability and nucleosynthesis and produces a smooth pattern, such as those seen in Figure 7.7.

Though all igneous geochemists normalize rare earth abundances to some set of chondritic values, there is no uniformity in the set chosen. Popular normalization schemes include the CI chondrite Orgueil, an average of 20 ordinary chondrites reported by Nakamura (1974), and the chondritic meteorite Leedy (Masuda et al., 1973). Although the absolute values of the normalizing values vary (for example, the Nakamura values are about 28% higher than those of Orgueil), the relative abundances are essentially the same. Thus the normalized rare earth *pattern* should be the same regardless of normalizing values. Some sets of normalizing values are listed in Table 7.3. A more complete tabulation can be found in Rollinson (1993).

Rare earth patterns for upper continental crust and average mid-ocean ridge basalt (MORB) are also shown in Figure 7.7. MORB exhibits a *light rare earth-depleted* pattern; upper continental crust is *light rare earth-enriched* with a negative 'Eu anomaly'. The light rare earth depletion of MORB reflects the incompatible element-depleted nature of the upper mantle from which these magmas are derived. This incompatible element depletion of the mantle is generally thought to have resulted from extraction of partial melts, in which the incompatible elements were concentrated. Those partial melts have crystallized to form the continental crust. If this is so, the complimentary nature of the rare earth patterns of MORB and continental crust is not coincidental. There are good reasons, which we will discuss in Chapters 10 and 11, to believe that the relative abundances of rare earths in the Earth as a whole are similar to those of chondrites, i.e., the rare earth pattern

of the Earth should be flat. Mass balance therefore requires the sum of all the various rare earth reservoirs in the Earth have a flat rare earth pattern. If we assume the continental crust and the mantle are the only two reservoirs with significant concentrations of rare earth elements, and if the continental crust is light rare earth-enriched, then the mantle should be light rare earth-depleted.

A negative Eu anomaly is typical of many continental rocks, as well as most sediments and seawater. The Eu anomaly probably arises because many crustal rocks of granitic and granodioritic composition were produced by intracrustal partial melting. The residues of those melts were rich in plagioclase, hence retaining somewhat more of the Eu in the lower crust, and creating a complimentary Eu-depleted upper crust. Sediments and seawater inherit this Eu anomaly from their source rocks in the upper continental crust.

Many sedimentary rocks, and seawater, have rare earth patterns that are similar to each other, and to that of the continental crust. To accentuate the difference in rare earth patterns between sediments, low temperature geochemists often normalize rare earth abundances to the concentrations in average shale. Again, there are several sets of normalizing values (one set is given in Table 7.3, others may be found in Rollinson, 1993), but the relative abundances are all similar. Figure 7.8 shows examples of shale-normalized rare earth patterns.

Table 7.3. Normalizing Values used for Rare Earth Plots

	Ordinary Chondrites	Orgueil (CI Chondrite)	Leedy	BSE	Ave. Shale
La	0.329	0.236	0.378	0.648	41
Ce	0.865	0.619	0.976	1.675	83
Pr	0.130	0.09		0.254	10.1
Nd	0.630	0.463	0.716	1.25	38
Sm	0.203	0.144	0.23	0.406	7.5
Eu	0.077	0.0547	0.0866	0.154	1.61
Gd	0.276	0.199	0.311	0.544	6.35
Tb	0.055	0.0353		0.099	1.23
Dy	0.343	0.246	0.39	0.674	5.5
Ho	0.077	0.0552		0.149	1.34
Er	0.225	0.162	0.255	0.438	3.75
Tm	0.035	0.022		0.068	0.63
Yb	0.220	0.166	0.249	0.441	3.53
Lu	0.034	0.0245	0.0387	0.0675	0.61

"Ordinary chondrites" is modified from Nakamura (1974), Orgueil are the values tabulated by Anders and Grevesse (1989), Leedy, an ordinary chondrite, is from Masuda (1973), BSE is Bulk Silicate Earth from McDonough and Sun (1994), and Average Shale is from Piper (1974).

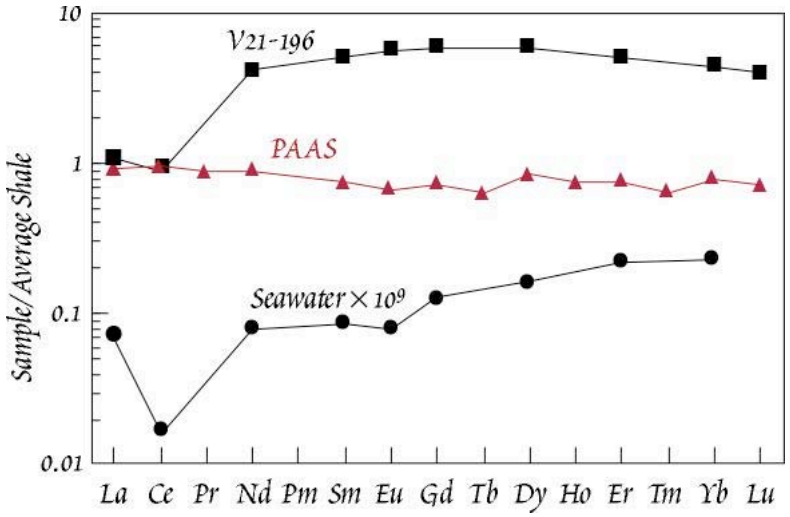

Figure 7.8. Shale-normalized REE earth patterns of a Pacific pelagic sediment (V21-196; Ben Othman et al., 1989), the Post-Archean shale composite (McLennan, 1989), and typical seawater (Elderfield and Greaves, 1982). Both the pelagic sediment and seawater display a negative Ce anomaly, a consequence of Ce being in the +4 oxidation state.

Because the rare earths are highly insoluble and immobile, rare earth patterns often remain unchanged during metamorphism. Hence rare earth patterns can provide information on the premetamorphic history of a rock. Indeed, even during the production of sediment from crystalline rock, the

rare earth patterns often remain little changed, and rare earth patterns have been used to identify the provenance, i.e., the source, of sedimentary rocks. Rare earth patterns have also become useful tools in chemical oceanography, now that modern analytical techniques allow their accurate determination despite concentrations in the parts per trillion range.

7.2.2.5 The HFS Elements

The *high field strength (HFS) elements* are so called because of their high ionic charge: Zr and Hf have +4 valence states and Ta and Nb have +5 valence states. Th and U are sometimes included in this group. As we noted, Th has a +4 valence state and U either a +6 or +4 valence state. Because of their high charge, all are relatively small cations, with ionic radii of 64 pm for Nb^{5+} and Ta^{5+}, and 72 and 76 pm for Zr^{4+} and Hf^{4+} respectively (U^{4+} and Th^{4+} are larger, however). Although they are of appropriate size for many cation sites in common minerals, their charge is too great and requires one or more coupled substitutions to maintain charge balance. As we noted earlier, such substitutions are energetically unfavorable. Thus Hf and Zr are moderately incompatible elements while Nb and Ta are highly incompatible elements. These elements are less electropositive than the alkalis, and alkaline and rare earths. That, as well as their high charge and the involvement of *d* orbitals (which are highly directional) in bonding in the case of Ta and Nb, means that there is a greater degree of covalency in the bonds they form. Thus the simple charged sphere is a less satisfactory model of their behavior.

As a consequence of their high ionic potential, or ionic charge to ionic radius ratio, the HFS elements are particularly insoluble. As a result, these elements tend to be very immobile during weathering and metamorphism. They are therefore particularly valuable in the study of ancient igneous rock suites as they can sometimes provide insights into the environment in which those rocks formed. Ta and Nb are present in anomalously low concentrations in magmas associated with subduction zones (indeed, this is considered a diagnostic feature of subduction-related volcanism). Although this depletion is not well understood, it is probably at least in part a consequence of the low solubility of these elements and the consequent failure of aqueous fluids generated by dehydration of the subducting oceanic crust to transport these elements into the magma genesis zone.

7.2.2.6 The First Series Transition Metals

The chemistry of the transition elements is considerably more complex than that of the elements we have discussed thus far. There are several reasons for this. First, many of the transition elements have two or more valence states in nature. Second, the transition metals have higher electronegativity than the alkali and alkaline earths, so that covalent bonding plays a more important role in their behavior. Bonding with oxygen in oxides and silicates is still predominantly ionic, but bonding with other nonmetals, such as sulfur, can be largely covalent. A final complicating factor is the geometry of the *d*-orbitals, which are highly directional and thus bestow upon the transition metals specific preferences for the geometry of coordinating anions, or ligands. We will discuss this aspect of their behavior in more detail in a subsequent section.

The solubility of the transition metals, though generally lower than that of the alkalis and alkaline earths, is quite variable and depends upon valence state and the availability of anions with which they can form soluble coordination complexes. Their behavior in magmas is also variable. They range from moderately incompatible (e.g., Ti, Cu, Zn) to very compatible (e.g., Cr, Ni, Co), but their exact behavior is generally a stronger function of composition (of both solid and melt phases) than that of the highly incompatible elements. With the exception of Mn, the first transition series metals are also siderophile and/or chalcophile.

7.2.2.7 The Noble Metals

The platinum group elements (Rh, Ru, Pd, Os, Ir, Pt) plus gold are often collectively called the *noble metals*. These metals are so called for two reasons: first they are rare, second they are unreactive and quite stable in metallic form. Their rarity is in part a consequence of their highly siderophilic character. The concentration of these elements in the silicate Earth is only about 1% of their concentrations in

chondrites. Presumably, the bulk of the Earth's inventory of these elements is in the core. As a result of their low concentrations, their behavior is still poorly understood.

These elements are all also chalcophile (i.e., all are enriched in sulfide liquids relative to silicate liquids), although to varying degrees. Ir appears to be the most chalcophile, Pt and Au the least. Considering the associations of their ore deposits, the platinum group elements (PGE) may be divided into two subgroups: the Ir group (Ir, Os, and Ru) and the Pd group (Rh, Pd, Pt). The former are often associated with chromites (chromite is $(Fe,Mg)Cr_2O_4$, part of the spinel solid solution) in ultramafic rocks as native metal alloys or sulfide (e.g., the Stillwater Complex of Montana), while the latter are associated with magmatic sulfides of Fe, Ni, and Cu associated with gabbros (e.g., the Sudbury Complex of Ontario). Besides forming compounds with sulfur, these elements form a variety of chloride and other halide complexes. These complexes may play an important role in the formation of some PGE deposits and certainly do in many gold deposits.

These elements are transition elements and, like the first transition series, can exist in multiple valence states, ranging from 0 to +8, and have bonding behavior influenced by the *d*-orbitals. Thus their chemistry is complex. When in high valence states, some, Os and Ru for example, form oxides that are highly volatile.

The nature of the host phase for these elements in the mantle is unclear. Mitchell and Keays (1981) found that they were concentrated in minerals in the order garnet<olivine<orthopyroxene <clinopyroxene<spinel, but that the total inventory in all minerals was less than that in the bulk rock. They concluded that 60-80% of the PGE's were present in intergranular sulfides. An alternative host is native metal grains, such as osmiridium (an approximately 50-50 Os-Ir alloy), which have been found in peridotites. A study by Brügmann et al. (1987) of komatiites revealed that the concentrations of Au and Pd increased with decreasing MgO while those of Ru, Os, and Ir decreased with decreasing MgO concentrations. This suggested that Au and Pd are moderately incompatible elements while are Ru, Os, and Ir are highly compatible. Subsequent work has confirmed this conclusion and shown that Rh is compatible while Pt is incompatible. Recent studies suggest that the elements dissolve in silicate melts in low valence states, +2 for Ir (and perhaps Os), and +1 for the other elements. The solubility of these elements in silicate melts, relative to native metal alloys, appears to be quite low, but is probably not exceeded in nature.

In a manner analogous to the rare earths, PGE data are sometimes presented as plots of the chondrite-normalized abundance, as in Figure 7.9. In this case, however, elements are not ordered by atomic number, but rather by decreasing melting point. This, as it turns out, places them in order of decreasing compatibility. The dunite in Figure 7.9 has a relatively flat noble metal pattern, as do many mantle peridotites. The remaining samples show varying degrees of enrichment in the Pd group elements relative to the Ir group elements. The chromites and sulfides in Figure 9 are highly enriched in noble metals relative to the silicate magmatic rocks, consistent with their chalcophile nature and demonstrated affinity for oxide phases such as the spinels.

7.2.2.8 Other Elements

Of the elements that do not fit into any of the above groups, several deserve special comment as they are of particular interest in isotope geochemistry. The first of these is boron. The geochemistry of boron remains incompletely understood, but knowledge of it has grown since the mid-1980's when it was shown that the relative proportions of its two isotopes, ^{10}B and ^{11}B, vary in nature. Boron is only mildly electropositive, meaning that the bonds it forms generally have a substantial covalent component. In nature, it is most often bound to three oxygens to form the borate complex. Borate is quite soluble, making borate one of the major ions in seawater. Furthermore, borate is mobile and easily leached or added to rocks during weathering and metamorphism. In igneous systems it is mildly incompatible. Boron appears to be quite readily removed from subducting oceanic crust and sediment by fluids and enriched in subduction-related magmas.

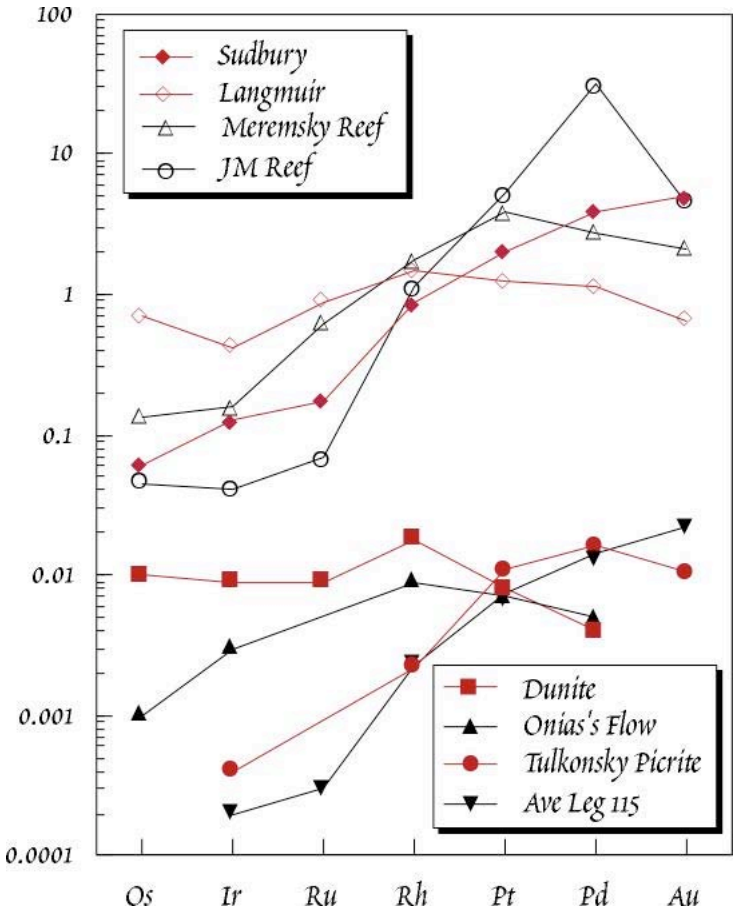

Figure 7.9. Chondrite-normalized abundances of the noble metals in a variety of igneous rocks and associated sulfides. "Sudbury" is the magmatic sulfide from the Little Strobie #1 Mine of the Sudbury intrusion (Naldrett et al., 1979), "Langmuir" is the sulfide of the Langmuir komatiite, Canada (Naldrett et al., 1979), "Merensky Reef" is a composite of the Merensky Reef chromite layer of the Bushveld Complex, South Africa (Heimstra, 1979), "JM Reef" is a chromite layer of the Stillwater Complex, Montana (Barnes et al., 1985), "Dunite" is a dunite from the Urals (Stockman, 1982), "Onias's Flow" is a komatiite flow From the Belingwe Greenstone Belt, Zimbabwe (Zhou, 1994), "Tulkonsky Picrite" is a picrite from the Siberia Traps (Brügmann et al., 1993), and "Ave Leg 115" is the average of basalts drilled from the Indian Ocean on ODP Leg 115 (Fryer and Greenough, 1982).

Rhenium is of interest because it decays radioactively to Os. Though it is not one of the platinum group elements, Re is adjacent to them in the periodic table and shares many of their properties, including being highly refractory under reducing conditions, being both highly siderophile and chalcophile, having a variety of potential valence states, having a large E_H, so that the metal is relatively resistant to oxidation, and forming a volatile (though only moderately so) oxide species. In oxidized aqueous solutions at the Earth's surface it is present as the perrhenate ion, ReO_4^-, and is quite soluble. However, it is readily adsorbed from solution under reducing conditions, leading to its concentration in organic-rich materials such as black shales and coals. In igneous systems, it is incompatible, though details of its behavior are not understood.

Lead is of great interest not only because of its economic importance but also because it is the product of radioactive decay of ^{232}Th, ^{235}U, and ^{238}U and is quite toxic. The latter is of concern because its widespread use, particularly in paint and gasoline, has led to widespread pollution. Pb is chalcophile, though not so much as the PGE's and Re, and perhaps slightly siderophile. It is also quite volatile. Pb is in the +2 state throughout virtually the entire range of natural redox conditions. Pb has an electronegativity of 1.9, indicating a greater degree of covalency in its bonding than for the alkalis, alkaline earths and rare earths. The solubility of Pb is reasonably low under most conditions, but it can form strong complexes with elements such as Cl and it can be readily transported in metamorphic and hydrothermal solutions. Its ionic radius is 119 pm in octahedral coordination, virtually identical to that of Sr. In igneous systems it is moderately incompatible, as might be expected from its ionic radius and charge.

The concentration of phosphorus is sometimes high enough that it is treated as a major element. With a valence of +5 and being moderately electropositive, it is generally present in nature as the oxyanion PO_4^{3-}, in which it is doubly bound to one of the oxygens and singly bound to the others. In

rocks, it forms the common mineral apatite ($Ca_3(PO)_4(OH,F,Cl)$) as well as rarer minerals such as monazite. It behaves as a moderately incompatible element in mafic and ultramafic igneous systems.

The elements of the U and Th decay series have no stable nuclei. They exist on the Earth only because they are continually created through decay of U and Th. They are of interest in geochemistry only because of their radioactivity. As we shall see in the next chapter, they can be useful geochronological tools. As radioactive substances, they represent potential environmental hazards and are of interest for this reason as well. Radon is perhaps the element that causes the greatest concern. As a noble gas, it is quite mobile. Relatively high levels of this gas can accumulate in structures built on uranium-rich soils and rocks. In this group we could also include the two "missing" elements, Tc and Pm. Like the U-decay series elements, they have no long-lived nuclei. They are, however, present in the Earth in exceedingly minute amounts, created by natural fission of U as well as by capture of fission-produced neutrons. Merely detecting them is a considerable challenge.

Ga and Ge can substitute, albeit with difficulty because of their larger radii, for their more abundant neighbors directly above them in the periodic table, Al and Si. Both are thus moderately incompatible elements. Their concentrations in the silicate Earth are somewhat low because of their siderophile nature. Germanium's greatest contribution to geochemistry may, however, be in experimental studies. Germanates created by substituting Ge for Si are used to simulate the properties of silicates at high pressures. This approach works because the oxygen ion is far more compressible than are cations. Thus the ratio of the ionic radius of oxygen to silicon at high pressure is similar to that of oxygen to germanium at low pressure. Such studies of "germanium analogs" considerably advanced the understanding of the Earth's deep interior decades before the technology for reproducing the pressure of the deep Earth in the laboratory existed. Studies of germanium analogs continue in parallel with ultrahigh pressure experiments.

The geochemistry of the remaining elements, particularly in igneous processes, is poorly understood. Because of their low abundances, there have been few analyses published of these elements. Progress is being made on this front, however. For example, Newsom et al. (1986) demonstrated that the behavior of the chalcophile element Mo closely follows that of the rare earth Pr. W appears to be highly incompatible and its behavior mimics that of Ba. In oxidizing solutions, Mo forms a very soluble oxyanion complex, MoO_4^{2-}, so that its concentration in seawater is relatively high. Tin (Sn) and antimony (Sb) behave as moderately incompatible elements, with behaviors in igneous systems that are similar to that of the rare earth Sm (Jochum et al., 1985, 1993). However, these elements appear to form soluble species so, unlike Sm, they can be relatively mobile. It appears, for example, that they are readily stripped from subducting oceanic crust and carried into the magma genesis zones of island arc volcanos.

7.3 Distribution of Trace Elements Between Co-existing Phases

7.3.1 The Partition Coefficient

Geochemists find it convenient to define a *partition or distribution coefficient* as:

$$\boxed{D_i^{\alpha-\beta} = \frac{C_i^\alpha}{C_i^\beta}} \qquad 7.1$$

where C is concentration, i refers to an element (or species) and α and β are two phases. By convention, if one phase is a liquid, the concentration ratio is written solid over liquid, i.e.:

$$D_i^{s/\ell} = \frac{C_i^s}{C_i^\ell} \qquad 7.2$$

where s refers to some solid phase and ℓ refers to the liquid phase. The distribution coefficient is a convenient concept for relating the concentration of some element in two different phases. It is also readily measured, either experimentally or 'observationally'. In the former, two phases are equilibrated at the temperature and pressure of interest and the concentration of i is subsequently measured in both. In

the latter, the concentration of element *i* is simply measured in two natural phases thought to be in equilibrium. In both cases, the catch is, of course, equilibrium. As we mentioned Chapter 5, kinetic effects can lead to apparent partition coefficients that differ from equilibrium ones.

Having introduced the partition coefficient, we can now quantitatively define two terms we have already introduced: compatible and incompatible. *Incompatible* elements are those with $D^{s/l} << 1$. *compatible* elements are those with $D^{s/l} \geq 1$. The partition coefficient for a given element will vary considerably between phases and can be less than one for one phase and greater than one for another. Hence the terms compatible and incompatible have meaning only when the phases are specified. These terms refer to partitioning *between silicate melts and phases common to mafic or ultramafic (i.e., basaltic or peridotitic) rocks*. It is this phase assemblage that dictates whether lithophile trace elements are concentrated in the Earth's crust, hence the significance of these terms.

7.3.1.1 Thermodynamic Basis

Though trace elements are often treated differently than major elements, we should remember that the principle governing their distribution is the same as that governing the distribution of major elements. We are already familiar with this principle: *at equilibrium, elements will distribute themselves between co-existing phases so that the chemical potential of that element is the same in every phase in the system*. The chemical potential of element *i* in phases α and β is given by equation 3.54:

$$\mu_i^\alpha = \mu_i^{o\alpha} + RT \ln X_i^\alpha \lambda_i^\alpha \qquad 7.3$$

and

$$\mu_i^\beta = \mu_i^{o\beta} + RT \ln X_i^\beta \lambda_i^\beta \qquad 7.4$$

At equilibrium, $\mu^\alpha = \mu^\beta$, so:

$$\mu_i^{o\beta} - \mu_i^{o\alpha} = RT \ln(X_i^\alpha \lambda_i^\alpha / X_i^\beta \lambda_i^\beta) \qquad 7.5$$

While equation 7.5 is expressed in mole fraction, the equation is identical when expressed in ppm because any difference in the molecular weights of the phases can be incorporated in the activity coefficients. A little algebra shows that the distribution coefficient is related to chemical potential as:

$$D_i^{\alpha-\beta} = \frac{C_i^\alpha}{C_i^\beta} = \frac{\lambda_i^\beta}{\lambda_i^\alpha} \exp\left(\frac{\mu_i^{o\beta} - \mu_i^{o\alpha}}{RT}\right) \qquad 7.6$$

The standard chemical potentials on the right hand side are the chemical potentials of *i* in pure *i* versions of phases α and β. Suppose, for example, we were interested in the partitioning of nickel between olivine and a silicate melt. In that case, $\mu_i^{\alpha o}$ would be the chemical potential of Ni in pure Ni olivine (i.e., Ni_2SiO_4) and $\mu_i^{\beta o}$ would be the chemical potential of Ni in Ni-silicate melt. This difference in chemical potential is the standard state Gibbs Free Energy change resulting from transfer of *i* between these two phases, so:

$$D_i^{\alpha-\beta} = \frac{\lambda_i^\beta}{\lambda_i^\alpha} \exp\left(\frac{-\Delta G_i^{o\alpha-\beta}}{RT}\right) \qquad 7.7$$

It is reasonable to expect that species present in trace quantities will obey Henry's Law. In that case, we can rewrite equ. 7.7 as:

$$D_i^{\alpha-\beta} = \frac{h_i^\beta}{h_i^\alpha} \exp\left(\frac{\mu_i^{o\beta} - \mu_i^{o\alpha}}{RT}\right) \qquad 7.8$$

where *h* is the Henry's Law constant (Chapter 3). Drake and Weill (1975) found that Sr and Ba obeyed Henry's Law in the system plagioclase-liquid up to concentrations of 5% or so of the element in the liquid, i.e., well above most natural concentrations. Many subsequent studies have confirmed that trace elements generally obey Henry's Law over their entire range of natural concentration.

Comparing our derivation of the partition coefficient with that of the equilibrium constant shows that the two are closely related. Indeed, the partition coefficient is a form of apparent equilibrium constant and effectively identical with the K_D as defined in equation 3.88 and 3.89. The terms partition coefficient, distribution coefficient, and K_D are synonymous and often used interchangeably.

In a system with three phases, α, β, and γ, if α and β are in equilibrium and α and γ are in equilib-

rium, then β and γ must also be in equilibrium. It follows that:

$$D^{\beta/\gamma} = D^{\alpha/\gamma}/D^{\alpha/\beta} \qquad 7.9$$

This relationship has practical use. For example, if we can determine the partition coefficient for an element between pyroxene and melt and between garnet and pyroxene, we can then calculate the garnet-melt partition coefficient for this element from equation 7.9.

7.4 Factors Governing the Value of Partition Coefficients

7.4.1 Temperature and Pressure Dependence of the Partition Coefficient

In ideal solutions, the temperature dependence of the partition coefficient is the same as that of the equilibrium constant, i.e.,:

$$D_i = \exp\left(\frac{-\Delta G_i^o}{RT}\right) \qquad 7.10$$

ΔG in equation 7.10 can be expanded into entropy and enthalpy terms, as in equation 4.38:

$$\left(\frac{\partial \ln D_i}{\partial T}\right)_P = \frac{\Delta H^o + (P - P^\circ)\Delta V}{RT^2} \qquad 7.11$$

In ideal solution, and assuming ΔV is independent of temperature and pressure, the pressure dependence is also the same as that of the equilibrium constant, i.e.:

$$\left(\frac{\partial \ln D_i}{\partial P}\right)_T = \frac{-\Delta V}{RT} \qquad 7.12$$

From equation 7.12, we would predict a strong pressure dependence when the ionic radius of an element differs greatly from that of the available crystal lattice site. Thus for example, we would predict the partition coefficient for K between pyroxene and melt would be strongly pressure dependent since the ionic radius of K is 150 pm and is much larger that the size of the M2 site in clinopyroxene, which is normally occupied by Ca, with a radius of about 100 pm. Conversely, where the size difference is small, e.g., Mn (83 pm) substituting for Fe (78 pm), we would expect the pressure dependence to be smaller.

For non-ideal solutions (which will be the usual case), the temperature and pressure dependence will be more complex than given in equations 7.11 and 7.12 because the ratio of Henry's Law constants in equation 7.0 will also be pressure and temperature dependent. The form of that dependence is usually difficult to deduce.

7.4.2 Ionic Size and Charge

Much of the interest in trace elements in igneous processes centers on the elements located in the lower left portion of the periodic table (alkalis K, Rb, Cs; alkaline earths Sr and Ba, the rare earths, Y, Zr, Nb, Hf and Ta). The reason for this focus of attention is in part due to the relative ease with which these elements can be analyzed. These elements are all lithophile and therefore present at *relatively* high abundance in the Earth's crust and mantle. There is another reason, however: their chemical behavior is comparatively simple. All have electronegativities less than 1.5 (Nb is the sole exception, with electronegativity of 1.6), and most have only a single valence state over the range of oxygen fugacity in the Earth. The difference in electronegativity between these elements and oxygen, effectively the only electronegative element in igneous rocks, is 2 or greater, so the bonds these elements will form are predominantly ionic. To a reasonable approximation then, the atoms of these elements behave as hard spheres containing a fixed point charge at their centers. Thus the two factors that most govern their chemical behavior are ionic radius and ionic charge. As we shall see, these elements have partition coefficients less than 1 for most common minerals. The term "incompatible elements" often refers specifically to these elements.

The other trace elements that receive the most attention from igneous geochemists are the first tran-

sition series elements. Though their electronic structures and bonding behavior are considerably more complex (as we shall see in a subsequent section), charge and size are also important in the behavior of these elements. Many of these elements, particularly Ni, Co, and Cr have partition coefficients greater than 1 in many Mg-Fe silicate minerals. Hence the term "compatible elements" often refers to these elements.

The effect of ionic charge and size is illustrated in Figure 7.10, which shows a plot of ionic radius vs. charge contoured for the clinopyroxene/melt partition coefficient. Those elements whose charge and ionic radius most closely matches that of the major elements present in the cation sites, Mg, Fe, and Ca, have partition coefficients close to 1, those whose charge or radius differs significantly have lower partition coefficients. Thus Ba, even though its charge is the same (2+), has an ionic radius of 135 pm and fits only with difficulty into the lattice site normally occupied by Ca (100 pm), Mg (72 pm) or Fe (78 pm). This strains the lattice, and hence additional energy is required for the substitution to occur. On the other hand, Zr, which has an ionic radius identical to that of Mg, is not accepted in this site because its charge, 4+, is too great. Substitution of Zr^{4+} for Mg^{2+} would require either leaving one cation site vacant or one or more coupled substitutions (e.g., Al^{3+} for Si^{4+}) to maintain charge balance. Both of these are energetically unfavorable. In addition, ions having a radius much smaller than that of the element normally occupying the site also have low partition coefficients because their substitution also induces strain in the lattice.

7.4.2.1 Goldschmidt's Rules of Substitution

The importance of ionic radius and charge have been long known. Indeed, Goldschmidt developed the following rules regarding substitutions of elements into crystal structures:

1. If 2 ions have the same radius and the same charge, they will enter a given lattice site with equal facility.

2. If two ions have similar radii and the same charge, the smaller ion will enter a given site more readily.

3. If two ions have similar radii, the ion with the higher charge will enter a given site more readily.

Ringwood‡ noted the need also to consider the electronegativity in substitution. His rule is:

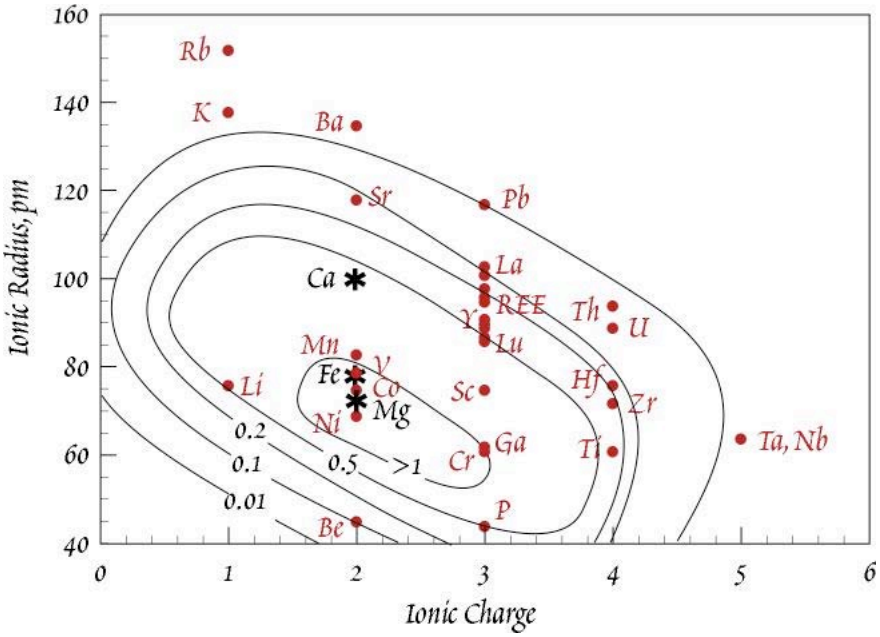

Figure 7.10. Ionic radius (picometers) vs. ionic charge contoured for clinopyroxene/liquid partition coefficients. Cations normally present in clinopyroxene are Ca^{2+}, Mg^{2+}, and Fe^{2+}, shown by ✲ symbols. Elements whose charge and ionic radius most closely match that of the major elements have the highest partition coefficients.

‡ Alfred E. Ringwood (1930-1993). After receiving his BSc and PhD degrees at the University of Melborne, Ringwood did a post-doctoral fellowship at Harvard University. His subsequent career was spent at the Australian National University, from where he exerted a strong influence on the development of earth science in Australia. Ringwood pioneered the post-war development of many aspects of geochemistry, including phase relationships of the mantle at very high pressures, the origin of basaltic magmas, the origin of the Earth and the Moon, as well as safe methods of long-term nuclear waste storage. Among his other contributions, he demonstrated that seismic discontinuities in the mantle were due to phase transitions, the existence of which he predicted using germanate analogs.

4. Whenever a substitution is possible between two elements with significantly different electronegativities (Δ > 0.1), the one with the lower electronegativity will be preferentially incorporated.
However, the bottom-line is: the stronger the bond, the more likely the substitution.

7.4.2.2 Quantitative Treatment of Ionic Size and Charge

Goldschmidt's rules are simple qualitative statements based on empirical observation. Can we turn these into quantitative tools? In the last 10 to 15 years, the answer has become yes. We can take advantage of the thermodynamic framework developed over the past century and incorporate into it the energetic effects of substituting a misfit ion into a specific lattice site to develop quantitative predictions of distribution coefficients. As we have seen, for example with the surface complexation model, thermodynamics generally, and the Gibbs Free Energy in particular, provide a wonderfully flexible framework into which we can incorporate new knowledge and understanding, often developed on the microscopic scale, to make quantitative predictions about the macroscopic behavior of chemical systems.

In brief, the idea is that when a trace element of different ionic radius is substituted for the ion that normally occupies a lattice site the lattice must adjust. This adjustment is accomplished through the expenditure of strain energy, which can be calculated by measurable parameters of the mineral. Since this strain energy contributes to the Gibbs Free Energy of reaction, and since the partition coefficient is related to ΔG, the effect of the lattice strain energy on the partition coefficient can be calculated.

Consider the formation of diopside containing metal ion M^{2+} in the site normally occupied by Ca^{2+}. We could write this reaction as:

$$MO^{\ell} + MgO^{\ell} + 2SiO_2^{\ell} \rightleftarrows MMgSi_2O_6 \qquad 7.13$$

where ℓ denotes the liquid phase. However, the mineral $MMgSi_2O_6$ may not exist in nature and may not be synthesizable in the laboratory, so it might not be possible to determine its thermodynamic properties. Instead, we can imagine two reactions. The first would be the crystallization of diopside from a melt:

$$CaO^{\ell} + MgO^{\ell} + 2SiO_2^{\ell} \rightleftarrows CaMgSi_2O_6 \qquad 7.13a$$

The second would be an exchange reaction such as the replacement of Ca^{2+} in the M2 site of diopside by metal ion M^{2+}:

$$M^{\ell} + CaMgSi_2O_6 \rightleftarrows Ca^{\ell} + MMgSi_2O_6 \qquad 7.13b$$

We can see that reaction 7.13 is simply the difference between reaction 7.13b and 7.13a. Hence, the Gibbs Free Energy change of this reaction can be expressed as:

$$\Delta G_r = \Delta G_{exchange}^{M-Ca} - \Delta G_{melting}^{Di} \qquad 7.14$$

The first term is the free energy change in involved in transferring a M^{2+} ion from the melt into the crystal lattice and simultaneously transferring a Ca^{2+} ion from the lattice site to the liquid. The second term is the free energy change associated with melting of diopside and in multi-component systems governs the distribution of Ca between diopside and the liquid. The distribution coefficient for element M then depends on these two components of free energy:

$$D_M^{Di/\ell} = \exp\left(\frac{\Delta G_{melting}^{Di} - \Delta G_{exchange}^{M-Ca}}{RT}\right) \qquad 7.15$$

According to the lattice strain energy theory of Beattie (1994) and Blundy and Wood (1994, 2003), $\Delta G_{exchnage}$ is dominated by the energy associated with the lattice strain that results from the M^{2+} ion being a different size than the Ca^{2+} ion normally occupying the lattice site. Because the melt (at least at low pressure) has a far less rigid structure and is more compressible than the solid, any strain in the melt is essentially negligible compared the strain in the solid. Hence:

$$\Delta G_{exchange}^{M-Ca} \cong \Delta G_{strain} \qquad 7.16$$

According to Brice (1975), the strain energy, ΔG_{strain}, maybe calculated from:

CHAPTER 7: TRACE ELEMENTS

$$\Delta G_{strain} = 4\pi E N_A \left[\frac{r_0}{2}(r_M - r_o)^2 + \frac{1}{3}(r_M - r_0)^3 \right] \quad 7.17$$

where r_0 is the optimal radius of the lattice site, r_M is the ionic radius of M, N_A is Avogadro's Number, and E is *Young's Modulus*. The Young's Modulus of a substance is the ratio of stress applied to the resulting strain and may be calculated as:

$$E = \frac{L_0 F}{\Delta L A} \quad 7.18$$

where L_0 is the original length of the object undergoing strain, ΔL is the length change under stress, F is the force applied over area A. E has units of pressure. Young's Modulus is related to the Bulk Modulus, K, (which, as we found in Chapter 2, is the inverse of compressibility) through Possion's ratio. Poisson's ratio is the ratio of the transverse contraction per unit dimension to elongation per unit length of a bar of uniform cross section when subjected to tensile stress and in most silicates is ~0.25. Consequently, $E \cong 1.5\ K$.

The $\Delta G_{melting}$ term in equation 7.15 governs the distribution of Ca between liquid and crystal, i.e.:

$$D_{Ca}^{Di/\ell} = \exp\left(\frac{\Delta G_{melting}^{Di}}{RT} \right) \quad 7.19$$

Substituting this and equation 7.17 into equation 7.15 we obtain:

$$D_M^{Di/\ell} = D_{Ca}^{Di/\ell} \exp\left(\frac{-\Delta G_{strain}^{M-Ca}}{RT} \right) = D_{Ca}^{Di/\ell} \exp\left(\frac{-4\pi E N_A \left[\frac{r_0}{2}(r_M - r_0)^2 + \frac{1}{3}(r_M - r_0)^3 \right]}{RT} \right)$$

More generally, this equation may be written as:

$$D_i^{s/\ell} = D^o \exp\left(\frac{-4\pi E N_A \left[\frac{r_0}{2}(r_M - r_0)^2 + \frac{1}{3}(r_M - r_0)^3 \right]}{RT} \right) \quad 7.20$$

where D° is the partition coefficient of an ion of radius r_o which has the same charge as i and enters the lattice site without strain (Blundy and Wood, 1994).

Now consider the case where the substituting trace element has a different charge than the ion normally occupying the site, for example:

$$La^{3+\ell} + CaMgSi_2O_6 \rightleftarrows Ca^{2+\ell} + LaMgSi_2O_6 \quad 7.21$$

The charge imbalance must be compensated in one of two ways: either through a coupled substitution, such as:

$$La^{3+\ell} + Na^{+\ell} + 2CaMgSi_2O_6 \rightleftarrows 2Ca^{2+\ell} + 2La_{0.5}Na_{0.5}MgSi_2O_6 \quad 7.22a$$

or

$$La^{3+\ell} + Al^{3+\ell} + CaMgSi_2O_6 \rightleftarrows Ca^{2+\ell} + Si^{4+}\ LaMgAlSiO_6 \quad 7.22b$$

or through a creation of a vacancy, e.g.:

$$2La^{3+\ell} + 3CaMgSi_2O_6 \rightleftarrows 3Ca^{2+\ell} + 2LaMgSi_2O_6 + MgSi_2O_6 \quad 7.23$$

If the charge balance mechanism is known, then free energy of exchange may be calculated as the sum of free energies associated with melting, strain, and the charge balance mechanism. From this, the distribution coefficient can be calculated. For example, if charge is balanced by the coupled substitution in 7.22a, then the distribution can be calculated as

CHAPTER 7: TRACE ELEMENTS

$$D_{La}^{Di/\ell} = e^{\frac{\Delta G_{melting}^{Di} - \Delta G_{strain}^{La-Ca} - \Delta G_{exchange}^{Na-Ca}}{RT}} \qquad 7.24$$

The free energy of the Na-Ca exchange reaction will, of course, also have a strain component. Equation 7.24 may be written as:

$$D_{La}^{Di/\ell} = e^{\frac{\Delta G_{melting}^{Di} - \Delta G_{exchange}^{Na-Ca}}{RT}} \; e^{\frac{-\Delta G_{strain}^{La-Ca}}{RT}} \qquad 7.24a$$

The first term on right may be replaced by D^o, so that equation 7.20 may also be applied to heterovalent exchanges.

Equations 7.20 suggests that the dependence of the partition coefficient on ionic radius should be highly non-linear, and experiments have proved this to be the case. Figure 7.11 compares clinopyroxene-liquid and plagioclase-liquid partition coefficients for the rare earths determined experimentally at 1225° C and 1.5 GPa with partition coefficients predicted using equation 7.20. Plots of partition coefficient vs. ionic radius are known as Onuma diagrams after Onuma et al. (1968).

The lattice strain model also helps us predict the effects of pressure on partitioning, as pressure will affect the dimension of the lattice site. For example, clinopyroxene incorporates an increasing amount of Na and Al as pressure increases, which results in a decrease in the radius of the M2 site. This shifts the partition coefficient parabola on the Onuma diagram. As illustrated in Figure 7.12, partition coefficients of large ions will decrease with increasing pressure, while those of small ions will increase.

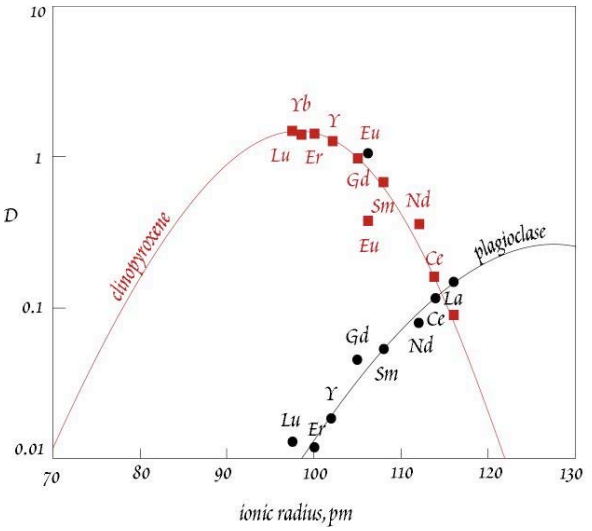

Figure 7.11. Experimentally determined clinopyroxene–liquid and plagioclase–liquid partition coefficients for rare earths as a function of ionic radius compared to predicted partition coefficients using equation 7.20. For clinopyroxene, the model assumes D^o = 1.47, E = 262 GPa, and r_0 = 98.1 pm. For plagioclase, these parameters are D^o = 0.26, E = 113 GPa, and r_0 = 128 pm. Data and model from Blundy et al. (1998).

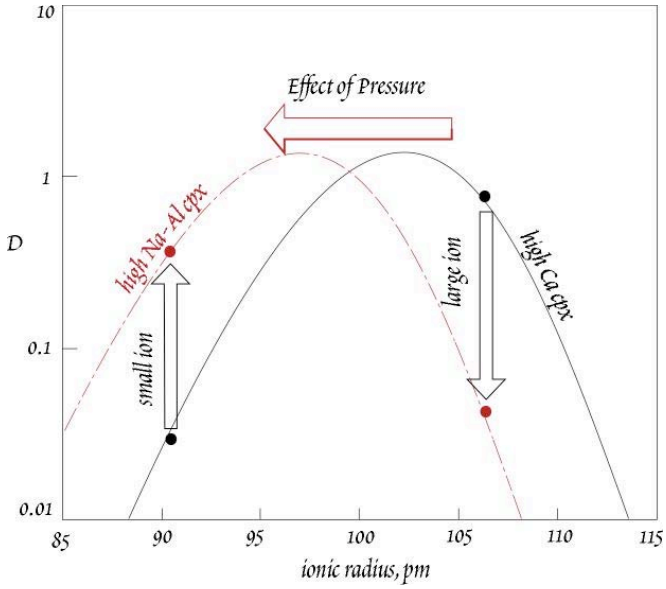

Figure 7.12. Because increasing pressure increases the amount of jadeite ($NaAlSi_2O_6$) in clinopyroxene, the radius of the M2 site decreases and partition coefficients for large ions decrease while those for small ions increase. After Wood et al. (1999).

7.4.3 Compositional Dependency

Equation 7.8 predicts that partition coefficients will depend on the composition of the phases involved since the Henry's Law constant will depend on the concentration of the major species. Experience has substantiated this prediction and shown that partition coefficients are composition-dependent. For example, elements that are incompatible in mafic (SiO_2-poor) systems often have partition coefficients equal to or greater than 1 in silicic (SiO_2-rich) systems. This behavior is illustrated by the solubility of zircon, $ZrSiO_4$. In basaltic liquids, zircon will not precipitate until the Zr concentration reaches 10000 ppm (1% Zr) or more. In granitic liquids, however, zircon crystallizes

at Zr levels around 100 ppm. In another example, Watson (1976) conducted two-liquid partitioning experiments in which the concentration of various elements was measured in coexisting immiscible mafic and silicic silicate liquids. P, the rare earth elements (REE), Ba, Sr, Mg, Zr, Mn, Ti, Cr, Ca, and Ta were found to be enriched in the mafic melt by factors of 1.5 to 10 (in the above order). Cs was enriched in the silicic melt by a factor of about 3.

Some of this compositional dependence results from the need for coupled substitutions to maintain charge balance. For example, Reactions 7.22a and 7.22b suggest clinopyroxene-liquid rare earth partition coefficients will depend on Na and Al concentrations. However, much of the compositional dependence can be related to structural changes in the melt phase. As we saw in Chapter 4, as the SiO_2 concentration of the melt increases, the polymerization of the melt increases as the Si tetrahedra become increasingly linked. On the other hand, Si-poor melts will be largely depolymerized as more non-bridging oxygens are needed to charge-balance network-modifying cations. The ratio of *non-bridging oxygens* to tetrahedral cations (Si^{4+} and Al^{3+}), written NBO/T, provides a measure of the degree of melt depolymerization. Kohn and Schofield (1994) carried out a series of experiments demonstrating the effect of melt polymerization on olivine/melt partitioning of Zn and Mn. Figure 7.12 shows that the Zn partition coefficient decreases from about 4.5 in highly polymerized melts (low NBO/T) to about 0.8 in depolymerized melts (high NBO/T). Zn is probably present in octahedral sites (i.e., surrounded by 6 oxygens) in silicates melts, though this remains uncertain. Changes in the partition coefficient most likely reflect the availability of suitably coordinated sites in the melt.

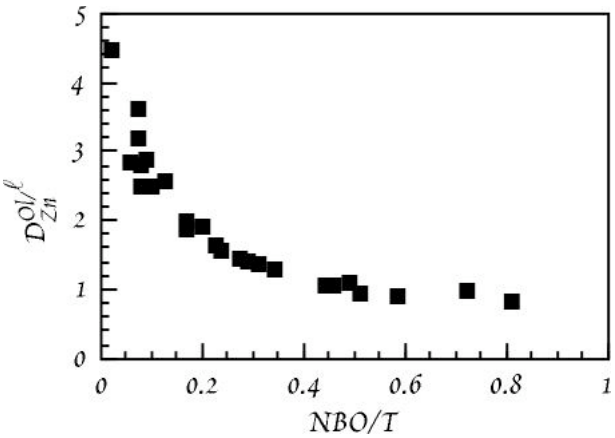

Figure 7.13. Variation of the zinc olivine/liquid partition coefficient as a function of the number of non-bridging oxygens per tetrahedral cation (NBO/T) in experiments by Kohn and Schofield (1994).

Another effect is a decrease in octahedral or other sites for transition and highly charged cations as melts become more polymerized. High-field strength elements, such as Zr^{4+} and Ta^{5+} need to be coordinated by a large number of anions. For example Zr is coordinated by 8 oxygens in zircon. Cations with large radii, such as Cs, do not easily fit in tetrahedral sites. Lacking suitable sites in silicic melts, they partition preferentially into solid phases.

7.4.3.1 Compositional Dependency of Clinopyroxene Partitioning

Because of its rather large M2 octahedral site and its capacity to accept Al in the tetrahedral site for charge balance, the clinopyroxene–melt partition coefficients for many incompatible elements are larger than for other phases occurring in mafic and ultramafic rocks. Consequently, clinopyroxene exerts a strong control on trace element fractionation during melting and crystallization in these rocks and related magmas. Thus considerable attention has been given to clinopyroxene-melt partition coefficients and there have been a number of attempts to quantify the temperature, pressure, and compositional dependencies of these partition coefficients. As an example, we will briefly consider the work of R. L. Nielsen and his colleagues on this problem.

Gallahan and Nielsen (1992) carried out experiments on the partitioning of Sc, Y, and several of the rare earth elements over a range of compositions with temperature held approximately constant. Based on this and previous work, they found that the alumina concentrations in the melt most strongly affected the partition coefficient (Figure 7.15). For Y and the rare earths, they assumed that the reaction:

$$Ree O^{\ell}_{1.5} + (Fe, Mg)O + Al O^{\ell}_{1.5} + SiO_2 \rightleftarrows Ree(Fe, Mg)AlSiO_6 \qquad 7.25$$

best described the formation of rare earth (here abbreviated Ree) pyroxene. The equilibrium constant

for this reaction is:

$$K = \left[\frac{a^{cpx}_{Ree}}{a^{\ell}_{Ree} a^{\ell}_{AlO_{1.5}} a^{\ell}_{SiO_2}}\right]\left[\frac{a^{cpx}_{Mg,Fe}}{a^{\ell}_{Mg,Fe}}\right] \qquad 7.26$$

where ℓ designates the liquid. It turns out the at any given temperature, the ratio of the activity of Fe^{2+} and Mg in the melt to their activity in the clinopyroxene is approximately constant, so that 7.26 simplifies to:

EXAMPLE 7.1. PARAMETERIZING PARTITION COEFFICIENTS

One approach to accounting for compositional variability when the underlying thermodynamics is not fully understood is to parameterize the partition coefficient, i.e., to express it as a function of other measurable or predictable variables. The Zn partition coefficients determined by Kohn and Schofield are clearly strong functions of the NBO/T parameter, suggesting we might usefully try to express the Zn partition coefficient as a function of NBO/T. From equation 7.7, we can expect that the partition coefficient will be a function of temperature as well. Furthermore, we can use equation 6.8 to predict the form of the equation. Taking the log of both sides of equation 7.7 we have:

$$\ln D = \ln\left(\frac{\lambda^{\beta}_i}{\lambda^{\alpha}_i}\right) - \frac{\Delta G^{\circ}}{RT}$$

The first term on the right expresses compositional dependence and the second term expresses the temperature dependence. Thus we might expect an equation of the form:

$$\ln D = a \ln\left(\frac{NBO}{T}\right) + \frac{b}{T}$$

We can then use a technique called *polynomial regression*, a multivariable extension of linear regression, to determine the constants *a* and *b*. Using this approach, we obtain the following equation:

$$\ln D = -0.405 \ln\left(\frac{NBO}{T} + 6.077\right) + \frac{3594}{T} \qquad 7.27$$

Figure 7.14 compares the observed Zn partition coefficients with those predicted by equation 7.27.

This approach does have limitations and dangers, however. In the experiments of Kohn and Schofield (1994), for example, temperature and NBO/T were highly correlated, thus some of the temperature dependence may actually be hidden in the first term of equation. Second, it is highly unlikely that all compositional effects on the partition coefficient can be adequately expressed by a single parameter. Furthermore, our equation does not take variations in the composition of olivine into account. Kohn and Schofield's experiments were performed using iron-free compositions, so the olivines were nearly pure forsterite. In real systems the composition of the solid may also affect partitioning behavior (though fosterite-fayalite system is nearly ideal, so the importance of this factor for olivine is less than for other minerals). Nevertheless, equation 7.27 is highly successful and accounts for over 96% of the variation in the partition coefficient observed by Kohn and Schofield (1994).

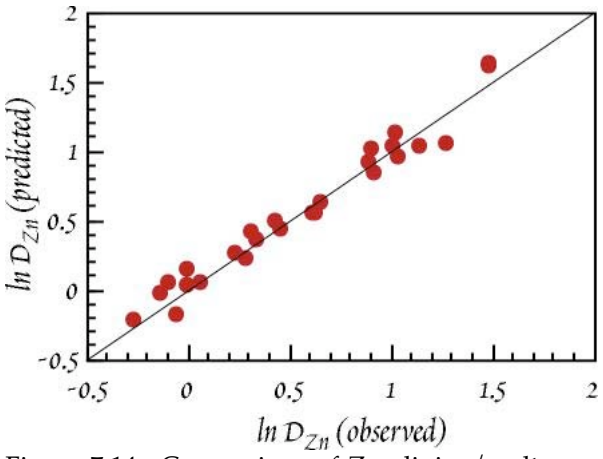

Figure 7.14. Comparison of Zn olivine/melt partition coefficients of Kohn and Schofield with values predicted by equation 7.27.

$$K \cong \left[\frac{a^{cpx}_{Ree}}{a^{\ell}_{Ree} a^{\ell}_{AlO_{1.5}} a^{\ell}_{SiO_2}} \right] \qquad 7.28$$

In addition to the compositional dependence, there is, of course, an expectation that the partition coefficient will depend on temperature as well. Gallahan and Nielsen addressed this problem by regressing the log of K as defined above against 1/T and determining the slope and intercept of the regression line, i.e., by expressing K as:

$$\ln K = a/T - b \qquad 7.29$$

(Compare equ. 7.29 to equ. 3.95. What should the *a* term represent? What should the *b* term represent?)

Gallahan and Nielsen's values for regression coefficients *a* and *b* are listed in Table 7.4. If we define $D^* = a^{cpx}_{REE} / a^{l}_{REE}$, the D can be written as:

$$D^*_{REE} = a^{\ell}_{AlO_{1.5}} a^{\ell}_{SiO_2} K \qquad 7.30$$

Taking the log of both sides of 7.30 and substituting equation 7.29 for ln K, we have:

$$\ln D^*_{REE} = \ln(a^{\ell}_{AlO_{1.5}} a^{\ell}_{SiO_2}) + \frac{a}{T} - b \qquad 7.31$$

For Sc, Gallahan and Nielsen (1992) found it necessary also to include CaO in the reaction:

$$ScO^{\ell}_{1.5} + Cao^{\ell} + AlO^{\ell}_{1.5} + SiO^{\ell}_2 \rightleftarrows ScCaAlSiO_6 \qquad 7.32$$

The corresponding equilibrium constant expression is:

$$K = \frac{a^{cpx}_{Sc}}{a^{\ell}_{Sc} a^{\ell}_{AlO_{1.5}} a^{\ell}_{SiO_2} a^{\ell}_{CaO}} \qquad 7.33$$

From this equation, an expression analogous to 7.31 may be derived. Activities for melt components are calculated using the 2-lattice model of Nielsen and Dungan (1983):

$$a^{\ell}_{AlO_{1.5}} = \frac{X_{AlO_{1.5}} - (X_{NaO_{0.5}} + X_{KO_{0.5}})}{\Sigma NM}$$

$$a^{\ell}_{SiO_2} = \frac{X_{SiO_2}}{\Sigma NF} \qquad a^{\ell}_{CaO} = \frac{X_{CaO}}{\Sigma NM} \qquad 7.34$$

where ΣNM is the sum of the 'network modifiers' and ΣNF is the sum of the 'network formers':

$$\Sigma NM = X_{AlO_{1.5}} + X_{CaO} + X_{MgO} + X_{FeO} + X_{P_2O_5} + X_{TiO_2} + X_{MnO} + X_{CrO_{1.5}} - X_{NaO_{0.5}} - X_{KO_{0.5}} \qquad 7.35$$

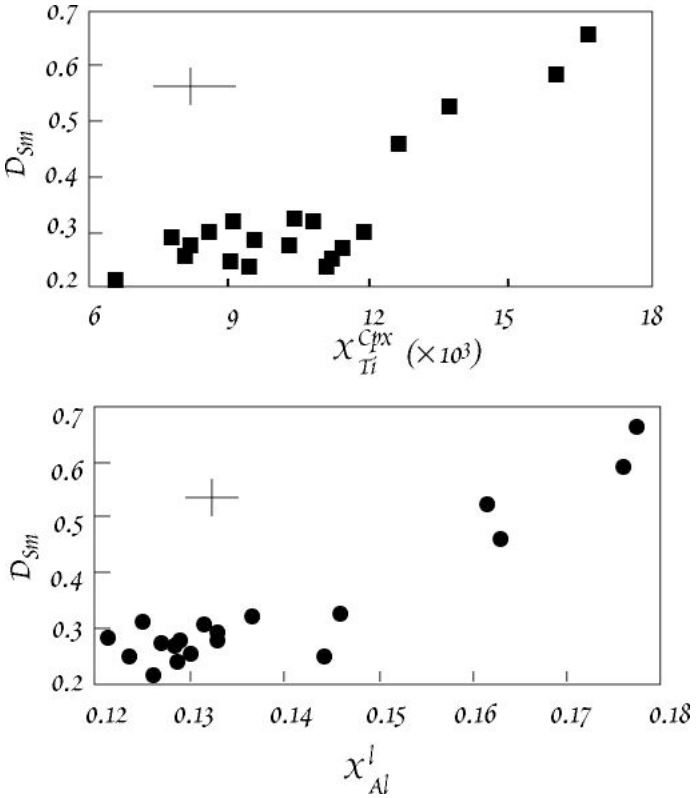

Figure 7.15. Experimentally determined clinopyroxene-liquid partition coefficient for Sm as a function the mole fraction of Al in the melt and the mole fraction of Ti in cpx. The correlation with Ti suggests Ti and REE partitioning is controlled by similar factors. Cross shows analytical error. From Gallahan and Nielsen (1992).

TABLE 7.4. REGRESSION CONSTANTS FOR CLINOPYROXENE-MELT PARTITIONING

	a	b
La	119	1.95
Sm	11371	8.60
Gd	8959	6.62
Ho	8651	7.62
Lu	19709	14.29
Y	12084	8.81
Sc	11956	16.83

From Gallahan and Nielsen (1992).

$$\Sigma NF = X_{SiO_2} + X_{NaO_{0.5}} + X_{KO_{0.5}} \qquad 7.36$$

The activities of Sc, Y, and the rare earths are assumed equal to:

$$a_i^{\ell} = \frac{X_i^{\ell}}{\Sigma NM} \qquad a_i^{cpx} = X_i^{cpx} \qquad 7.37$$

where *i* is Sc, Y, La, etc.

How does the D* we defined above relate to D as defined in equation 7.2? With activities as defined in equation 7.34, D is related to D* as:

$$D_i = D_i^* \frac{\sum moles\ \ oxides\ \ cpx \times Mol.\ Wt.\ i}{\sum NM \sum moles\ \ oxides\ \ liq. \times Mol.\ Wt.\ i} \qquad 7.38$$

The molecular weight terms cancel, of course, and the molar sums for cpx and basaltic liquid will generally be equal to within about 5%, so that 7.38 simplifies to:

$$D_i \approx \frac{D_i^*}{\Sigma NM} \qquad 7.39$$

Hack et al. (1994) extended the work of Gallahan and Nielsen (1994) to include the effects of pressure. They found the equilibrium constant for reaction 7.25 could be expressed as follows:

$$\ln K = c_1 + c_2 \times \frac{10000}{T} + \frac{c_3}{P} + c_4 X_{Ca}^{cpx} c_5 D_{Ti}^{cpx/\ell} + c_6(Al + Si - Na - K)$$

where T is temperature (in kelvins), P is pressure (in kbar), X_{Ca} is the mole fraction of clinopyroxene octahedral sites occupied by Ca, D_{Ti} is the clinopyroxene–melt partition coefficient for Ti, (Al + Si – Na – K) refer to the mole fraction of the corresponding oxides in the melt, and c_1 ...c_6 are regression coefficients. This equation is considerably more complex than equation 7.30, but is only marginally more accurate. It does have the advantage of including the pressure term.

Beattie (1993) used a modification of the two-lattice model to predict the partitioning of Mg, Fe, Mn, Co, and Ni between olivine, orthopyroxene, and melt as a function of temperature and composition. Beattie relaxes the assumption that the network-forming lattice is ideal and introduces an empirical function to calculate the activity of SiO_2. He then calculated values of ΔH_m, ΔV_m, and ΔS_m from experiments on mineral melt pairs. The resulting thermodynamic data were used to calculate the equilibrium constant for the exchange reaction, e.g.,

$$2MO^{\ell} + Mg_2SiO_4^{ol} \rightleftarrows 2MgO^{\ell} + M_2SiO_4^{ol}$$

where M is Fe, Mn, Co, etc. The equilibrium constant is:

$$K = \left(\frac{D_M^{\alpha/\ell} \lambda_{MO}^{\alpha} \lambda_{MgO}^{\ell}}{D_{Mg}^{\alpha/\ell} \lambda_{MgO}^{\alpha} \lambda_{MO}^{\ell}} \right)^2 \exp\left(\frac{\Delta S}{R} - \frac{\Delta H + (P - P^{\circ})\Delta V}{RT} \right) \qquad 7.40$$

where γ is the activity coefficient, ΔS, ΔH, and ΔV refer to the difference in entropy, enthalpy, and volume changes of fusion between the Mg version and the M version of phase α (e.g., $\Delta S = \Delta S_m^{M-\alpha} - \Delta S_m^{MgO-\alpha}$).

7.4.4 Mineral-Liquid Partition Coefficients for Mafic and Ultramafic Systems

As we have seen, partition coefficients depend on temperature, pressure, and the composition of the phases involved. There are nevertheless circumstances when a general set of partition coefficients is useful. For example, temperature or melt composition may not be known, or great accuracy may not be needed. Table 7.5 is a set of mineral–melt partition coefficients for mafic and ultramafic magmas. They have been assembled from a variety of literature sources and adjusted where necessary to make them self-consistent. The assembly of any set of partition coefficients will always be somewhat subjective. The following principles have guided selection of this partition coefficient set.

EXAMPLE 7.2. CALCULATING PARTITION COEFFICIENTS

Using the composition of the basalts given below, calculate the clinopyroxene-matrix partition coefficients for La and Sm using the Gallahan and Nielsen equations and the coefficients given in Table 7.4. Assume a temperature of 1080° C.

Oxide	Mauna Loa tholeiite wt %	Mount Hope alkali basalt wt %
SiO_2	49.56	50.95
TiO_2	4.28	1.38
Al_2O_3	14.09	17.87
FeO	12.47	8.64
MnO	0.22	0.21
MgO	4.62	6.18
CaO	9.63	11.29
Na_2O	3.03	2.32
K_2O	1.18	0.95
P_2O_5	1.02	0.51

Answer: Once again this is a problem that is best done in a spreadsheet. Our first task will be to convert the wt. percent to mole fractions. We calculate the moles of each component (Gallahan and Nielsen chose their components as single cation oxides, except for P_2O_5) by dividing by the molecular weight. We convert this to mole fractions by dividing by the sum of the moles of all components. Then we calculate the sums of the network formers and network modifiers (equations 7.33 and 7.36), and finally the activities of SiO_2 and $AlO_{1.5}$ using equation 7.34. We calculate K using equation 7.28 (temperature in kelvins, as in all thermodynamically based formulae). The distribution coefficient, D* can then be calculated using equation 7.31. Finally, we convert to D using equation 7.39.

Though the temperature is the same and the compositions of these magmas are similar (both are basalts), there is a large difference, almost a factor of 2, in the partition coefficients we have calculated.

Oxide	Mauna Loa			Mt. Hope			Mole. Wt
	wt %	moles	mol fract.	wt %	moles	mol fract.	
SiO2	49.56	0.826	0.472288	50.95	0.8492	0.473491	60
TiO2	4.28	0.0536	0.030636	1.38	0.0173	0.009633	79.88
Al2O3	14.09	0.2764	0.158029	17.87	0.3505	0.195454	50.98
FeO	12.47	0.1736	0.099235	8.64	0.1203	0.067051	71.85
MnO	0.22	0.0031	0.001773	0.21	0.003	0.001651	70.94
MgO	4.62	0.1146	0.065532	6.18	0.1533	0.085486	40.31
CaO	9.63	0.1717	0.098185	11.29	0.2013	0.112255	56.08
Na2O	3.03	0.0977	0.055887	2.32	0.0748	0.04173	31
K2O	1.18	0.0251	0.014325	0.95	0.0202	0.011247	47.1
P2O5	1.02	0.0072	0.004109	0.51	0.0036	0.002003	141.94
Total	100.1	1.7489	1	100.3	1.7934	1	
NM			0.387289			0.420556	
NF			0.5425			0.526468	
aSiO2			0.870578			0.899374	
aAlO1.5			0.065156			0.126982	
ln(aSiO2*aAlO1.5)			-2.86958			-2.16977	
T	1353						
	La	Sm	Mauna Loa			Mount Hope	
a	119	11371	lnD La	lnD Sm		lnD La	lnD Sm
b	1.95	8.6	-4.73162	-3.0653		-4.03182	-2.3655
ln K	-1.86205	-0.1957	D* La	D* Sm		D* La	D* Sm
D*			0.008812	0.0466		0.017742	0.0939
D			**0.02275**	**0.1204**		**0.04219**	**0.22329**

- Errors in measurement and experimental limitations are such that measured partition coefficients will be too large more often than too low. Thus low values are generally preferred.
- In situ microanalytical techniques (e.g., ion probe) of experiments on natural basaltic liquids were preferred over bulk analysis of natural samples. Undoped experiments were preferred over doped experiments.
- Knowing relative relationship of the partition coefficient of one element to that of another is more important than knowing absolute values. Accuracy of relative values is maximized when partition coefficients for all elements are measured in a single experiment or series of experiments. Thus studies where partition coefficients for a large number of elements were determined were preferred over more limited set of elements.
- Partition coefficients measured experimentally using natural basaltic liquids with temperatures in the range of 1200-1400°C were preferred.
- Elements known to have partition coefficients that depend strongly on composition or temperature (e.g., Ni) have not been included.

Figure 7.16 illustrates the rare earth partition coefficients from this data set. In general, the minerals clinopyroxene, garnet and plagioclase and, when present, amphibole (amphibole is not usually present in basalts because it is not stable at low pressure or above 1100 ° C) will control the patterns of incompatible element parti-

Table 7.5. Mineral-Melt Partition Coefficients for Basalts

	Olivine	Opx	Cpx	Plag	Spinel	Garnet	Amph
Li	0.041	0.11	0.59	0.45			
Be	0.035		0.047	0.36			
B	0.034	0.027	0.117		0.08		
K	0.00017		0.0028	0.18		0.002	0.35
Sc	0.37	0.6	0.8	0.065	0.048	0.688	
V	0.3	2.6	1.81	0.04	38	1.48	
Ga	0.024		0.74	0.86	4.6		
Ge	0.097	0.25	1.4	0.51	0.1		
Rb	0.000044		0.0033	0.025		0.007	0.437
Sr	0.000063	0.0068	0.157	2.7		0.0099	0.184
Y	0.0098	0.014	0.62	0.013		5.42	0.634
Zr	0.00068	0.004	0.195	0.001	0.06	2.12	0.3
Nb	0.00005	0.015	0.0081	0.033	0.08	0.0538	0.197
Cs	0.0015		0.0039	0.026			
Ba	0.0000034	0.0067	0.0022	0.33		0.0007	0.282
La	0.0000088	0.0056	0.052	0.082	0.01	0.0164	0.058
Ce	0.000019	0.0058	0.108	0.072		0.065	0.116
Pr	0.000049	0.006		0.056			0.178
Nd		0.007	0.277	0.045		0.363	0.273
Sm	0.000445	0.0085	0.462	0.033	0.0064	1.1	0.425
Eu		0.0078	0.458	0.55	0.0061	2.02	0.387
Gd		0.011		0.034			0.725
Tb	0.00324	0.011			0.0078		0.779
Dy		0.015	0.711	0.03		4.13	0.816
Ho	0.00927	0.019					0.783
Er		0.021	0.66	0.02		3.95	0.699
Tm		0.025					
Yb	0.0366	0.032	0.633	0.014	0.0076	3.88	0.509
Lu		0.042	0.623			3.78	0.645
Hf	0.001	0.021	0.223		0.05	1.22	0.638
Ta	0.00005	0.015	0.013	0.11	0.06	0.11	
Pb	0.0076		0.01	1.07		0.0001	
Th	0.000052	0.0056	0.014	0.19		0.0014	0.016
U	0.00002	0.015	0.013	0.34		0.0059	

Data sources: Beattie (1994), Chaussidon and Libourel (1993), Chazot et al. (in press), Dunn and Sen (1994), Hart and Brooks (1974), Hart and Dunn (1993), Hauri et al. (1994), Kennedy et al. (1993), Nagasawa et al. (1980), and compilations by Green (1994), Irving (1978), and Jones (1995).

tioning during melting and crystallization of basaltic magmas because they have the highest partition coefficients. Olivine, though by far the most abundant mineral in the mantle, will produce little fractionation§ of incompatible elements because its partition coefficients are so low. Spinel, which is usually not pres??ent in more than a few volume percent, will also have little effect on relative trace element abundances. On the other hand, olivine largely controls the fractionation of the compatible transition metals.

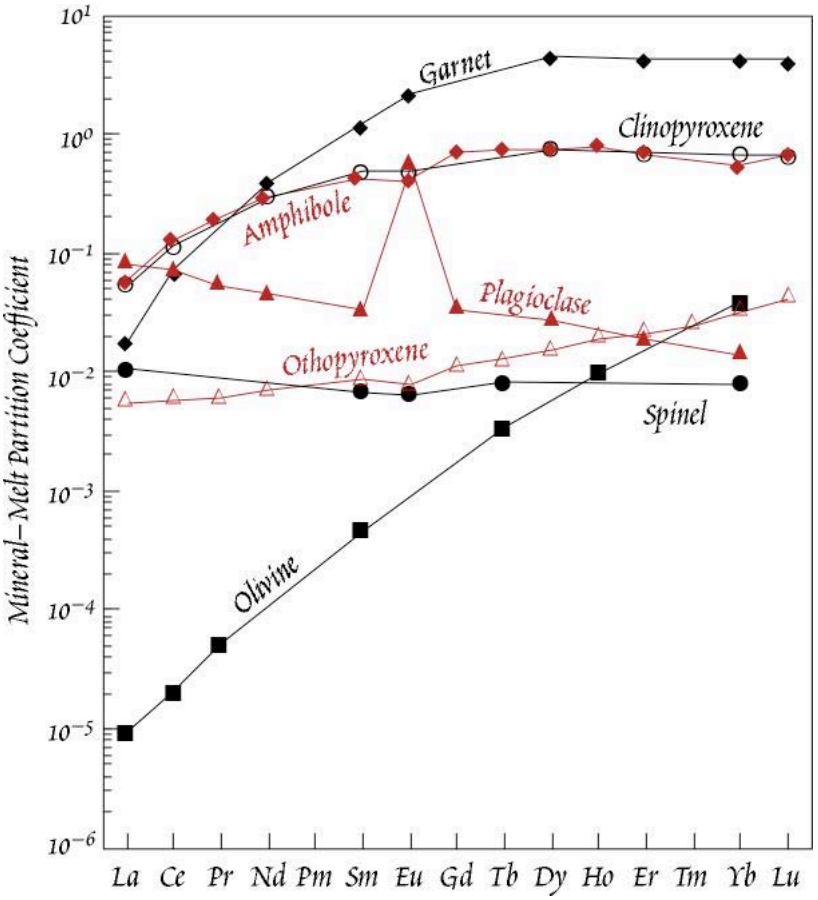

Figure 7.16. Rare earth mineral–melt partition coefficients for mafic magmas. Data from Table 7.5.

7.5 Crystal-Field Effects

We pointed out earlier that the ions of the alkalis, alkaline earths and rare earths can be satisfactorily modeled as hard spheres containing point charges at their centers. This model of ionic behavior is notably less satisfactory for many of the transition metals, because of the complex geometry of the bonding electron orbitals, illustrated in Figure 7.17. A more accurate prediction of bonding and substitution requires consideration of the electrostatic field of surrounding ions on the electron structure of transition elements.

Crystal-Field Theory, which was developed in 1929 by physicist Hans Bethe, describes the effects of electrostatic fields on the energy levels of a transition-metal ion in a crystal structure. These electrostatic forces originate from the surrounding negatively charged anions or dipolar groups, known as ligands. Crystal Field Theory is the simplest of several theories that attempt to describe the interaction and bonding between ligands and transition metals. In crystal field theory, the ligands are regarded simply as negative point charges about the transition metal ion. The electromagnetic field produced by these ligands, the "crystal field", destroys the spherical symmetry possessed by an isolated transition metal. The changes induced depend on the type, position, and symmetry of the coordinating ligands, as well as the nature of the transition metal.

In the usual case, electron orbitals are filled successively from inner to outer as one proceeds 'up' the periodic table to heavier elements. In transition metals, however, filling of the outermost *s* orbital is begun before the *d* orbitals are completely filled. Ions are formed when the outermost *s* and, in some cases, some of the outermost *d* electrons (outermost will be *4s* and *3d* for the first transition series, *5s* and *4d* for the second, etc.) are removed from the metal.

§ *Fractionation*, in this context, refers to a change in the relative abundances, or ratios, of elements. For example, if the ratio of La to Sm changes during a process, these elements are said to have been fractionated by that process.

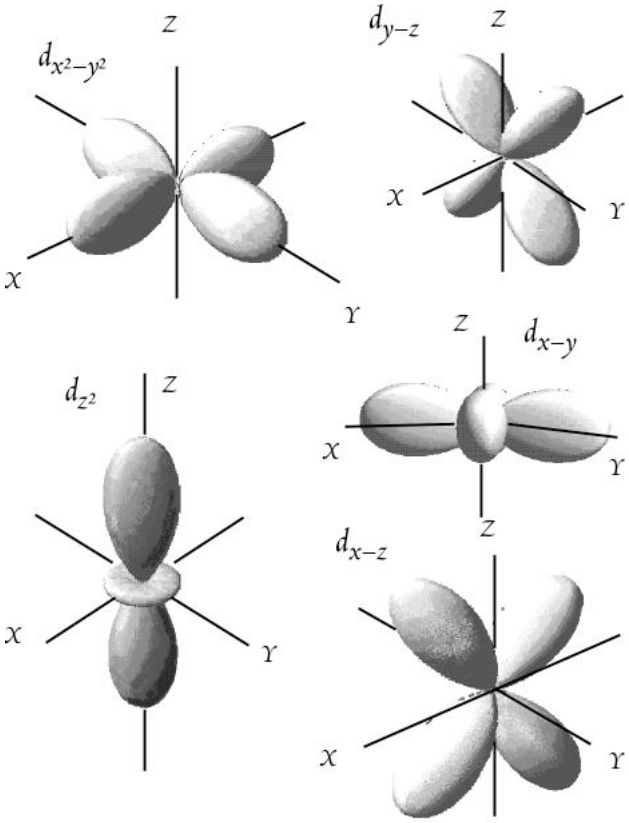

Figure 7.17. Geometry of the *d* orbitals.

In an isolated first series transition metal, the 5 *3d* orbitals (each containing up to 2 electrons: a total of 10 electrons are possible in the *d* orbitals) are energetically equivalent and have equal probability of being filled: they are said to be *degenerate*. They possess, however, different spatial configurations (Figure 7.17). One group, the e_g orbitals, consisting of the d_{z^2} and the $d_{x^2-y^2}$ orbitals, has lobes directed along the Cartesian coordinates, while the t_{2_g} group, consisting of the d_{xy}, d_{yz}, and d_{xz}, possess lobes between the Cartesian axes. In a crystal field the *3d* orbitals are no longer degenerate, and some have lower energy than others. Thus there can be a relative energy gain by preferentially filling low-energy *d* orbitals. This energy gain is traded off against the energy cost of placing two electrons in a single orbital. Depending on this trade off, preferentially filling low energy *d* orbitals can lower the overall energy of some transition metal ions, hence stabilizing them, in certain lattice configurations relative to other configurations. *The effect is a lattice site preference of some transition metals that would not be predicted simply from consideration of ion charge and size.*

In octahedral coordination, the transition metal is surrounded by six identical ligands (Figure 7.18). Electrons in all orbitals are repelled by the negatively charged ligands, but electrons in the e_g orbitals, the orbitals directed toward the ligand, are repelled to a greater extent than those in the t_{2_g} orbitals. *The energy separation between the t_{2g} and the e_g orbitals is termed octahedral crystal-field splitting and is denoted by Δ_o. The t_{2_g} orbitals are lowered by $^2/_5\Delta_o$ while the e_g orbitals are raised by $^3/_5\Delta_o$ relative to the mean energy of an unperturbed ion.* Therefore each electron in a t_{2_g} orbital stabilizes a transition metal ion by $^2/_5\Delta_o$

TABLE 7.6. ELECTRONIC CONFIGURATIONS AND CRYSTAL FIELD STABILIZATION ENERGIES OF FIRST TRANSITION SERIES METAL IONS IN OCTAHEDRAL CONFIGURATION.

Number of 3*d* electrons	Ion	High Spin State Electronic Configuration t_{2g}	e_g	Unpaired Electrons	CFSE	Low Spin State Electronic Configuration t_{2g}	e_g	Unpaired Electrons	CFSE
0	Sc^{3+}, Ti^{4+}			0	0			0	0
1	Ti^{3+}	↑		1	$2/5\Delta_o$	↑		1	$2/5\Delta_o$
2	Ti^{2+}, V^{3+}	↑ ↑		2	$4/5\Delta_o$	↑ ↑		2	$4/5\Delta_o$
3	V^{2+}, Cr^{3+}, Mn^{4+}	↑ ↑ ↑		3	$6/5\Delta_o$	↑ ↑ ↑		3	$6/5\Delta_o$
4	Cr^{2+}, Mn^{3+}	↑ ↑ ↑	↑	4	$3/5\Delta_o$	↑↓ ↑ ↑		2	$8/5\Delta_o$
5	Mn^{2+} Fe^{3+}	↑ ↑ ↑	↑ ↑	5	0	↑↓↑↓ ↑		1	$10/5\Delta_o$
6	Fe^{2+}, Co^{3+},Ni^{3+}	↑↓ ↑ ↑	↑ ↑	4	$2/5\Delta_o$	↑↓↑↓↑↓		0	$12/5\Delta_o$
7	Co^{2+},Ni^{3+}	↑↓↑↓ ↑	↑ ↑	3	$4/5\Delta_o$	↑↓↑↓↑↓	↑	1	$9/5\Delta_o$
8	Ni^{2+}	↑↓↑↓↑↓	↑ ↑	2	$6/5\Delta_o$	↑↓↑↓↑↓	↑ ↑	2	$6/5\Delta_o$
9	Cu^{2+}	↑↓↑↓↑↓	↑↓ ↑	1	$3/5\Delta_o$	↑↓↑↓↑↓	↑↓ ↑	1	$3/5\Delta_o$
10	Zn^{2+}	↑↓↑↓↑↓	↑↓↑↓	0	0	↑↓↑↓↑↓	↑↓↑↓	0	0

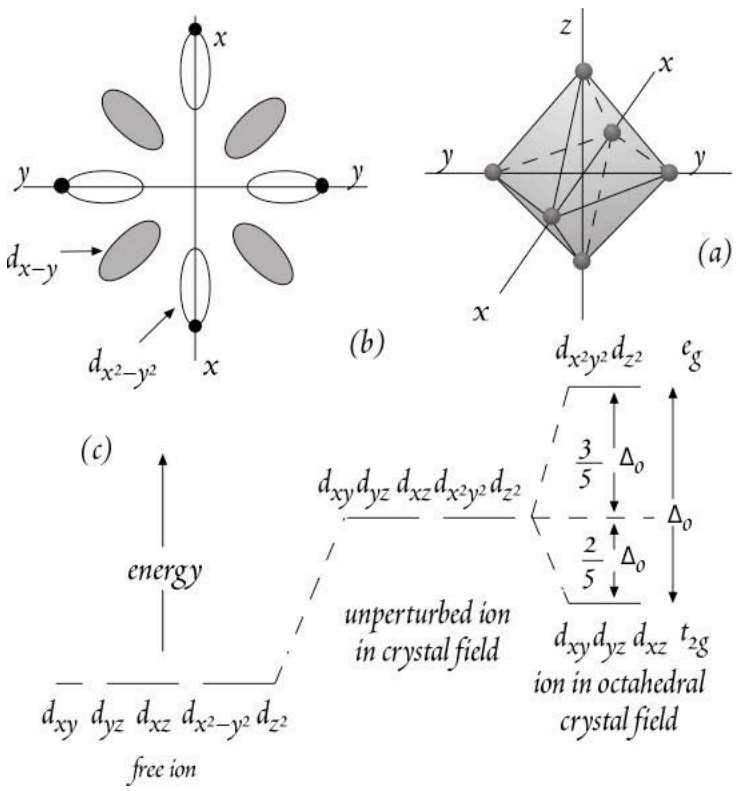

Figure 7.18. (a) Orientation of ligands and Cartesian coordinates for a metal ion in octahedral coordination. (b) Orientation of ligands (points) and d_{xy} (shaded) and $d_{x^2-y^2}$ (unshaded) orbitals in the x-y plane of a metal in octahedral coordination. (c) Energy level diagram for d orbitals of a free transition metal ion, and ion in a spherically symmetric crystal field and an octahedral crystal field. In an octahedral crystal field, the energy of the *d* orbitals projected between the coordinates and the ligands (the t_{2g} orbitals) are lowered relative to the energy of the orbitals projected toward the ligands (e_g orbitals). From Burns (1970).

and each electron in an e_g orbital diminishes stability by $^3/_5\Delta_o$. The resultant net stabilization energy, i.e., $\Sigma\Delta_o$, is called the *octahedral crystal field stabilization energy* or octahedral CFSE.

How electrons are distributed in an octahedrally coordinated transition metal is governed by two opposing tendencies. Coulomb forces between electrons cause them to be distributed over as many orbitals as possible, but crystal-field splitting favors the occupation of lowest energy orbitals. These two factors in turn depend on the number of *d* electrons possessed by the metal and the strength of the crystal field.

In ions having 1, 2 or 3 *d* electrons all electrons will be in only t_{2g} orbitals, regardless of the strength of the crystal field, since there is only 1 electron per orbit. In ions having 8, 9, or 10 electrons in *d* orbitals, each orbital must contain at least 1 electron and three orbitals must contain 2 electrons, so all the 3 t_{2g} orbitals will be filled even for weak ligands. But in ions having 4, 5, 6 and 7 *d* electrons there is a choice. If the crystal-field splitting is large, as it is in the case of strong field ligands, all electrons are in t_{2g} orbitals. This is the *low-spin* case, because the spins of electrons are anti-aligned (recall the Pauli exclusion principle that electron can only occupy the same orbit if their spins are opposite). When the crystal-field splitting is small, the energy cost of placing two electrons in the same orbit is greater than the energy gain from the octahedral CFSE, and electrons are distributed over both t_{2g} and e_g orbitals. This is known as the *high spin* case because the electrons will preferentially occupy different orbitals with their spins parallel. Apart from Co^{3+} and Ni^{3+}, all first series transition metals exist in the high-spin state on the Earth's surface. Cr^{3+}, Ni^{2+}, and Co^{3+} have particularly high CFSE in octahedral coordination.

The distinction between high and low spin configurations is important in understanding magnetic properties of transition metal compounds because magnetism relates to spin alignment of electrons. Also, the crystal-field splitting energies are in the visible light band and hence relate to the coloration of transition-metal-bearing minerals. For example, consider titan-augite (a variety of clinopyroxene containing appreciable amounts of Ti). In Ti^{+3}, the single *d* electron is normally in the t_{2g} orbital. Absorption of light of appropriate frequency $\nu = \Delta_o/h$ excites the electron into an e_g orbital. This energy corresponds to violet light, which is emitted when the electron returns to the t_{2g} orbital.

In tetrahedral coordination (Figure 7.19), the e_g orbitals become more stable than the t_{2g} orbitals, but the tetrahedral crystal-field splitting parameter, Δ_t, is smaller than Δ_o. Other things being equal,

$\Delta_t = 4/9\Delta_o$.

The crystal field splitting parameter, Δ, depends on a number of things, but some generalizations can be made:

1. Values of Δ are higher for +3 ions than +2 ions.

2. The values are 30% higher for each succeeding transition element (left to right in the periodic table).

3. Δ depends on the ligands coordinating the transition metal. Δ may be arranged to increase as follows: halides < OH^- (hydroxides)< silicates < H_2O < SO_4.

4. Δ depends on the symmetry of the coordinating ligands (as we have seen).

5. Δ varies with interatomic distance (inversely proportional to the 5^{th} power).

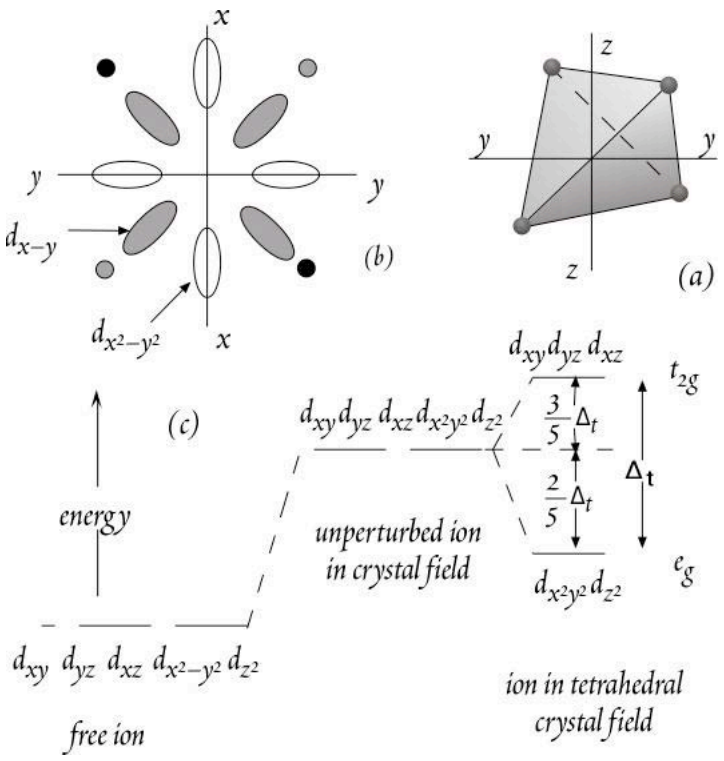

Figure 7.19. (a) Orientation of ligands and Cartesian coordinates for a metal ion in tetrahedral coordination. (b) Orientation of ligands (points) and d_{xy} (shaded) and $d_{x^2y^2}$ (unshaded) orbitals in the *x*-*y* plane of a metal in tetrahedral coordination. Black points are in front of plane of orbitals, gray points are behind the plane. Energy level diagram for *d* orbitals of a free transition metal ion, and ion in a spherically symmetric crystal field and a tetrahedral crystal field. From Burns (1970).

In silicates, oxygen atoms frequently form distorted coordination polyhedra about cations and metal-oxygen interatomic distances are not constant. Distortion of coordinated polyhedra is expected from the *Jahn-Teller Theorem*, which states that if the ground state of a molecule is degenerate, it will distort to make one of the energy levels more stable (Figure 7.20). For example, if one of the *d* orbitals is filled or empty while another is half-filled, the environment about the transition metal ion is predicted to distort spontaneously to a different geometry in which a more stable electronic configuration is attained by making the occupied orbital lower in energy. Further splitting of *d* orbital energy levels occurs when transition metal ions are in distorted coordination.

This can be illustrated for the case of Mn^{3+} in octahedral coordination with oxygen. The Mn^{3+} ion has the high spin configuration (Table 7.6) in which each t_{2g} orbital is occupied by 1 electron and the fourth electron may occupy either of the e_g orbitals. If the four oxygen atoms in the *x*-*y* plane move toward, and the two oxygens along the *z*-axis move away from, the central Mn^{3+} ion (Figure 7.20a), then the one e_g electron will favor the d_{z^2} orbital in which the repulsion by the O ions is smaller than in the $d_{x^2-y^2}$ orbital. Thus the e_g orbital group separates into two energy levels with the d_{z^2} becoming more stable. The t_{2g} orbital group is also split, with the d_{xz} and d_{yz} becoming more stable than the d_{xy} orbital. If the two O ions along the *z*-axis move closer to the Mn^{3+} ion (Figure 7.20c), the $d_{x^2-y^2}$ becomes more stable than the d_{z^2}. In either of the distorted environments, the Mn^{3+} becomes more stable than in an undistorted octahedral site. Transition metals subject to Jahn-Teller distortions in octahedral coordination are those with d^4, d^9, and low-spin d^7 configurations, in which one or three electrons occupy e_g orbitals. Looking at Table 7.6, we can see that these are Cr^{2+}, Mn^{3+}, Cu^{2+}, Co^{2+} and Ni^{3+} ions.

CHAPTER 7: TRACE ELEMENTS

As noted, electronic transition energies are related to color. Because of the distortion, additional electronic transitions become possible. The differing probabilities of the various electronic transitions in polarized radiation in one of the causes of *pleochroism*[*] in minerals.

Crystal-field effects lead to irregularities in the interatomic distances, or ionic radii of transition metals. As you might expect, they depend on the nature of the site, and for a given site, there need not be a smooth contraction of interatomic distances with increasing atomic number.

The application of crystal field theory is restricted to compounds where the transition metal forms a dominantly ionic bond with surrounding ligands. In sulfides, and related minerals, the effects of covalent bonding, in which the orbitals become hybridized, must be considered, but such consideration is beyond the scope of our treatment.

7.5.1 Crystal Field Influences on Transition Metal Partitioning

We can now return to the transition metals and crystal-field theory to explain some of the peculiarities of their behavior. We noted that the energy of some *d* orbitals is reduced (stabilized) by the effects of the electrostatic field of coordinating ligands in both octahedral and tetrahedral sites and that the octahedral CFSE is always greater than the tetrahedral CFSE. We now introduce one more quantity: the octahedral site preference energy (OSPE), which is defined as the octahedral CFSE less the tetrahedral

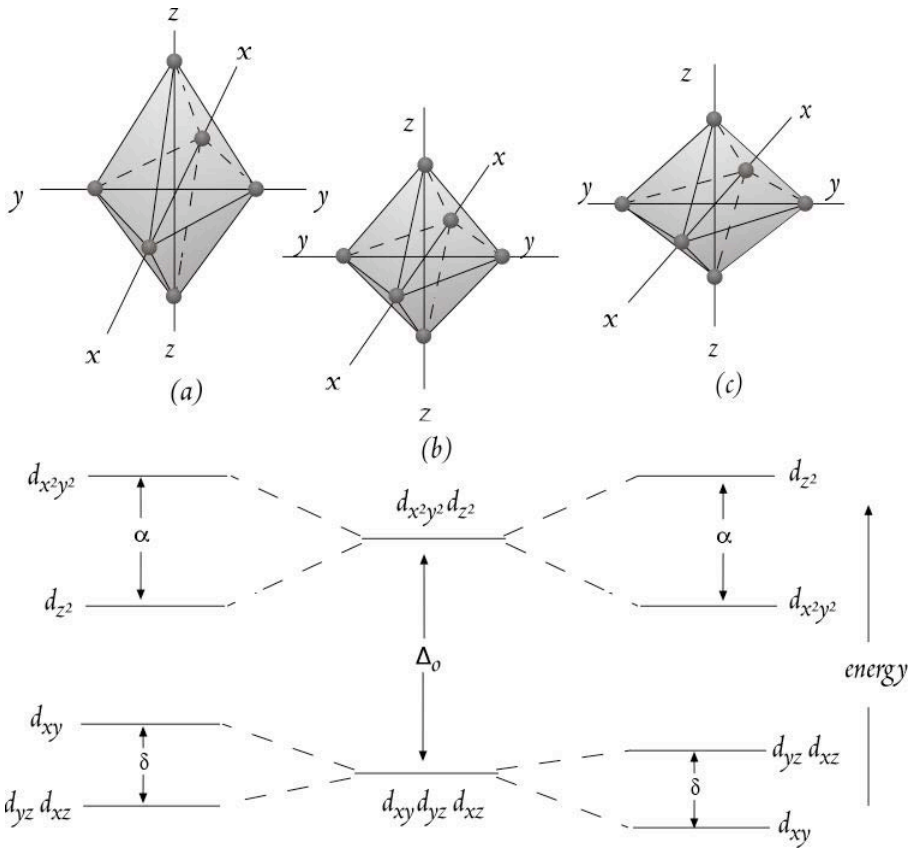

Figure 7.19. Arrangement of ligands and energy levels for (a) an octahedral site distorted along the *z* axis. (b) an undistorted site, and (c) an octahedral site distorted along the *y* axis. After Burns (1970).

[*] Pleochroism refers to property possessed by some crystals of exhibiting different colors when viewed along different axes in polarized light.

CFSE. Table 7.7 lists these energies for various first transition series metals. Silicate melts contain both octahedral and tetrahedral sites, but transition metals, with a few exceptions, occupy only octahedral sites in silicate minerals. Thus the OSPE is a indicator of the preference of the transition ion for solid phases over liquid phases: the higher the OSPE, the more readily it is partitioned into a solid phase. Predicted order of uptake is: Ni>Co>Fe^{+2}>Mn for 2+ ions and Cr>V>Fe^{+3} for 3+ ions, which agrees with observation. Since the number of octahedral sites in the liquid decrease with increasing SiO_2 concentration, crystal field theory explains why Ni partition coefficients are highly composition dependent, increasing with increasing SiO_2 concentration.

It should be emphasized that there are no crystal field effects for transition metals such as Sc^{2+}, Ti^{+4}, Y^{3+}, Zr^{4+}, Nb^{5+}, Hf^{4+}, and Ta^{5+} where the *d* electrons are not present in the ion, or where the *d* shell is completely filled (Zn^{2+}) in the usual valence state, at least when the electrons are in their ground state. However color, which arises from excitation of electrons into higher orbitals and subsequent decay to the ground state, may still relate to crystal field effects even when the *d* orbitals are not filled in the ground state. The second and third transition series metals for which crystal-field effects are expected are all highly siderophile or chalcophile and highly depleted in the Earth's crust and mantle. Little information is available on their behavior in silicate systems.

An understanding of crystal field theory solves an interesting dilemma. A phase (T-X) diagram for the binary system Mg_2SiO_4 — Ni_2SiO_4 is shown schematically in Figure 7.21. It is apparent from a quick glance that for any coexisting liquid and solid in the system, the solid will be poorer in Ni than the liquid, i.e., $(Ni/Mg)_{ol} < (Ni/Mg)_{liq}$. However, olivine crystallizing from basaltic liquids is always richer in Ni than the liquid. The reason for this is that in the pure olivine system, only octahedral sites exist in the melt and the solid, and thus Ni has no particular preference for the solid due to crystal field effects. But basaltic melts have both tetrahedral and octahedral sites, while olivine has only octahedral sites (available to Ni). The greater availability of octahedral sites in the solid provides an added incentive for Ni to partition into olivine relative to basaltic liquid.

Table 7.7. Crystal-Field Splittings and Stabilization Energies in Transition-Metal Ions

Number of 3*d* electrons	Ion	Electronic Configuration		Δ (cm^{-1}) $M(H_2O)_6^{n+}{}_{(aq)}$	CFSE hydrate (KJ/mole)	Octahedral CFSE (kJ/mole)	Tetrahedral CFSE (kJ/mole)	Octahedral Site Preference Energy (kJ)
1	Ti^{3+}	$(t_{2g})^1$		20,300	$2/5\Delta = 97.1$	87.4	58.6	28.9
2	V^{3+}	$(t_{2g})^2$		17,700	$4/5\Delta = 169.0$	160.2	106.7	53.6
3	Cr^{3+}	$(t_{2g})^3$		17,400	$6/5\Delta = 249.4$	224.7	66.9	157.7
4	Cr^{2+}	$(t_{2g})^3$	$(e_g)^1$	13,900	$3/5\Delta = 99.6$	100.7	29.3	71.1
4	Mn^{3+}	$(t_{2g})^3$	$(e_g)^1$	21,000	$3/5\Delta = 150.6$	135.6	40.2	95.4
5	Mn^{2+}	$(t_{2g})^3$	$(e_g)^2$	7,800	0	0	0	0
5	Fe^{3+}	$(t_{2g})^3$	$(e_g)^2$	13,700	0	0	0	0
6	Fe^{2+}	$(t_{2g})^4$	$(e_g)^2$	10,400	$2/5\Delta = 49.8$	49.8	33.1	16.7
6	Co^{3+}	$(t_{2g})^6$		18,600	$12/5\Delta = 533.5$*	188.3	108.8	79.5
7	Co^{2+}	$(t_{2g})^5$	$(e_g)^2$	9,300	$4/5\Delta = 89.1$	92.9	61.9	31.0
7	Ni^{3+}	$(t_{2g})^6$	$(e_g)^1$	–	$9/5\Delta =$			
8	Ni^{2+}	$(t_{2g})^6$	$(e_g)^2$	8,500	$6/5\Delta = 29.6$	122.2	36.0	86.2
9	Cu^{2+}	$(t_{2g})^6$	$(e_g)^3$	12,600	$3/5\Delta = 21.6$	90.4	26.8	63.6

* Low-spin complexes. The calculated CFSE must be reduced by the energy required to couple two electrons in a t_{2g} orbital. Data from Orgel (1966) and McClure (1957).

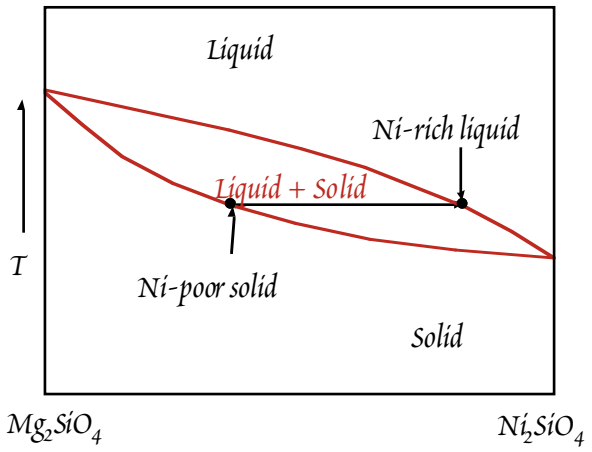

Figure 7.21. Schematic phase diagram for the system forsterite—Ni olivine showing Ni-poor olivine in equilibrium with Ni-rich liquid.

7.6 TRACE ELEMENT DISTRIBUTION DURING PARTIAL MELTING

In igneous geochemistry, trace elements are useful in understanding magmatic processes and in evaluating the composition of magma sources such as the mantle and lower crust. To make use of trace elements in such studies, we need to understand how magmatic processes such as partial melting and fractional crystallization will affect trace element abundances.

The task of the igneous geochemist is often to make inferences about the sources of magma, the mantle and lower crust, from the composition of the magmas themselves. This can be done through a mathematical model of the melting. In the following sections, we will consider two simple alternative models of melting: batch, or equilibrium, melting, and fractional melting. In fractional melting, the melt is extracted as soon as it is created, and only an infinitesimal increment of melt will be in equilibrium with the solid residue at any given time. In batch melting, a finite amount of melt, for example 5 or 10%, is produced and equilibrates completely with the solid residue.

Once a melt is created and begins to rise, it may further interact with the surrounding "wallrock". We will also consider one possible model of this interaction: "zone refining". Choosing between alternative models of partial melting requires a knowledge of how melting and melt extraction actually occurs. Unfortunately, melting and melt extraction in the Earth remain poorly understood because we are unable to observed them directly. Although melting experiments are useful in determining phase relationships, melting temperatures, and distribution coefficients, they do not provide much direct information on how melt is extracted. By and large, our knowledge of the melt extraction process comes from indirect inferences. Rarely, we can identify partial melting residues that have been tectonically emplaced at the surface of the Earth, and studies of these have provided some insights into the melting process. We will consider some of these insights in a subsequent section.

7.6.1 EQUILIBRIUM OR BATCH MELTING

Equilibrium crystallization or melting implies complete equilibration between solid and melt. This means that the entire batch equilibrates with the residue before it is removed. From mass balance we may write:

$$C_i^o = C_i^s(1-F) + C_i^\ell F \qquad 7.41$$

where i is the element of interest, C° is the original concentration in the solid phase (and the concentration in the whole system), C^ℓ is the concentration in the liquid, C^s is the concentration remaining in the solid and F is the melt fraction (i.e., mass of melt/mass of system). Since $D = C^s/C^\ell$, and rearranging:

$$C_i^o = C_i^\ell D_i^{s/\ell}(1-F) + C_i^\ell F$$

$$\boxed{\frac{C_i^\ell}{C_i^o} = \frac{1}{D^{s/\ell}(1-F)+F}} \qquad 7.42$$

This equation is an extremely useful one and describes the relative enrichment or depletion of a trace element in the liquid as a function of degree of melting. Two approximations are often useful and give us a feel for this equation. First consider the case where D<<F. In this case $C^\ell/C^\circ \approx 1/F$, that is, the enrichment is inversely proportional to the degree of melting. This is the case for highly incompatible elements at all but the smallest degrees of melting. Now consider the case where F approaches 0. In this

case $C^\ell/C^\circ \approx 1/D$, the enrichment is inversely proportional to the partition coefficient. Thus the maximum enrichment possible in a partial melt is 1/D. For highly compatible elements, that is those with large D such as Ni, the depletion in the melt is 1/D when F is small and is relatively insensitive to F.

7.6.2 Fractional Melting

Now consider the case where only an infinitesimally small amount of melt equilibrates with the solid residue, in other words, imagine we remove the liquid as fast as we make it. If i^s is the mass of element i in the solid phase being melted, S the mass of the solid phase, L the mass of the liquid phase, i^l the mass of i in the liquid, S° the original mass of the solid (and mass of the system), and i° the original mass of i in the solid (and system), then:

$$C_i^s = \frac{i^s}{S} = \frac{i^\circ - i^l}{S^\circ - L} \qquad \text{and} \qquad C_i^\ell = \frac{1}{D_i}\frac{i^\circ - i^\ell}{S^\circ - L} = \frac{di^\ell}{dL}$$

This can be rearranged so that we can integrate it to obtain:

$$\boxed{\frac{C_i^\ell}{C_i^o} = \frac{1}{D}(1-F)^{1/D-1}} \qquad 7.43$$

If we subsequently mix the various melt fractions produced over a melt interval from 0 to F, the composition of this *aggregate liquid*, $\bar{C}$ is:

$$\boxed{\frac{\bar{C}_i^\ell}{C_i^o} = \frac{1}{F}\left(1-(1-F)^{1/D_i}\right)} \qquad 7.44$$

Figure 7.22 illustrates the variation of the liquid enrichment (C^ℓ/C^o) with degree of melting for both batch and fractional melting. The aggregate liquid of fractional melting, which may be the most realistic of the 3 equations we have considered so far, follows a trend close to that of batch melting.

7.6.3 Zone Refining

If melt percolates slowly through the source region, trace element fractionation may be best approximated by equations governing zone refining. The term zone refining comes from the industrial purification process in which a melt zone is caused to migrate along a column of material. Several passes of this process efficiently extract low melting-temperature components. The relevant equation is:

$$\frac{C_i^\ell}{C_i^o} = \frac{1}{D_i} - \left(\frac{1}{D_i} - 1\right)e^{-D_i R} \qquad 7.45$$

where R is the ratio of host, or wallrock, to melt. Note that for large R, $C^l/C^\circ \sim 1/D$.

7.6.4 Multiphase Solids

The above equations are relevant when the solid undergoing melting is homogeneous. If it consists of several phases, we need to replace D with a *bulk* distribution coefficient, which is simply the weighted mean of the

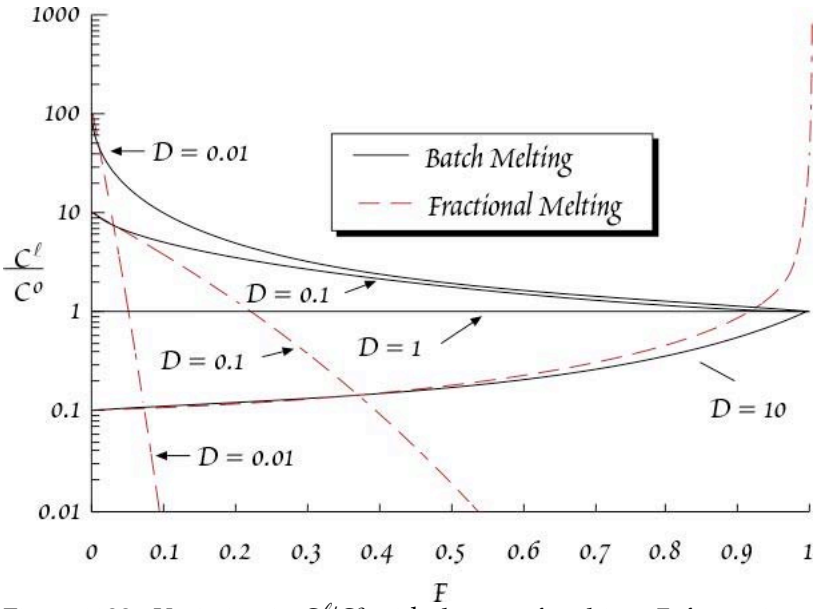

Figure 7.22. Variation in C^ℓ/C^o with degree of melting, F, for various partition coefficients for batch and fractional melting.

individual solid/liquid partition coefficients:

$$\overline{D}_i = D_i^o = \sum_\phi m_\phi D_i^{\phi/\ell} \qquad 7.46$$

where m is simply the *modal mass fraction* of phase ϕ, that is the fraction of phase ϕ as it exists in the rock.

In general, minerals do not enter the melt in the proportion in which they exist in a rock, i.e., their modal proportions. Thus a realistic melting model requires we modify our equations to account for this. We need to define a new parameter P, which is simply the average individual partition coefficients weighted according the proportions in which the minerals enter the melt:

$$P_i = \sum_\phi p_\phi D_i^{\phi/\ell} \qquad 7.47$$

where p is the proportion in which phase ϕ enters the melt. It is often assumed that the p_ϕ values are constants. In reality, they will be functions of F. The equations for batch and fractional melting in this *non-modal melting* case become:

Non-Modal Batch Melting

$$\frac{C_i^\ell}{C_i^o} = \frac{1}{F(1-P_i) + D_i^o} \qquad 7.48$$

Non-Modal Fractional Melting

$$\frac{C_i^\ell}{C_i^o} = \frac{1}{D_i^o}\left(1 - \frac{P_i F}{D_i^o}\right)^{1/P_i - 1} \qquad 7.49$$

The aggregate liquid for non-modal fractional melting is given by:

Aggregate:

$$\frac{\overline{C}_i^\ell}{C_i^o} = \frac{1}{F}\left(1 - (1 - \frac{P_i F}{D_i^o})^{1/P_i}\right) \qquad 7.50$$

These equations are from Shaw (1970).

EXAMPLE 7.3. MODELLING PARTIAL MELTING

Geochemists are often interested in the ratios of incompatible trace elements. For one thing, ratios of incompatible elements are less affected by fractional crystallization than are trace element abundances. To illustrate the effect of partial melting on a trace element ratio, we will calculate how the ratio of La to Sm varies in basalts produced by different extents of melting in the mantle.

We need to make some assumptions about the composition and mineralogy of the mantle. These assumptions are: (1) the mantle 'source' is composed of 58% olivine, 27% orthopyroxene, 12% clinopyroxene, and 3% spinel (2) these minerals enter the melt in the proportions 20% olivine, 25% orthopyroxene, 45% clinopyroxene, and 10% spinel, (3) that this source contains 1 ppm La and 1 ppm Sm. Using the partition coefficients for peridotite mantle listed below, we calculate the La and Sm concentrations at 2% and 10% melting using the batch melting model.

Our first step is to calculate the D_o and P values for each element using equations 7.46 and 7.47. Doing so, we find $D_{La} = 0.007$, $D_{Sm} = 0.047$, $P_{La} = 0.025$, $P_{Sm} = 0.166$. Using equation 7.48, we find that at 10% melting, [La] = 9.5 ppm and [Sm]= 7.66 ppm. So a 10% melt (F = 0.1) of a mantle having La/Sm = 1 will have La/Sm = 9.5/7.66 = 1.25. For the same calculation at 2% melting we obtain [La] = 37.3 ppm and [Sm] = 15.65 ppm and La/Sm = 2.38. Thus at a fairly large degree of melting (10%), the La/Sm ratio was only 25% greater than that of the source. At a small degree of melting, the La/Sm ratio was more than a factor of 2 greater than that of the source.

PARTITION COEFFICIENTS

	Ol	Opx	Cpx	spinel
La	0.0003	0.002	0.053	0.01
Sm	0.0013	0.011	0.36	0.01

7.6.5 Continuous Melting

In most circumstances, the way in which rock melts in the Earth is probably intermediate between our batch and fractional melting models: only part of the melt is extracted continuously, some fraction remains to fill the pore spaces between the mineral grains. This process has been called *continuous melting*. Let's look at how we can modify our fractional melting equation (equation 7.43) for this situation.

Consider a rock undergoing melting. We assume that it has a melt-filled porosity of ϕ, where ϕ is defined by mass. We can replace the partition coefficient in equation 7.43 with an effective partition coefficient, D´, which takes account of a fraction of liquid, ϕ, in the rock with a partition coefficient of 1 (Albarède, 1995). Equation 7.43 thus becomes:

$$\frac{C_i^\ell}{C_i^o} = \frac{1}{D_i'}\left(1-F\right)^{1/D_i'-1} \qquad 7.51$$

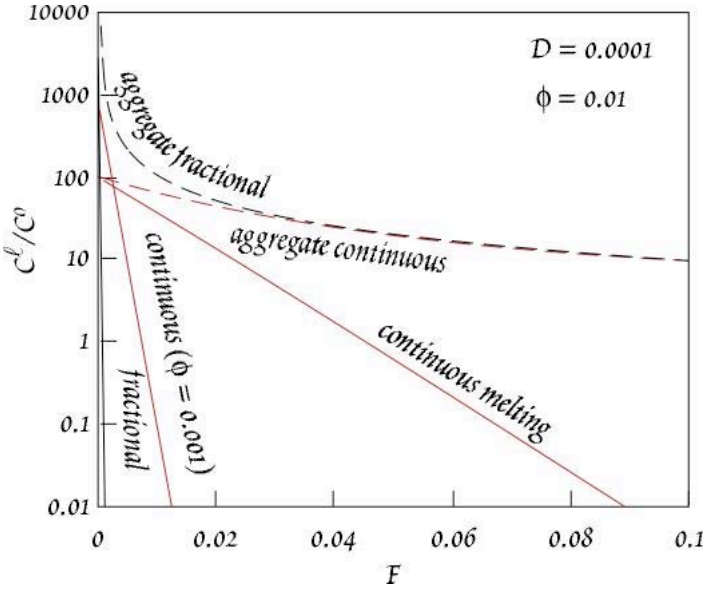

Figure 7.23. Comparison of continuous and fractional melting for D = 0.0001 and ϕ = 0.01. The aggregate melt is similar in both cases when F is greater than about 2%. A separate curve for continuous melting is shown for ϕ = 0.001.

F in this case is the fraction of melt extracted, which differs from the total amount of melt produced by an amount equal to ϕ. D' is related to the usual partition coefficient, D, (equation 7.1) as:

$$D_i' = (1-\phi)D_i + \phi \qquad 7.52$$

The exponential term in 7.51, $1/D'$-1, is related to D by:

$$\frac{1}{D_i'} - 1 = \frac{1-\phi}{(1-\phi)D_i + \phi}\left(1-D\right) \qquad 7.53$$

Substituting these back into equation 7.51, our expression for continuous melting written in terms of the usual partition coefficient is:

$$\frac{C_i^\ell}{C_i^o} = \frac{1}{(1-\phi)D_i + \phi}(1-F)^{\frac{(1-\phi)(1-D_i)}{(1-\phi)D_i+\phi}} \qquad 7.54$$

Porosity is normally defined in terms of volume, but the above equations use a porosity defined in terms of mass. The relationship between the mass porosity and the volume porosity is:

$$\phi = \frac{\rho_\ell \varphi}{\rho_s(1-\varphi) + \rho_\ell \varphi} \qquad 7.55$$

where ϕ is the mass porosity, φ volume porosity, ρ_s is the density of the solid and ρ_ℓ is the density of the liquid.

We can also derive an equation for an aggregate continuous melt simply by replacing D with D´ in equation 7.44. Figure 7.23 compares continuous and fractional melting for D = 0.0001 and ϕ = 0.001. Leaving residual melt in the pores has the effect of buffering the depletion of the solid, so that the concentration of an incompatible element does not decrease as fast in the case of continuous melting as for fractional melting. As Figure 7.23 shows, for high values of F, the aggregate melts produced by fractional and continuous melting have almost identical compositions. The compositions of the residual solids, however, will be far different, with the residue of fractional melting being far more depleted in incompatible elements than the residue of batch melting.

7.6.6 Constraints on Melting Models

To summarized the discussion above, we may say that the concentration of a trace element in a melt is a function of (1) the solid phases (i.e., minerals) present in the system before and during melting (2) the extent of melting (i.e., F), (3) the manner of melting (e.g., fractional vs. batch), (4) the concentration of the element in the original solid (i.e., C°), and (5) the partition coefficients. The partition coefficients, as we have seen, are functions of temperature, pressure, and composition of the phases involved. Two tasks of trace element geochemistry are to deduce something about the melting process and about the composition of the source of magmas. If we are to use trace elements for these purposes, it is essential we independently constrain some of these variables.

Most magmas are generated by partial melting of the upper mantle. Although temperature increases with depth in the mantle, the solidus temperature (i.e., the temperature where melting begins) increases more rapidly, so that the deep mantle is generally well below its solidus[†]. Though they have played a very important role in the evolution of the Earth, magmas produced by melting of the deep crust are very much rarer. So our discussion here will be limited to the melting process in the upper mantle. The phases present in the upper mantle, and their compositions, are discussed in more detail in Chapter 11, so we will omit that topic from the discussion here.

7.6.6.1 Relationship Between Melt Fraction and Temperature and Pressure

We can shorten our list of variables if we can somehow relate the degree of melting to temperature and ultimately to pressure. We can do this through a simplified thermodynamic analysis.

Most melting in the mantle, with the notable and important exception of subduction zones, appears to result from decompression: packets of mantle moving upward. Pressure in the Earth is related to depth, (h), by the simple relationship:

$$\frac{dP}{dh} = \rho g \qquad 7.56$$

where ρ is density and g is the acceleration of gravity. For a typical upper mantle density, pressures increases by about 1 GPa every 35 km depth.

Because of the scales generally involved (kilometers to hundreds of kilometers) and the low thermal conductivity of rock, it is reasonable to assume that a rising packet of mantle is adiabatic. As we learned Chapter 2, this means it can do work or have work done on it, but it does not exchange heat with its surroundings, i.e., $dQ = 0$. We also learned in Chapter 2 that an adiabatic system is an isoentropic one, i.e., $dS = 0$. The constraint that the system is isoentropic allows us to relate the amount of melting that will occur to the temperature and pressure of the rising mantle.

The variation of entropy with temperature and pressure can be expressed as:

$$dS = \left(\frac{\partial S}{\partial T}\right)_P dT + \left(\frac{\partial S}{\partial P}\right)_T dP \qquad 7.57$$

Substituting equations 2.105 and 2.106 into 7.57, we have:

$$dS = \frac{C_P}{T} dT - \alpha V dP \qquad 7.58$$

Since the system is isoentropic, $dS = 0$, and we can solve 7.58 to obtain:

$$\left(\frac{\partial T}{\partial P}\right)_S = \frac{T\alpha V}{C_P} \qquad 7.59$$

This equation describes the *adiabat*, the P-T path that adiabatically rising mantle follows. (By the way, we can see that the adiabat will be curved, since its slope depends on T). The solidus temperature will also change with pressure. It's slope is given by the *Clapeyron Equation* (equation 3.3):

[†] Recent seismic studies suggest the possible presence of melt pockets in the lowermost mantle, near the core-mantle boundary.

$$\left(\frac{dT}{dP}\right)_{sol} = \frac{\Delta V_m}{\Delta S_m}$$

The slope of the solidus is steeper than that of the adiabat, so that rising mantle will eventually intersect the solidus (Figure 7.24). For simplicity, let's assume the solid consists of a single phase. When the solidus is reached, the system will consist of two phases, solid and liquid, and we can write one version of equation 7.57 for the solid and one version for any melt that has formed. Now let's specify that the two phases coexist at equilibrium along a univariant reaction curve, whose slope in T-P space is $(dT/dP)_{2\phi}$. We can solve equation 7.57 to determine how entropy of each phase changes with pressure, for example, for the solid:

$$\frac{dS^s}{dP} = \frac{C_P^s}{T}\left(\frac{dT}{dP}\right)_{2\phi} - \alpha^s V^s \qquad 7.60$$

The total specific entropy (i.e., entropy per unit mass) of the system, S_o, can be expressed as the sum of the entropy of the solid and the melt.

$$FS^{\ell} + (1-F)S^s = S_0 \qquad 7.61$$

where S^{ℓ} and S^s are specific entropies of the melt and solid respectively and F is the fraction of melt. If we solve 7.61 for F, we have:

$$F = \frac{S_0 - S^s}{S^{\ell} - S^s} \qquad 7.62$$

The term S^{ℓ} - S^s is just entropy of melting, ΔS_m, so 7.61 can be written as:

$$F = \frac{S_0 - S^s}{\Delta S_m} \qquad 7.63$$

So long as the melt is not extracted the system remains isoentropic and S_0 is a constant; however, neither S^{ℓ} nor S^s are necessarily constant. Let's assume for the moment, that ΔS_m is also constant (equivalent to assuming that S^{ℓ} and S^s change in an identical way). If we now differentiate 7.63 with respect to pressure, we have:

$$\left(\frac{\partial F}{\partial P}\right)_S = \frac{1}{\Delta S_m}\left(\frac{C_P^s}{T}\left(\frac{dT}{dP}\right)_{2\phi} - \alpha^s V^s\right) \qquad 7.64$$

Equation 7.64 shows that even assuming that all the thermodynamic parameters in 7.64 are constant, the amount of melt produced by rising mantle will be a function of its temperature.

Once melting begins, rising mantle follows a P-T path that is steeper than adiabatic (Fig. 7.24), since some energy is consumed in melting. Let's call the temperature that the system would have attained had melting not occurred the potential temperature, T_{pot}. The difference between that temperature and the actual temperature T is related to the entropy change during melting ΔS_m. We can determine the entropy change due to the difference between T and T_{pot} by integrating equation 2.105:

$$\Delta S = \int_T^{T_{pot}} \frac{C_P}{T} dT \qquad 7.65$$

Since we are interested in a simple, approximate analysis, let's assume that C_P is constant. In that case, equation 7.65 becomes:

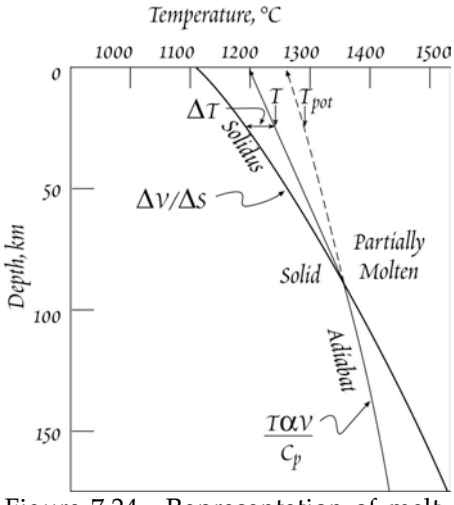

Figure 7.24. Representation of melting of an ascending packet of mantle in temperature and pressure space. Below the solidus, the mantle rises along the adiabat. Once packet intersects the solidus, the T-P path of the mantle packet is deflected by ΔT.

$$\Delta S == C_p \ln \frac{T_{pot}}{T} \qquad 7.66$$

To find a simple linear solution, let's approximate 7.66 with a Taylor Series expansion about T_{act}, which yields:

$$\Delta S \cong \frac{C_p}{T}(T_{pot} - T) \qquad 7.67$$

So long as melt has not been lost, the system remains isoentropic, so the entropy difference in 7.67 must simply be the entropy consumed in melting:

$$\Delta S = \Delta S_m F \qquad 7.68$$

equating the two, we have:

$$\Delta S_m F \cong \frac{C_p}{T}(T_{pot} - T) \qquad 7.69$$

Rearranging, and letting $\Delta T = (T_{pot} - T)$, we have:

$$T_{pot} - T \cong \frac{T}{C_p}\Delta S_m F \qquad 7.70$$

This difference, $T_{pot} - T$ is the temperature deflection due to melting in the T-P path and is shown in Figure 7.24. If we differentiate 7.70 with respect to P (and still holding S constant), we have:

$$\left(\frac{\partial (T_{pot} - T)}{\partial P}\right)_S \cong \frac{\Delta S_m}{C_p}\left(\frac{\partial (TF)}{\partial P}\right)_S = \frac{\Delta S_m}{C_p}\left[F\left(\frac{\partial T}{\partial P}\right)_S + T\left(\frac{\partial F}{\partial P}\right)_S\right]$$

and finally:

$$\left(\frac{\partial \Delta T}{\partial P}\right)_S \cong \frac{\Delta S_m}{C_p}F\left(\frac{\partial T}{\partial P}\right)_S + \frac{\Delta S_m}{C_p}T\left(\frac{\partial F}{\partial P}\right)_S \qquad 7.71$$

Solving for $(\partial T/\partial P)_S$, we have:

$$\left(\frac{\partial T}{\partial P}\right)_S \cong \left(\frac{\partial T_{pot}}{\partial P}\right)_S - \frac{T}{C_p}\Delta S_m\left(\frac{\partial F}{\partial P}\right)_S \qquad 7.72$$

The term $(\partial T_{pot}/\partial P)_s$ is just the adiabatic gradient, given by equation 7.58, and substituting that into 7.72 we have:

$$\left(\frac{\partial T}{\partial P}\right)_S \cong \frac{T\alpha V}{C_P} - \frac{T}{C_p}\Delta S_m\left(\frac{\partial F}{\partial P}\right)_S \qquad 7.73$$

Equation 7.73 describes the P-T path that a system undergoing isoentropic melting will follow as it rises.

The degree of melting will be a function of excess temperature, i.e., the difference between the solidus temperature and the actual temperature, which we shall call ΔT. In Figure 7.24, ΔT can be found by subtracting the solidus temperature from temperature path of the mantle packet, i.e.:

$$\left(\frac{\partial \Delta T}{\partial P}\right)_S \cong \left[\frac{T\alpha V}{C_P} - \frac{T}{C_p}\Delta S_m\left(\frac{\partial F}{\partial P}\right)_S\right] - \left(\frac{\partial T}{\partial P}\right)_{solidus} \qquad 7.74$$

There have been many attempts to determine the relationship between melting and temperature for mantle materials. Such melting curves are notoriously difficult to determine. Figure 7.25 shows an experimentally determined melting curve for a peridotite composition at 3.5 GPa. The curve has several breaks in slope that correspond to elimination of phases. Despite the kinks, one can extract from this

kind of experiment a relationship between degree of melting and excess temperature, i.e., a value for $(\partial F/\partial T)_P$. For example, Langmuir et al. (1993) adopted a value of about 0.00285 for $(\partial F/\partial T)_P$ below 22% melting and 0.0015 for $(\partial F/\partial T)_P$ above 22% melting. We want to incorporate this information into our analysis. We do this as follows. First, we express the variation in temperature as a function of melt fraction and pressure:

$$dT = \left(\frac{\partial T}{\partial P}\right)_F dP + \left(\frac{\partial T}{\partial F}\right)_P dF \qquad 7.75$$

If we differentiate 7.75 with respect to pressure, specifying that entropy be held constant, we can derive the following relationship:

$$\left(\frac{\partial T}{\partial P}\right)_S = \left(\frac{\partial T}{\partial P}\right)_F + \left(\frac{\partial T}{\partial F}\right)_P \left(\frac{\partial F}{\partial P}\right)_S$$

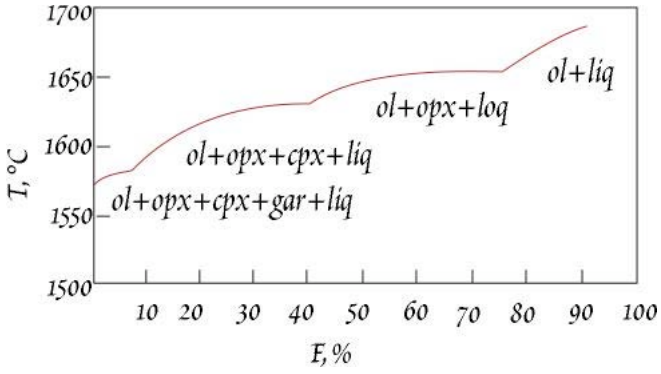

Figure 7.25. Relationship between extent of melting, F, and temperature in peridotite at 3.5 GPa determined experimentally in graphite capsules by Harrison (1979). Kinks in the curve correspond to consumption of phases, in the order garnet (gar), clinopyroxene (cpx), and orthopyroxene (opx).

This can be substituted into 7.72 to obtain:

$$\left(\frac{\partial T}{\partial P}\right)_F + \left(\frac{\partial T}{\partial F}\right)_P \left(\frac{\partial F}{\partial P}\right)_S \cong \frac{T\alpha V}{C_P} - \frac{T}{C_p}\Delta S_m \left(\frac{\partial F}{\partial P}\right)_S \qquad 7.76$$

Rearranging:

$$\left(\frac{\partial T}{\partial P}\right)_F - \frac{T\alpha V}{C_P} \cong \left[-\frac{T}{C_p}\Delta S_m - \left(\frac{\partial T}{\partial F}\right)_P\right]\left(\frac{\partial F}{\partial P}\right)_S$$

and finally:

$$\left(\frac{\partial F}{\partial P}\right)_S \cong \frac{\frac{T\alpha V}{C_P} - \left(\frac{\partial T}{\partial P}\right)_F}{\frac{T}{C_p}\Delta S_m + \left(\frac{\partial T}{\partial F}\right)_P} \qquad 7.77$$

Equation 7.77 gives the *melt fraction as a function of pressure above the pressure where the mantle intersects the solidus*.

Let's now attempt to evaluate equation 7.77 by substituting some real values into it. The term $(\partial T/\partial P)_F$ is the slope in T-P space of lines of constant melt fraction. We can make two simplifying assumptions: (1) the lines of constant melt fraction are parallel to the solidus, and (2) the solidus can be adequately described by a Clapeyron slope, equation 3.3 (because the composition of both melt and solid can vary in the real mantle, the solidus will not be a simple univariant curved described by the Clapeyron equation), so 7.77 becomes:

$$\left(\frac{\partial F}{\partial P}\right)_S \approx \frac{\frac{T\alpha V}{C_P} - \frac{\Delta V_m}{\Delta S_m}}{\frac{T}{C_p}\Delta S_m + \left(\frac{\partial T}{\partial F}\right)_P} \qquad 7.78$$

The coefficient of thermal expansion, α, is about $3 \times 10^{-5} K^{-1}$, V is about 0.3175 cm^3/g (=0.3175 J $MPa^{-1}g^{-1}$), C_p is about 1.15 J $K^{-1}g^{-1}$. Thus the adiabatic gradient at 1673 K (1400°C) is about 14K/GPa. The term $(\partial T/\partial F)_P$ is, of course, just the inverse of $(\partial F/\partial T)_P$ and has a value of 1/0.00285 = 350.88 K. ΔV_m

is about 0.0434 cm^3/g (0.0434 J $MPa^{-1}g^{-1}$) and ΔS_m is about 0.362 J K^{-1} g^{-1}, which corresponds to a slope of the solidus of about 120 K/GPa. From this we calculate a value for $(\partial F/\partial P)_S$ of about -0.12 GPa^{-1}, or about -1.2%/kbar (it is negative because the extent of melt *increases* as pressure *decreases*). Of course, we have greatly simplified matters here by neglecting the pressure and temperature dependencies of all thermodynamic functions. Thus this relationship is only approximate and considering the uncertainty in our assumptions and the thermodynamic parameters, this value could anywhere between -0.08/GPa and –0.2/GPa. So, for example, if a rising packet of mantle intersects the solidus at 100 km depth (≈ 3 GPa), upon reaching a depth of 30 km (~1 GPa) that packet would have undergone 24% melting.

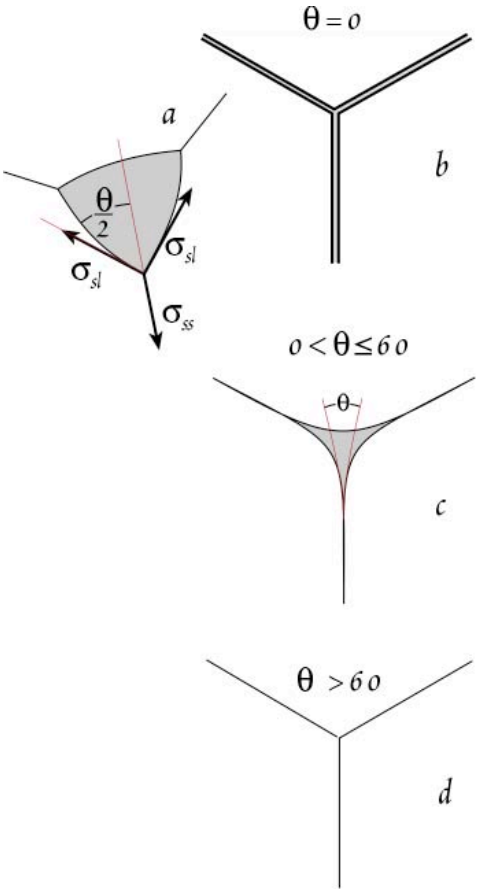

Figure 7.26. Relationship between dihedral angle, θ, and melt distribution at grain triple junctions. (a) Illustrates the balance of solid-solid and solid-liquid interfacial energies, σ_{ss} and σ_{sl}, at the junction. In case (b), the θ = 0, and the melt (shaded) is distributed along grain-grain boundaries as well as triple junctions. In case (c) the melt forms and interconnected network along grain triple junctions. In case (d) θ is greater than 60° and melt is present only at 4-grain junctions. After Kingery (1960) and Kohlstedt (1993).

The solidus temperature of silicates can be substantially lowered by the addition of water and, at high pressures, of CO_2. In the presence of either H_2O or CO_2, the melting curve will be different from that shown in Figure 7.23, and the relationship we deduced between melt, temperature, and pressure will also be different.

A final point to make is that once melt is extracted, the system is no longer isoentropic because the extracted melt carries away some of the entropy of the system. Thus our analysis would be strictly limited to batch melting, where the melt remains in equilibrium with the solid. A complete treatment of the thermodynamics of melting, including fractional melting can be found in Azimov et al. (1997). Morgan (2001) discusses the situation where the material undergoing melting is lithologically heterogeneous.

7.6.6.2 Mantle Permeability and Melt Distribution and Withdrawal

Whether the melting process approximates the batch (equilibrium) model or the fractional model depends on the permeability of the source region. If the source region is highly permeable, melt will flow out as it is created, approximating the fractional melting model; if it is impermeable, it will build up in place before ascending, approximating the equilibrium model. Permeability depends on the degree to which the melt is interconnected, and this in turn depends on the crystal-liquid interfacial energy.

We explored the effects of interfacial energy on nucleation in Chapter 5 (section 5.5.3.3). We found that the difference in interfacial energy determined the geometry of nucleation. Here we wish to consider the case of how a liquid will distribute itself between grains of a solid undergoing melting. We assume that the solid consists of a single phase (e.g., olivine) and that the interfacial energy between these grains is σ_{ss}. Now consider the intersection between 3 such grains (Figure 7.26). When melt is present, there will also be an interfacial energy between the grains and the melt, σ_{sm}. If θ is the angle formed by a melt pocket at a grain triple junction, the balance of forces may be described as:

$$\sigma_{ss} = 2\sigma_{s\ell}\cos\frac{\theta}{2} \qquad 7.79$$

Rearranging, we have:

$$\cos\frac{\theta}{2} = \frac{\sigma_{ss}}{2\sigma_{s\ell}} \qquad 7.80$$

and

$$\theta = 2\arccos\left(\frac{\sigma_{ss}}{2\sigma_{s\ell}}\right) \qquad 7.80a$$

The bottom line is that the lower the solid-liquid interfacial energy, the more extensively melt will interconnect (the more extensively grains will 'wet') and the more readily melt will flow. Considering equation 7.80 in greater detail reveals that, depending on the value of θ, the melt can distribute itself in number of ways. These are illustrated in Figure 7.26. The first case occurs when the solid-solid interfacial energy is twice that of the solid-melt interfacial energy; if so, then cos $\theta/2 = 1$ and $\theta \approx 0$. In this case, solid-solid interfaces are energetically unfavorable and melt will form a thin film that coats all grain boundaries (Figure 7.26b). The second case is where the solid-solid interfacial energy is more than 1.73 times but less than twice that of the solid-melt interfacial energy ($2\sigma_{sl} > \sigma_{ss} > 1.73\sigma_{sm}$) which corresponds to $0 < \theta < 60°$ (Fig. 7.25c). In this case, the melt will form interconnected channels along grain triple junctions, as is illustrated in Figure 7.26, but is absent from grain-grain surfaces. The third case corresponds to $\sigma_{ss} < 1.73\sigma_{sl}$ and $\theta > 60$ (Fig. 7.25d). In this case, melt forms isolated pockets at junctions between 4 or more grains and but is absent elsewhere. These pockets become connected only at relatively high melt fractions (several percent). Permeability will be high for the first two cases where melt forms films or channels that allow melt to flow, but low for the last case of isolated melt pockets. The interfacial energy, and hence θ, depends on temperature, pressure, and the composition of the melt and solid phase, and hence will vary even within a single rock.

Scanning electron microscopy of experiments in which basaltic melt is allowed to come to textural equilibrium with olivine indicate show that θ is characteristically between 25° and 50°. The dihedral angle is larger, typically greater than 60°, for junctions between pyroxene grains and for H_2O and CO_2 fluids (though addition of water to a silicate rock reduces θ). Since the upper mantle consists of over 60% olivine, however, it is likely that melt forms an interconnected network such as that illustrated in Figure 7.27, resulting in high permeability. Experiments in which melt is induced to migrate, either a result of a gradient in melt fraction in the experimental charge or a result of stress, confirm that permeability of mantle material undergoing melting will be high. From our perspective, this means melt is likely to be extracted fairly quickly after it is created, and that very small melt fractions, perhaps as low as 0.1%, can segregate from the mantle. Thus the fractional melting model may more closely approximate melting in the mantle.

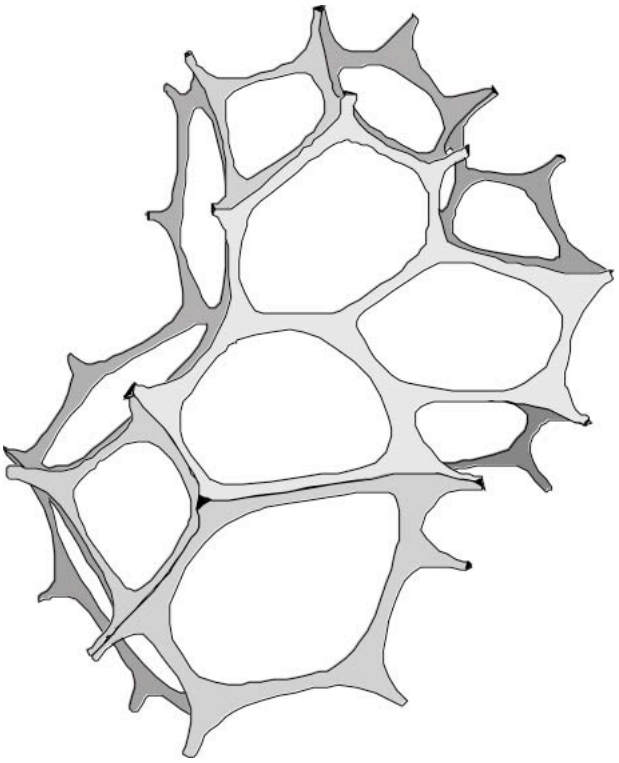

Figure 7.27. Three-dimensional network of formed by melt along triple junctions of olivine grains. From Riley and Kohlstedt (1990).

Laporte (1994) carried out similar experiments with quartz and hydrous silicate melts and found that the dihedral is in the range of 12 to 18°, indicting a high ratio of σ_{ss}/σ_{sl}. This in turn indicates that the permeability within regions of the crust undergoing melting will be relatively high. However, the rate at which melt segregates from its

source depends on melt viscosity as well as permeability. Because the viscosity of even hydrous granitic magmas is 4 orders of magnitude greater than that of basalt, segregation of granitic melt requires a higher melt fraction than does segregation of basaltic melt. Nevertheless, Laporte argues that melt fractions as low as 10% will segregate on time scales of 10^5 yrs, whereas it had been previously believed that melt fractions as high as 30% would not segregate on reasonable geologic time scales.

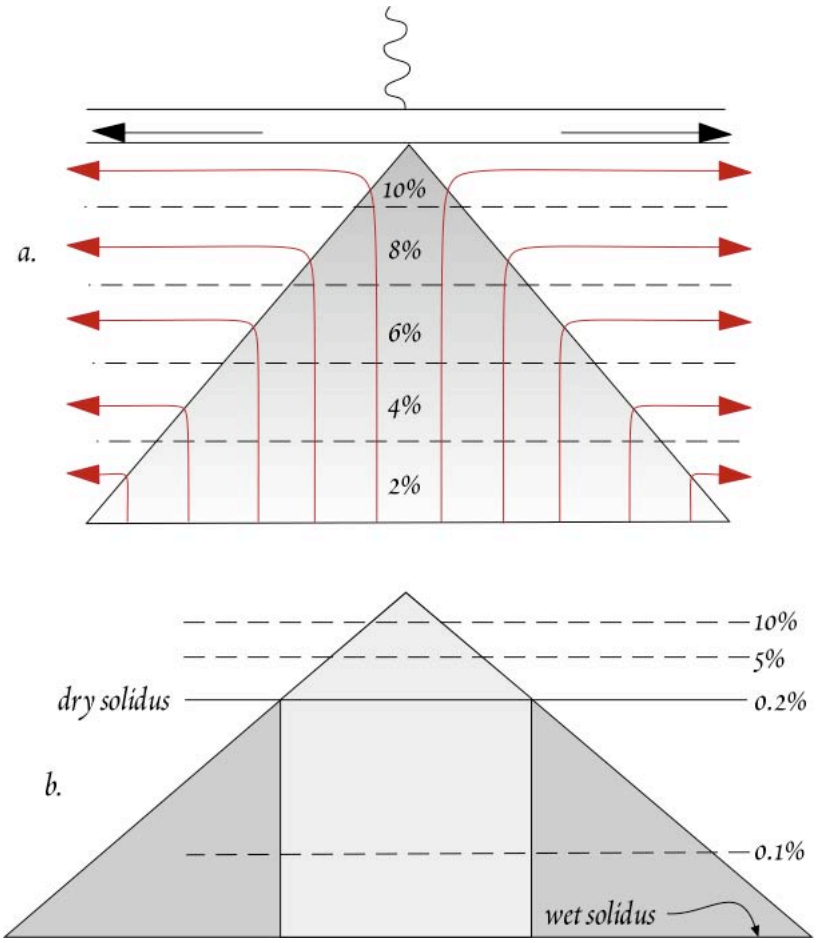

Figure 7.28. (a). Melting regime under a mid-ocean ridge. Red lines show flow of mantle induced by passive spreading of overlying plates. Since melting results from decompression, no further melting occurs once motion becomes horizontal. Only those parts of the mantle directly under the ridge reach the maximum extent of melting. The melting regime along ridge can be assumed to uniform parallel to the ridge, hence the process is two-dimensional. The cartoon is, however, readily adapted to mantle-plume related volcanism by assuming radial symmetry. (b) Low degree melts generated between the "wet" and "dry" solidi could enrich higher degree melts from the normal mantle column (light shading) in highly incompatible elements. However, the volume of this region must be large (typically 10 times that of the normal mantle column) for this to be effective, requiring efficient transport and focussing of melt over scales of hundreds of kilometers. After Plank and Langmuir (1992).

7.6.6.3 Realistic Models of Mantle Melting

As we pointed out above, in most circumstances melting in the mantle occurs because of decompression. (A possible exception is in subduction zones; here the generation of melt is still poorly understood, but may ultimately be due to hydration of the mantle wedge. Addition of water lowers the melting temperature, so this is a form of flux melting.) Decompression melting is necessarily a dynamic process: a parcel of mantle will begin to melt at some depth and will continue to melt as it rises. The fraction of melt produced will increase with height above the initial melting depth. If, as we have argued above, melt segregates readily, melt will rise faster than the solid. As a result, once the parcel of mantle has risen above the depth where melting begins, melt from below will continually stream through it. The melt entering the parcel from below will initially not be in equilibrium with the solid within the parcel, having been produced as a smaller melt fraction at greater depth (and hence greater pressure and temperature). Thus melt passing through the parcel will react with the solid in an attempt to reach equilibrium with it. This is similar to the process we described above as zone refining.

The situation then is analogous to diagenesis in sediments, which we discussed in Chapter 5. There are some differences, however.

In diagenesis, the fraction of solid relative to fluid does not change, except through expulsion of fluid. In the melting process, solid is converted to fluid by nature of the process. In the melting process, length scales are such that diffusion does not significantly contribute to the flux and bioturbation does not exist, so advection is the only significant flux. Furthermore, our reduction of the problem to 1 dimension by assuming lateral uniformity will not be valid for the melting process. This is because the extent of melt will also decrease with distance from the some central point (a point under a volcano or under a spreading mid-ocean ridge), and because melt will be focussed in from these peripheral regions toward the center. With these caveats, however, the diagenetic equation (equ. 5.171) may be directly applicable to the melting process.

Unfortunately, a truly thorough quantitative treatment of the melting process has not yet been undertaken. In one of the more thorough discussions to date, Langmuir et al. (1993) concluded that despite the complexity of the melting process, the batch melting equation gives a reasonably good approximation of incompatible element concentrations in the melt as a function of the *average* degree of melting. Beneath mid-ocean ridges, the average degree of melting will be less than the maximum degree of melting, because different parcels of mantle follow different paths. Only mantle directly beneath the ridge is able to rise the maximum amount, and hence melt the maximum amount. In the simple case illustrated in Figure 7.28a, the average extent of melting is one half the maximum extent. Other ratios are possible for other models of mantle flow.

There are two situations where batch melting may not be a good approximation of incompatible element concentrations. The first is where there is a large volume of mantle from which only very low degree melts are extracted. This situation might arise as a result of suppression of the solidus by H_2O or CO_2 fluid, a well-established phenomenon. If melting is such that a small fraction of melt, say 0.1% or so, is generated between the "wet solidus" (i.e., H_2O or CO_2 present) and the "dry solidus" and the temperature between the two is large, there could be a large region at great depth where very small degree melts are produced (Figure 7.28b). Mixing of these small degree melts with larger degree ones produced above the dry solidus then results in melt compositions different from those predicted by the batch melting equation (Plank and Langmuir, 1992). The second situation occurs when there is a phase change within the melting region. For example, spinel is replaced by garnet as the aluminous phase in the mantle at about 60-90 km depth. These two minerals have very different partition coefficients for some elements (Table 7.5), hence melts produced in the garnet stability region will have different incompatible element concentrations (and in particular, different rare earth patterns) than those in the spinel stability region.

7.7 TRACE ELEMENT DISTRIBUTION DURING CRYSTALLIZATION

7.7.1 EQUILIBRIUM CRYSTALLIZATION

Equilibrium crystallization occurs when the total liquid and total solid remain in equilibrium throughout the crystallization. If we define X as the fraction of material crystallized, then

$$\boxed{\frac{C_i^l}{C_i^0} = \frac{1}{DX + (1 - X)}} \qquad 7.81$$

where C^ℓ is the concentration in the remaining liquid and C° is the concentration in the original liquid (we derive this equation in a manner exactly analogous to equation 7.42). The limit of trace element enrichment or depletion, occurs when $X = 1$ when $C_l/C_0 = 1/D$. Equilibrium crystallization requires the liquid keep contact with all crystals. Crystal interiors would have to maintain equilibrium through solid state diffusion, a slow process. Thus equilibrium crystallization is probably relevant only to a limited range of situations, such as the slow crystallization of an intrusion.

7.7.2 FRACTIONAL CRYSTALLIZATION

Fractional crystallization, which assumes only instantaneous equilibrium between solid and liquid, is a more generally applicable model of crystallization. In this case, trace element concentrations in the

melt are governed by:

$$\frac{C_i^\ell}{C_i^o} = (1-X)^{D-1} \qquad 7.82$$

There is no limit to the enrichment or depletion of the liquid in this case. If D is very large, C^ℓ/C^o approaches 0 as X approaches 1, and it approaches ∞ as X approaches 1 if D is very small. What happens when D=O?

For multiphase crystallization, we need to replace D in equations 7.81 and 7.82 with the bulk distribution coefficient as we defined it in equation 7.46, where m_ϕ in that equation would become the fraction of phase ϕ in the crystallizing mass.

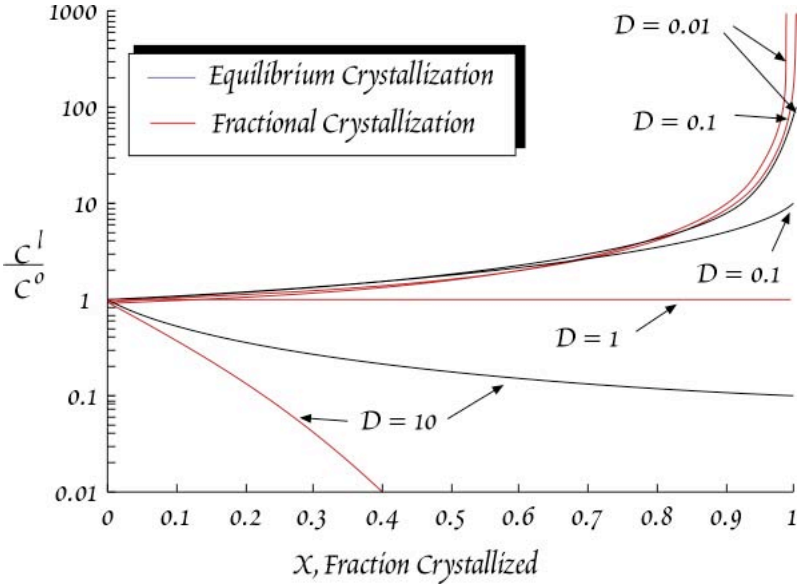

Figure 7.29. Variation of relative trace element concentration in a liquid undergoing crystallization.

Though fractional crystallization can, in principle, produce extreme trace element enrichment, this rarely occurs. A melt that has crystallized 90% or more (which would produce a ten-fold enrichment of a perfectly incompatible element in the melt) would have major element chemistry very different from its parent. From our knowledge of the compositional dependence of partition coefficients we could predict that incompatible elements would have partition coefficients close to 1 for such an acid melt[§]. This limits the enrichment of incompatible elements. However, highly *compatible* elements (elements with solid/liquid partition coefficients greater than 1 such as Ni) do have concentrations that approach 0 in fractionated melts (generally they disappear below detection limits). Variation of relative trace element concentration as a function of the fraction of liquid remaining is shown in Figure 7.29.

In summary, for moderate amounts of fractionation, crystallization has only a moderate effect on trace element concentrations, given that these concentrations vary by orders of magnitude.

7.7.3 *In Situ* Crystallization

A magma chamber is likely to be substantially hotter than the rock surrounding it, which will result in a substantial thermal gradient at the margin of the chamber. Thus the margins, particularly the roof and walls, are likely to be cooler than the interior and it is here where crystallization will primarily occur. Crystals sloughed from the walls and roof would accumulate on the floor. When crystallization is restricted to marginal zones of the chamber, magma composition will evolve in a somewhat different manner than for simple fractional crystallization. Langmuir (1989) called this process *in situ crystallization*.

Imagine a magma chamber that is bounded by a zone of well-consolidated crystals at the margin. There may be some liquid within this zone, but we assume that the permeability is sufficiently low that it will never return to the magma chamber. Between this 'cumulate zone' and the free magma is a transition zone of higher permeability, which we call the 'solidification zone' (Figure 7.30). Magma is added to the solidification zone as crystallization advances into the chamber. As crystallization and compaction proceed within the solidification zone, liquid is expelled back into the central magma. The

§ Silica-rich, or silicic, melts are sometimes referred to as "acidic" and Mg and Fe-rich ones as "basic". The reason is historical: it was once though that silica was present in melts as H_4SiO_4. This is not the case, but the terminology persists.

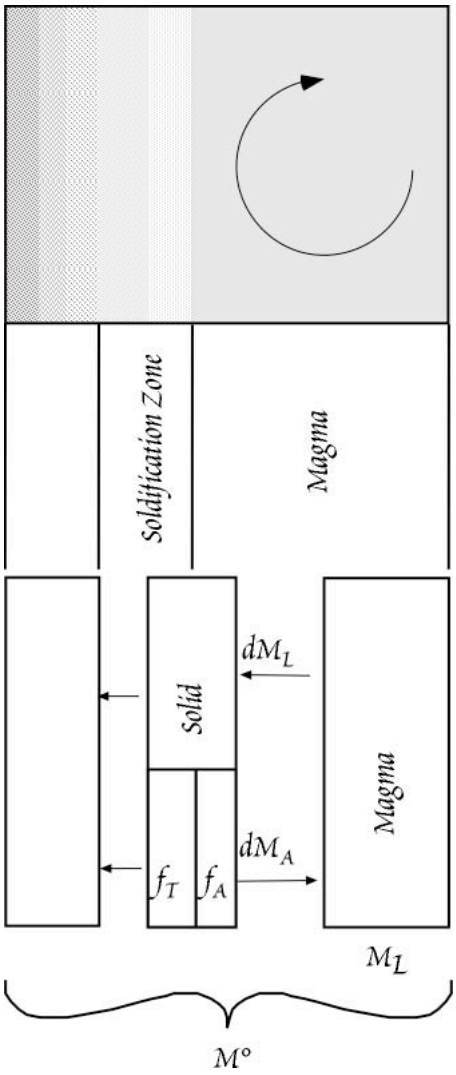

Figure 7.30. Cartoon of magma chamber undergoing *in situ* crystallization. The solidification zone is the transition region between consolidated cumulates (that nevertheless retain some trapped liquid) and the magma chamber. As crystallization proceeds, some liquid will be expelled from the solidification zone back into the magma. After Langmuir (1989).

flux of magma to the solidification zone we will designate dM_I and the return flux as dM_A. We let f be the fraction of interstitial liquid remaining after crystallization within the solidification zone, and $(1 - f)$ be fraction of liquid crystallized within this zone. Some fraction f_T of the liquid remains to form the trapped liquid within the cumulate zone, and some fraction f_A returns to the magma, so that $f = f_T + f_A$. Hence:

$$dM_A = f_A dM_I \qquad 7.83$$

If the magma plus cumulates form a closed system, then the change in mass of liquid within the chamber is the difference between the flux into and out of the solidification zone:

$$dM_L = dM_A - dM_I = dM_I(f_A - 1) \qquad 7.84$$

If C_L is the concentration of some element in the magma and C_f is the concentration in the liquid returning from the solidification zone, then the change in mass of the element is:

$$d(M_L C_L) = C_L dM_L + M_L dC_L = C_f dM_A - C_L dM_I \qquad 7.85$$

We define the parameter E as ratio of the concentration in the magma to that in the returning liquid:

$$E = C_f / C_L \qquad 7.86$$

E will depend on the partition coefficient for the element of interest and on the manner in which crystallization proceeds within the solidification zone. If, for example, we assume that there is complete equilibration between crystals and liquid within the zone, then from equ. 7.81:

$$E = \frac{1}{D(1-f)+f} \qquad 7.87$$

Substituting equation 7.83, 7.85, and 7.86 into 7.84 and rearranging, we have:

$$\frac{dC_L}{C_L} = \frac{dM_L}{M_L}\left(\frac{f_A(E-1)}{f_A - 1}\right) \qquad 7.88$$

Assuming E and f_A are constants, we can integrate 7.88 to yield:

$$\frac{C_L}{C^0} = \left(\frac{M_L}{M^0}\right)^{f_A(E-1)/(f_A-1)} \qquad 7.89$$

Figure 7.31 compares the change in concentration due to *in situ* crystallization and fractional crystallization for two values of D and several values of f. In general, *in situ* crystallization results in less enrichment of incompatible elements and less depletion of compatible elements for a given degree of crystallization of a magma body than does fractional crystallization. The degree of enrichment depends on f, the fractional of liquid remaining when liquid is expelled from the solidification zone. For very small values of f, that is, complete crystallization within the solidification zone, the composition of the magma remains nearly constant. For f=1, that is, for no crystallization within the solidification zone, equation 7.89 reduces to equation 7.82, and the *in situ* curves in Figure 7.31 coincide with the fractional crystallization curves.

CHAPTER 7: TRACE ELEMENTS

7.7.4 CRYSTALLIZATION IN OPEN SYSTEM MAGMA CHAMBERS

Thus far, we have treated crystallization only in closed systems, that is, where a certain volume of magma is intruded and subsequently cools and crystallizes without withdrawal or further addition of magma. This is certainly not a very realistic model of magmatism and volcanism. In the well-studied Hawaiian volcanoes for example, injections of new magma into crustal magma chambers are fairly frequent. Indeed, it appears that addition of magma to the Kilauean magma chamber is nearly continuous. Furthermore, many igneous rocks show petrographic evidence of mixing of differentiated magmas with more primitive ones. In this section, we consider the concentrations of trace elements in open magma chambers; that is, the case where new 'primary' magma mixes with a magma that has already undergone some fractional crystallization. Magma chambers where crystallization, eruption and addition of new magma are sometimes called RTF magma chambers, the RTF referring to "refilled", "tapped", and "fractionated".

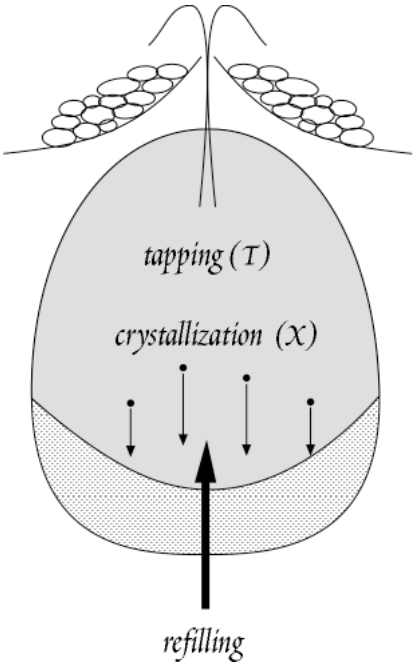

Figure 7.32. Schematic illustration of a steady-state and periodically refilled, fractionally crystallized, and tapped magma chamber beneath a mid-ocean ridge.

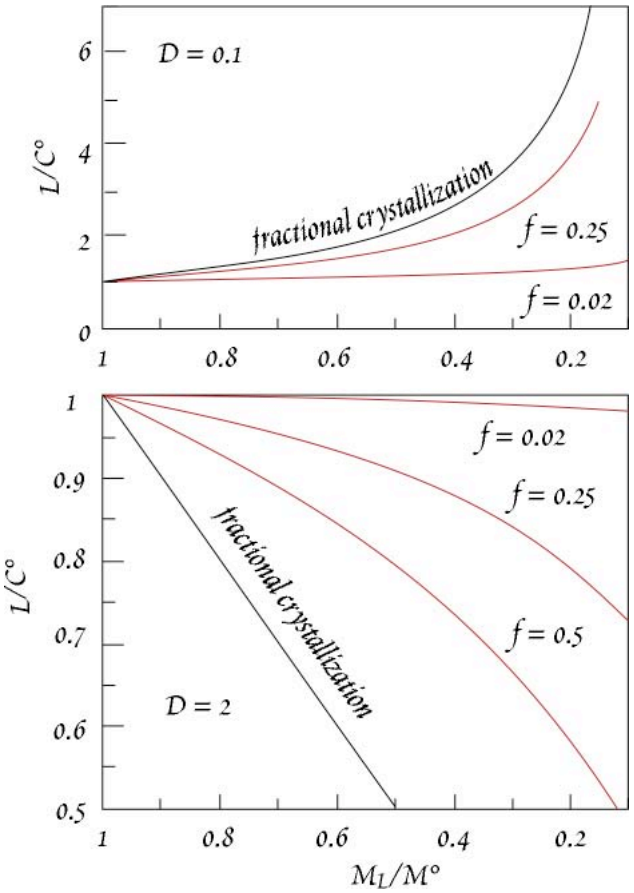

Figure 7.31. Comparison of the effects of *in situ* and fractional crystallization on concentration for two values of the distribution coefficient, D, and several values of f. f_A is assumed to equal f, i.e., no trapped liquid remains in the cumulate zone. After Langmuir (1989).

The extreme case of an RTF magma chamber is a *steady state* system, where magma resupply rate equals the rate of crystallization and eruption, thus maintaining a constant volume of liquid (Figure 7.32). In such a magma chamber, the concentrations of all elements eventually reach steady state after many cycles of refilling, eruption, and fractional crystallization. Steady state occurs when the rate of supply of the elements (due addition of new magma) becomes equal to the rate of loss (due to crystallization and withdrawal and eruption of magma).

To understand how steady state is achieved, consider a cyclic process where a volume C is lost by crystallization and a volume T is lost by eruption and a volume $(T + C)$ is added to the magma chamber during each cycle. For incompatible elements, the concentration in the liquid initially increases because a greater mass of these elements is added by refilling than is lost by crystallization and eruption. As the concentration in the liquid increases, so

does the concentration in the solid since $C^s = D^{s/l} C^l$ ($D^{s/l}$ would be a bulk distribution coefficient if more than 1 phase is crystallizing). Eventually a point is reached where the concentration in the solid is so great, that loss of the element by crystallization and eruption equals the gain resulting from crystallization.

We can quickly derive an expression for the steady-state concentration of an element in the *equilibrium crystallization* case. In the steady-state, the losses of an element must equal gains of that element, so:

$$C^\circ(X + T) = TC^{ssl} + XC^s \qquad 7.90$$

where C° is the concentration in the primary magma being added to the chamber, C^{ssl} is the concentration in the steady-state liquid, and C^s is the concentration in the solid. Since $C^s = D^{s/l}C^{ssl}$:

$$C^\circ(X + T) = TC^{ssl} + XDC^{ssl} \qquad 7.91$$

We can rearrange this to obtain the enrichment in the steady-state liquid relative to the primary magma:

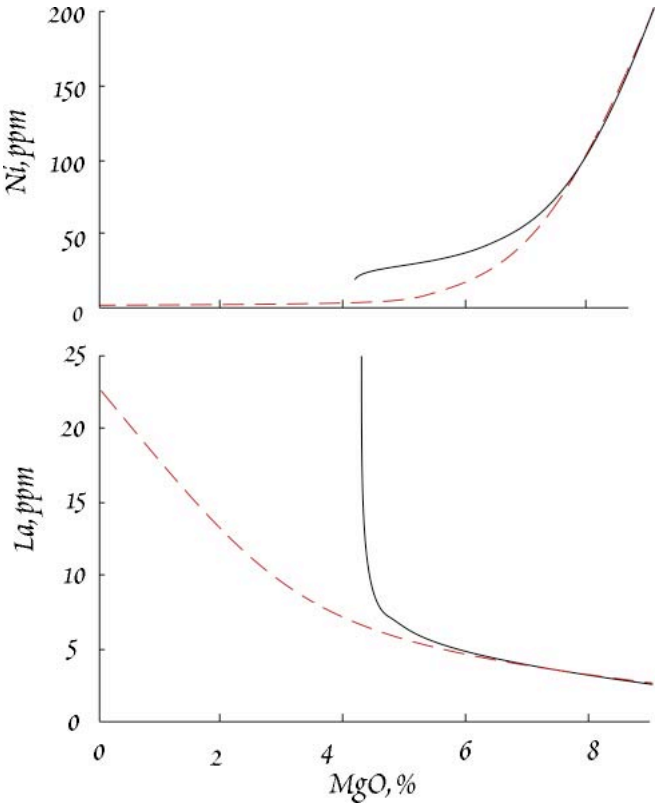

Figure 7.34. La and Ni concentrations plotted against MgO concentration in a basalt undergoing closed system fractional crystallization (dashed line) and in a steady-state magma chamber where the mass of new magma equals the mass crystallized in each cycle.

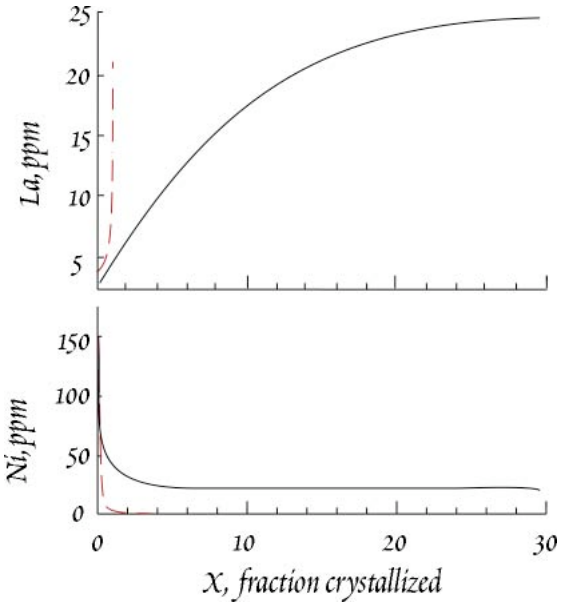

Figure 7.33. Concentration of Ni and La in closed system fractional crystallization (dashed line) and open system crystallization (solid line) as a function of the fraction crystallized. In the open system case the mass injected into the chamber is equal to the mass crystallized (i.e., Y = 0).

$$\frac{C^{ssl}}{C^0} = \frac{X + T}{X + TD^{s/l}} \qquad 7.92$$

For the fractional crystallization case, the enrichment factor is:

$$\frac{C^{ssl}}{C^0} = \frac{(X + T)(1 - X)^{D-1}}{1 - (1 - X - T)(1 - X)^{D-1}} \qquad 7.93$$

These equations are from O'Hara (1977).

Compatible element concentrations reach steady state after few cycles than do incompatible elements. This is illustrated in Figure 7.33, which shows how the concentrations of La, an incompatible element, and Ni, a compatible element, vary as function of the total amount crystallized in a steady-state system. The Ni concentration, which is 200 ppm in the primary magma, reaches a steady-state concentration of about 20 ppm after the equivalent of 5 magma chamber masses has crystallized. After the equivalent of 30 magma chamber masses crystallization, La has not quite reached its steady state concentration of around 25 ppm.

Unfortunately, it is never possible to measure

the fraction of magma that has crystallized. In place of our parameter, X, petrologists often use the concentration of some 'index species', i.e., some species whose behavior is relatively well understood and whose concentration should vary smoothly as a function of the fraction crystallized. In basalts, MgO is commonly used as the index species, SiO_2 is a more common index in more acid magmas such as andesites and dacites. Figure 7.34 shows the La and Ni concentrations in the same steady-state system. Since MgO is a compatible element (though not a trace element, we could treat it using the same equations we have derived for trace elements) it quickly reaches a steady state concentration around 4.25% while the La concentration continues to increase. Lavas erupted from this magma chamber could thus have essentially constant MgO and Ni concentrations, but variable La concentrations. This apparent 'decoupling' of compatible and incompatible element concentrations is a feature of open magmatic systems.

7.8 Summary of Trace Element Variations during Melting and Crystallization

For moderate amounts of crystallization, fractional crystallization does not have dramatic effects on *incompatible* elements concentrations. Concentrations of highly *compatible* elements are, however, dramatically affected by fractional crystallization. The RTF model does have significantly greater effects on incompatible element concentrations than simpler models, however.

Partial melting has much more dramatic effects on *incompatible* element concentrations. It is likely much of the incompatible element variations observed in magmas and magmatic rocks are related to variations in degree of melting. Depth of melting also has an effect, in that the phases with which melts equilibrate vary with depth. For example, the presence of garnet dramatically affects rare earth element (REE) abundances. The heavy rare earths are accepted into the garnet structure and have D's > 1. The lights are, however, highly rejected. The presence of garnet in the partial melting residua thus can lead to strong light rare earth enrichment of the melt.

Two simplifications are important for partial melting (both batch and fractional). *When $D << F$, the enrichment is $1/F$.* Thus for small D, the enrichment is highly dependent on the degree of melting. If D is large, i.e., $D > 1$ and $D >> F$, the depletion of the element in the melt is rather insensitive to F. In either case, *when F approaches 0, the maximum enrichment or depletion is $1/D$.*

Highly *compatible* elements are, of course, depleted in a partial melt. But the degree of depletion is rather insensitive to the degree of melting for values of F likely to occur in the mantle (<.25). It must be emphasized that we have no good constraints on the absolute values of F.

This all works out nicely: *compatible element are good qualitative indicators of the extent of fractional crystallization and incompatible elements are good indicators of the degree of melting.*

Both geochemical and (experimental) petrological evidence indicates that alkali basalts and their kin are the result of lower degrees of melting than tholeiites. Highly undersaturated rocks such as nephelinites are probably produced by the smallest degrees of melting (1% or less). At the same time, alkali basalts are probably also the products of deeper melting.

Ratios of incompatible elements are generally less sensitive to fractional crystallization and partial melting than are absolute abundances, particularly if they are of similar incompatibility. For relatively large extents of melting, the ratio of two incompatible elements in a magma will be similar to that ratio in the magma source. For this reason, trace element geochemists are often more interested in the ratios of elements than in absolute abundances.

One approach commonly used is to plot the ratio of two incompatible elements against the abundance of the least compatible of the two. This kind of plot is sometimes referred to as a *process identification plot* because fractional crystallization and partial melting result in very different slopes on such a diagram. Figure 7.35 is a schematic version of a process identification plot. Crystallization, both fractional and equilibrium produce rather flat slopes on such a diagram, as does crystallization in an open system magma chamber. Partial melting produces a much steeper slope and the slope of produced by aggregates of fractional melts is similar to that of equilibrium partial melting. *In Situ* crystallization can produce a range of slopes depending on the value of f. Langmuir (1989) found a that a value for f of

0.25 best matched the variation observed in the Kiglapait Intrusion in Labrador, a classic large layered intrusion. Assuming this value of f is typical, then the change in a trace element ratio due to *in situ* crystallization should be only moderately greater than for fractional crystallization.

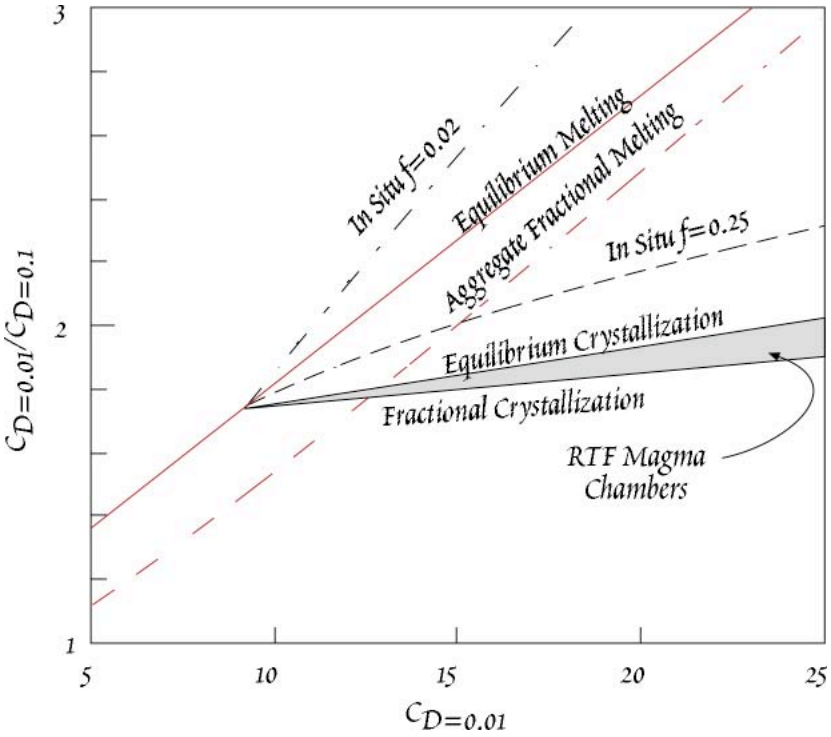

Figure 7.35. Plot of the ratio of two incompatible elements (one with D=0.01, the other with D=0.1) vs. the concentration of the more incompatible element. Plot shows calculated effects of equilibrium partial melting and aggregate partial melting assuming concentrations of 1 in the source for both elements. Other lines show the effect of crystallization on the composition of a liquid produced by 10% equilibrium melting. Fractional crystallization, equilibrium crystallization, and open system crystallization (RTF magma chambers) produce less variation of the ratio than does partial melting. *In Situ* crystallization can mimic the effect of partial melting if the value of f, the fraction of liquid returned to the magma, is sufficiently small.

REFERENCES AND SUGGESTIONS FOR FURTHER READING

Albarède, F. 1995. *Introduction to Geochemical Modeling*. Cambridge: Cambridge Univ. Press.

Azimov, P. D., M. M. Hirschmann and E. Stolper, 1997. An analysis of variations in isentropic melt productivity, *Phil Trans R Soc Lond A*, 355:255-281.

Beattie, P. 1993. Olivine-melt and orthopyroxene-melt equilibria. *Contrib. Mineral. Petrol.* 115: 103-111.

Beattie, P. 1994. Systematics and energetics of trace-element partitioning between olivine and silicate melts: implications for the nature of mineral/melt partitioning. *Chem. Geol.* 117: 57-71.

Beattie, P., M. Drake, J. Jones, W. Leeman, J. Longhi, et al. 1993. Terminology for trace-element partitioning. *Geochim. Cosmochim. Acta*. 57: 1605-1606.

Ben Othman, D., W. M. White and J. Patchett. 1989. The geochemistry of marine sediments, island arc magma genesis, and crust-mantle recycling. *Earth Planet. Sci. Lett*. 94: 1-21.

Blundy, J. D., J. C. Robinson and B. J. Wood, 1998. Heavy REE are compatible in clinopyroxene on the spinel lherzolite solidus, *Earth Planet. Sci. Lett.*, 160:493-504.

Blundy, J. and B. Wood, 1994. Prediction of crystal-melt partition coefficients from elastic moduli, *Nature*, 372:452-454.

Blundy, J. and B. Wood, 2003. Partitioning of trace elements between crystals and melts, *Earth Planet. Sci. Lett.*, 210: 383-397.

Brice, J. C., 1975. some thermodynamic aspects of the growth of strained crystals, *J. Cryst. Growth*, 28:249-253.

Brügmann, G. E., A. J. Naldrett, M. Asif, P. C. Lightfoot, N. S. Gorbachev, et al. 1993. Siderophile and chalcophile metals as tracers of the evolution of the Siberian Trap in the Noril'sk region, Russia. *Geochim. Cosmochim. Acta*. 57: 2001-2018.

CHAPTER 7: TRACE ELEMENTS

Brügmann, G. E., N. T. Arndt, A. W. Hofmann and H. J. Tobschall. 1987. Noble metal abundances in komatiite suites from Alexo, Ontanrio, and Gorgona Island, Columbia. *Geochim. Cosmochim. Acta*. 51: 2159-2171.

Burns, R. G. 1970. *Mineralogical Applications of Crystal Field Theory*. Cambridge: Cambridge Univ. Press.

Burns, R. G. 1973. The partitioning of trace transition elements in crystal structures: a provocative review with applications to mantle geochemistry. *Geochimica et Cosmochimica Acta*. 37: 2395-2403.

Carroll, M. R. and D. S. Draper. 1994. Noble gases as trace elements in magmatic processes. *Chem. Geol.* 117: 37-56.

Chaussidon, M. and G. Libourel. 1993. Boron partitioning in the upper mantle: an experimental study. *Geochim. Cosmochim. Acta*. 57: 5053-5062.

Chazot, G., M. Menzies and B. Harte. in press. Determination of partition coefficients between apatite, clinopyroxene, amphibole and melt in natural spinel lherzolites from Yemen: implications for wet melting of the lithospheric mantle. *Geochim. Cosmochim. Acta*.

Drake, M. J. and D. F. Weill, 1975. Partition of Sr, Ba, Ca, Y, Eu^{2+}, Eu^{3+}, and other REE between plagioclase feldspar and magmatic liquid: an experimental study, *Geochim. Cosmochim. Acta*, 39, 689–712.

Dunn, T. and C. Sen. 1994. Mineral/matrix partition coefficients for orthopyroxene, plagioclase, and olivine in basaltic to andesitic systems: a combined analytical and experimental study. *Geochim. Cosmochim. Acta*. 58: 717-734.

Elderfield, H. and M. J. Greaves. 1982. The rare earth elements in seawater. *Nature*. 296: 214-219.

Fryer, B. J. and J. D. Greenough. 1992. Evidence for mantle heterogeneity from platinum-group element abundances in Indian Ocean basalts. *Can. J. Earth Sci.* 29: 2329-2340.

Gallahan, W. E. and R. L. Nielsen, 1992. The partitioning of Sc, Y and the rare earth elements between high-Ca pyroxene and natural mafic to intermediate lavas at 1 atmosphere, *Geochim. Cosmochim. Acta*, 56, 2387-2404.

Green, T. H. 1994. Experimental studies of trace-element partitioning applicable to igneous petrogenesis: Sedona 16 years later. *Chem. Geol.* 117: 1-36.

Hack, P. J., R. L. Nielsen and A. D. Johnston. 1994. Experimentally determined rare-earth element and Y partitioning behavior between clinopyroxene and basaltic liquids at pressures up to 20 kbar. *Chem. Geol.* 117: 89-105.

Hanson, G. N., 1980. Rare earth elements in petrogenetic studies of igneous systems, *Ann. Rev. Earth Planet. Sci.*, 8, 371-406.

Hart, S. R. 1993. Equilibration during mantle melting: a fractal tree model. *Proc. Natl Acad. Sci. USA*. 90: 11914-11918.

Hart, S. R. and C. Brooks. 1974. Clinopyroxene-matrix partitioning of K, Rb, Cs, Sr, and Ba. *Geochim. Cosmochim. Acta*. 38: 1799-1806.

Hart, S. R. and C. J. Allègre, 1980. Trace element constraints on magma genesis, in *Physics of magmatic processes*, edited by R. B. Hargraves, p. 121-159, Princeton University Press, Princeton.

Hart, S. R. and T. Dunn. 1993. Experimental cpx/melt partitioning of 24 trace elements. *Contrib. Mineral. Petrol.* 113: 1-8.

Hauri, E. H., T. P. Wagner and T. L. Grove. 1994. Experimental and natural partitioning of Th, U, Pb and other trace elements between garnet, clinopyroxene and basaltic melts. *Chem. Geol.* 117: 149-166.

Hie}stra, S. A. 1979. The role of collectgors in the formation of platinum deposits in the Bushveld Complex. *Can. Mineral.* 17: 469-482.

Irving, A. J. 1978. A review of experimental studies of crystal/liquid trace element partitioning. *Geochim. Cosmochim. Acta*. 42: 743-770.

Jochum, K. P., A. W. Hofmann and H. M. Seufert. 1993. Tin in mantle-derived rocks: Constraints on Earth evolution. *Geochim. Cosmochim. Acta*. 57: 3585-3595.

Jochum, K.-P., A. W. Hofmann and H. M. Seifert. 1985. Sn and Sb in oceanic basalts and the depletion of the siderophile elements in the primitive mantle (abs). *EOS*. 66: 1113.

Jones, J. H.1995. Experimental trace element partitioning. in *Rock Physics and Phase Relations: a Handbook of Physical Constants, AGU Reference Shelf 3*, ed. T. J. Ahrens. 73-104. Washington: AGU.

Kennedy, A. K., G. E. Lofgren and G. J. Wasserburg. 1993. An experimental study of trace element partitioning between olivine, orthopyroxene and melt in chondrules: equilibrium values and kinetic effects. *Earth Planet. Sci. Lett.* 115: 177-195.

Kohlstedt, D. L., 1993. Structure, rheology and permeability of partially molten rocks at low melt fractions, in *Mantle flow and melt generation at mid-ocean ridges, Geophysical Monograph 71*, edited by J. P. Morgan, D. K. Blackman and J. M. Sinton, p. 103-121, AGU, Washington.

Kohn, S. C. and P. F. Schofield. 1994. The implication of melt composition in controlling trace-element behavior: an experimental study of Mn and Zn partitioning between forsterite and silicate melts. *Chem. Geol.* 117: 73-87.

Langmuir, C. H., 1989. Geochemical consequences of *in situ* crystallization, *Nature*, 340, 199-2059.

Langmuir, C. H., E. M. Klein and T. Plank, 1993. Petrological systematics of mid-ocean ridge basalts: constraints on melt generation beneath oceanic ridges, in *Mantle flow and melt generation at mid-ocean ridges, Geophysical Monograph 71*, edited by J. P. Morgan, D. K. Blackman and J. M. Sinton, p. 183-280, AGU, Washington.

Laporte, D. 1994. Wetting behavior of partial melts during crustal anatexis: the distribution of hydrous silicic melts in polycrystalline aggregates of quartz. *Contrib. Mineral. Petrol.* 116: 486-499.

McClure, D. S. 1957. The distribution of transition metal cations in spinel. *J. Phys. Chem. Solids*. 3: 311-317.

McClure, D. S., 1957. The distribution of transition metal ions in spinels, *J. Chem. Solids*. 3, 311-317.

McLennan, S. M. 1989. Rare earth elements in sedimentary rocks: influence of provenance and sedimentary processes. in *Geochemistry and mineralogy of the rare earths, Reviews in Mineralogy 21*, ed. B. R. Lipin and G. A. McKay. 169-200. Washington: Mineral. Soc. Am.

Mitchell, R. H. and R. R. Keays. 1981. Abundance and distribution of gold, palladium and iridium in some spinel and garnet lherzolites: implications for the nature and origin of precisou metal-rich intergranular components in the upper mantle. *Geochim. Cosmochim. Acta*. 45: 2425-2442.

Morgan, J. P., 2001. Thermodynamics of pressure release melting of a veined plum pudding mantle, *Geochem. Geophys. Geosyst.*, 2: paper number 2002GC000049.

Mysen, B. O., 1976. Partitioning of samarium and nickel between olivine, orthopyroxene, and liquid: preliminary data at 20 kbar and 1025°C, *Earth Planet Sci. Lett.*, 31: 1-7.

Mysen, B. O., 1978. Experimental determination of nickel partition coefficients between liquid, paragasite, and garnet peridotite minerals and concentration limits to behavior according to Henry's Law at high pressure and temperature, *Am. J. Sci.*, 278: 217-243.

Nagasawa, H., H. D. Schrieber and R. V. Morris. 1980. Experimental mineral/liquid partition coefficients of the rare earth elements (REE), Sc and Sr for perovskite, spinel, and melilite. *Earth Planet. Sci. Lett.* 46: 431-437.

Nakamura, N., 1974. Determination of REE, Ba, Fe, Mg, Ba, and K in carbonaceous and ordinary chondrites, *Geochim. Cosmochim. Acta*, 38: 7577-775.

Newsom, H. E., W. M. White, K. P. Jochum and A. W. Hofmann. 1986. Siderophile and chalcophile element abundances in oceanic basalts, Pb isotope evolution and growth of the Earth's core. *Earth Planet. Sci. Lett.* 80: 299-313.

O'Hara, M. J., 1977. Geochemical evolution during fractional crystallization of a periodically refilled magma chamber, Nature, 266: 503-507.

O'Hara, M. J., 1985. Importance of the 'shape' of the melting regime during partial melting of the mantle. *Nature*, 314: 58-62.

Onuma, N., H. Higuchi, H. Wakita and H. Nagasawa, 1968. Trace element partition between two pyroxenes and the host lava, *Earth Planet. Sci. Lett.*, 5:47-51.

Orgel, L. E. 1966. *An Introduction to Transition Metal Chemistry: Ligand Field Theory*. London: Methuen.

Orgel, L. E., 1960. *An Introduction to Transition-Metal Chemistry: Ligand-Field Theory*, Methuen and Co., London.

Piper, D. Z. 1994. Rare earth elements in the sedimentary cycle: a summary. *Chem. Geol.* 14: 285-304.

Plank, T. and C. H. Langmuir. 1992. Effects of the melting regime on the composition of the oceanic crust. *J. Geophys. Res.* 97: 19749-19770.

Riley, G. N. and D. L. Kohlstedt, 1990. Kinetics of melt migration in upper mantle-type rocks, *Earth Planet. Sci. Lett.*, 105, 500-521.

Rollinson, H. 1993. *Using Geochemical Data: Evaluation, Presentation, Interpretation*. Essex: Longman Scientific and Technical.

Shaw, D.M., 1970. Trace element fractionation during anatexis, *Geochim. Cosmochim. Acta*, 34: 237-243.

Stockman, H. W. 1982. *Noble metals in the Ronda and Josephine peridotites*, PhD dissertation. Cambridge. M.I.T., 1982.

Taylor, S. R., and S. M. McLennan, 1985. *The Continental Crust: its Composition and Evolution*. 312 p., Blackwell Scientific Publications, Oxford.

Van Westenen, W., J. D. Blundy and B. J. Wood, 2001. High field strength element/rare earth element fractionation during partial melting in the presence of garnet: Implications for identification of mantle heterogeneities, *Geochem. Geophys. Geosyst.*, 2: paper number 2000GC000133.

Watson, E. B., 1976, Two-liquid partition coefficients: experimental data and geochemical implications, *Contrib. Mineral. Petrol.*, 56: 119-134.

Wood, B. J., J. D. Blundy and J. C. Robinson, 1999. The role of clinopyroxene in generating U-series disequilibrium during mantle melting, *Geochim. Cosmochim. Acta*, 63:1613-1620.

PROBLEMS

1. For one element in the "other" category in Figure 7.3, write several paragraphs on its geochemistry. Include answers to the following: what valence state (or states) will it have in nature? What is its ionic radius in its most common valence state (preferably in octahedral coordination)? What is its electronegativity? What kinds of bonds will it most likely form? How will it behave, in particular what it its solubility, in aqueous solution? What element will it most easily substitute for in silicate rocks? Is it volatile or does it form volatile compounds? Is it siderophile or chalcophile? Will it behave as a compatible or incompatible element? What are its uses? What are the primary sources of the element for use by man?

2. Make rare earth plots for the following two samples. For the granite, plot it normalized to one of the chondritic values in Table 7.3. For the Mn nodule, make one plot normalizing it to chondrites and one plot normalizing it to average shale. Describe the features of the REE patterns.

	La	Ce	Pr	Nd	Sm	Eu	Gd	Tb	Dy	Ho	Er	Tm	Yb	Lu
Granite	41	75		25	3.6	0.6	2.7		1.3				0.4	
Mn-nodule	110	858		116	24	4.9	24		24.1		14.4		13	1.92

3. Using the Blundy and Wood model, calculate the partition coefficients for the alkali metals in plagioclase at 1250° C. Assume that the site radius in 124 nm and that an ion of this radius would have a partition coefficient of 1. Assume that the value of Young's Modulus in plagioclase is 64 GPa and that ionic radii for the alkali are as follows: Li: 76 pm, Na 102 pm, K 138 pm, Rb 152 pm, and Cs 167 pm.

4. Relatively Ca-rich garnets (i.e., grossular-rich) appear to accept high field strength elements in both the X (normally occupied by Ca^{2+}, Mg^{2+}, Fe^{2+}, etc.) and Y (normally occupied by Al^{3+}, Fe^{3+}, etc.) crystallographic sites. The garnet/liquid partition coefficient should be the sum of the individual partition coefficients for each site. Assume that D_0, r_0, and E for the X site are 7, 91 pm and 1350 GPa respectively, and the corresponding values for the Y site are 1.9, 67 pm, and 920 GPa respectively. Ions in the X site will be in 8-fold coordination, while ions in the Y site will be in six-fold coordination. In 8-fold coordination, the ionic radii of Zr^{4+}, Hf^{4+}, Th^{4+}, and U^{4+} are 84 pm, 83 pm, 105 pm, and 100 pm respectively; in six fold coordination they will be 72 pm, 71 pm, 94 pm, and 89 pm respectively. Calculate the garnet/liquid partition coefficients for these 4 elements at 1250°C using the Blundy and Wood model.

5. Does Gallahan and Nielsen's (1992) equation for the cpx/liquid partition coefficient (equation 7.31) have the form you expect from thermodynamics? If so, what does the *a* parameter represent? What does the *b* parameter represent? Derive this equation from the thermodynamic relationships we developed in Chapter 3.

6. Calculate the cpx/melt partition coefficients for La and Sm using the method of Gallahan and Nielsen (1992) for the following basalt from Reunion Island:

SiO_2	46.99	
TiO_2	2.66	
Al_2O_3	13.57	
Fe_2O_3	13.38	(total Fe as Fe_2O_3)
MnO	0.18	
MgO	9.78	
CaO	9.51	
Na_2O	2.91	
K_2O	0.88	
P_2O_5	0.35	

7. Construct a table similar to Table 7.3 showing electronic configuration and CFSE (in terms of Δ_t) for both high spin and low spin states in *tetralhedral* coordination for Ti^{2+}, V^{2+},Fe^{2+}, Co^{2+}, Ni^{2+}, and Cu^{2+}.

8. The Table below gives the spectroscopically measured octahedral crystal-field splitting parameter (Δ_o) of oxides for several transition metal ions.

(a) For each ion below, calculate the octahedral CFSE (crystal-field stabilization energy), in joules per mole, for the high spin state. The data are given in terms of wavenumber, which is the inverse of wavelength, λ. Recall from your physics that $\lambda = c/\nu$, and that $e = h\nu$. Useful constants are: $h = 6.626 \times 10^{-34}$ joule-sec, $c = 2.998 \times 10^{10}$ cm/sec, $N_A = 6.023 \times 10^{23}$ atoms/mole.

(b) Assuming $\Delta_t = {}^4/_9\Delta_o$, use the table you constructed in problem 1 to calculate the tetrahedral CFSE for the high spin state.

(c) Calculate the OSPE (octahedral site preference energy) for each. (OSPE = Octa. CFSE – tetra. CFSE)

Ion	Δ_O (cm^{-1})
Ti^{2+}	16,100
V^{2+}	13,550
Fe^{2+}	11,200
Co^{2+}	8,080
Ni^{2+}	7,240
Cu^{2+}	12,600

9. Calculate the relative concentrations (i.e., C^l/C^o) in a partial melt at increments of F = 0.1, under the following assumptions:

(a.) Homogeneous solid phase, equilibrium (batch) melting for D = 0.01 and D = 10.

(b.) Calculate the relative concentration in the aggregate liquid for fractional melting for D = 0.01 and D = 10.

(c.) Plot C^l/C^o vs. F for a and b on the same graph, labeling each curve (use different colors or line types as well).

10. Calculate the enrichment in rare earth elements in an equilibrium partial melt of a mantle consisting of 10% cpx, 5% gar, 25% opx and 60% ol, assuming *modal* (phases enter the melt in the same proportion as they exist in the solid) melting for F = 0.02 and F = 0.10. Assume the concentrations in the mantle are chondritic. Use the partition coefficients given in Table 7.5. *Where data is missing in this table,*

interpolate the values of partition coefficients. Use only the following 8 rare earths: La, Ce, Nd, Sm, Eu, Gd, Dy, and Lu. Plot the results on a semi-log plot of chondrite-normalized abundance vs atomic number (i.e. typical REE plot). Draw a smooth curve through the REE, interpolating the other REE. (Hint: *work only with chondrite-normalized abundances, don't worry about absolute concentrations, so the* C^0 *values will all be 1*).

11. Calculate the relative enrichments of La and Sm and the La/Sm ratio in an aggregate melt produced by continuous melting. Assume bulk distribution coefficients for these two elements of 0.01 and 0.05 respectively. Do the calculation for porosities (ϕ) of 0.001 and 0.01.

a.) Plot your results as a function of extent of melting, F, letting F vary from 0.001 to 0.1.

b.) Plot your results on a process identification diagram, i.e., plot La/Sm vs. La, assuming initial La and Sm concentrations of 1.

c.) Do the same calculation for and batch melting. Compare the two processes, aggregate continuous and batch on a plot of plot La/Sm vs. La.

12. Calculate the change in the La/Sm ratio of a melt undergoing *in situ* crystallization assuming bulk partition coefficients for La and Sm of 0.05 and 0.2 respectively. Assume the melt initially has a La/Sm ratio of 1. Do the calculation for values of f of 0.05 and 0.25 and assume that $f_A = f$.

a.) Plot your results as a function of M^l/M°.

b.) Plot your results on a process identification diagram, i.e., plot La/Sm vs. La, assuming initial La and Sm concentrations of 1.